INFORMATION TO USERS

This reproduction was made from a copy of a document sent to us for microfilming. While the most advanced technology has been used to photograph and reproduce this document, the quality of the reproduction is heavily dependent upon the quality of the material submitted.

The following explanation of techniques is provided to help clarify markings or notations which may appear on this reproduction.

1. The sign or "target" for pages apparently lacking from the document photographed is "Missing Page(s)". If it was possible to obtain the missing page(s) or section, they are spliced into the film along with adjacent pages. This may have necessitated cutting through an image and duplicating adjacent pages to assure complete continuity.

2. When an image on the film is obliterated with a round black mark, it is an indication of either blurred copy because of movement during exposure, duplicate copy, or copyrighted materials that should not have been filmed. For blurred pages, a good image of the page can be found in the adjacent frame. If copyrighted materials were deleted, a target note will appear listing the pages in the adjacent frame.

3. When a map, drawing or chart, etc., is part of the material being photographed, a definite method of "sectioning" the material has been followed. It is customary to begin filming at the upper left hand corner of a large sheet and to continue from left to right in equal sections with small overlaps. If necessary, sectioning is continued again beginning below the first row and continuing on until complete.

4. For illustrations that cannot be satisfactorily reproduced by xerographic means, photographic prints can be purchased at additional cost and inserted into your xerographic copy. These prints are available upon request from the Dissertations Customer Services Department.

5. Some pages in any document may have indistinct print. In all cases the best available copy has been filmed.

University Microfilms International
300 N. Zeeb Road
Ann Arbor, MI 48106

8302552

Yao, Shing Shwang

THE EMISSION AND ABSORPTION CHARACTERISTICS OF CHALCOGENIDE SEMICONDUCTORS USING STEADY STATE AND TIME RESOLVED PICOSECOND SPECTROSCOPY

City University of New York PH.D. 1982

University
Microfilms
International 300 N. Zeeb Road, Ann Arbor, MI 48106

THE EMISSION AND ABSORPTION CHARCTERISTICS OF CHALCOGENIDE SEMICONDUCTORS USING STEADY STATE AND TIME RESOLVED PICOSECOND SPECTROSCOPY

by

Shing Shwang Yao

A dissertation submitted to the graduate faculty in Physics in partial fulfillment of the requirement for the degree of the Doctor of Philosophy, The City University of New York.

1982

This manuscript has been read and accepted for the Graduate Faculty in Physics in satisfaction of the dissertation requirement for the degree of Doctor of Philosophy.

August 2/1982 — date

Robert R. Alfano — Chairman of Examining Committee

9/7/82 — date

Executive Officer

Prof. F. Smith

Prof. N. Tzoar

Prof. R. Marino

Dr. W. J. Miniscalco

Supervisory Committee

The City University of New York

Dedication

To my father Mr. Gee-shoon Yao and my mother Mrs. Tse-ling Wang Yao.

Acknowledgements

First of all, I would like to thank my adviser Prof. R. R Alfano for his kind and helpful advice during the last several years. I also appreciate him giving me the chance to work with him in one of the most advanced picosecond laser spectroscopy laboratories in the world. I am grateful to a lot of help from my colleagues in USL laboratory, particularly Dr. Doukas, Dr. Buchert, Dr. Dorsenville, Dr. Lu, Dr. Pellegrino, Mr. Yu, Mr. Junnarkar, Mr. Rosen, Mr. Franklin, Mr. Zarrabi and Mr. Yury. Without their help, my thesis work could not be finished now. I also like to thank Mrs. Megan Gibbs for her help. Dr. Miniscalco and Dr. Lempicki at GTE labs. gave me the opportunity to begin my thesis work in the field of ferromagnetic semiconductors. I am indebted to them for their assistance.

Abstract

The Emission and Absorption Characteristics of Chalcogenide Semiconductors Using Steady State and Time Resolved Picosecond Spectroscopy

by

Shing Shwang Yao

Adviser: Professor R. R. Alfano

In this thesis, two chalcogenide semiconductors were studied by optical spectroscopy: a ferromagnetic semiconductor cadmium chromium selenide($CdCr_2Se_4$) with a Curie temperature 130K and a nonmagnetic layered semiconductor gallium selenide(GaSe).

Using steady state and time resolved picosecond emission spectroscopy, the fundamental energy gap between the S-conduction band and P-valence band has been determined in $CdCr_2Se_4$. The steady state photoluminescence spectra at low temperatures consists of two bands with an energy difference of 3.5 mev. This splitting was attributed to the exchange effect between the S-conduction electrons and the localized magnetic moments. From the theory of Nolting and Olés, the exchange constant was estimated to be 2.3 mev. The temperature dependence of the relaxation decay time and the steady state integrated intensity of the photoluminescence from $CdCr_2Se_4$ was explained by the relationship that the photoluminescence intensity is nearly proportional to the square power of the excitation intensity. $CdCr_2Se_4$ was

determined to be a direct bandgap semiconductor from the analysis of the spectral profiles of the electron-hole plasma emission from $CdCr_2Se_4$.

Using time resolved picosecond absorption spectroscopy, hot photogenerated carriers in GaSe were found to relax to the sample temperature by the emissions of nonpolar optical phonons $A_1'^{(1)}$(16.7 mev) which were related to the lattice vibration modes perpendicular to the layers. When the density of photogenerated carriers increased, the relaxation process of hot carriers decreased because the risetime increased from within our resolution to 100ps when the carrier density increased to $1.5x10^{19}cm^{-3}$ in the time resolved emission spectroscopy. This was attributed to the screening effect on the emissions of nonpolar optical phonons $A_1'^{(1)}$ from relaxing holes. From the analysis of time integrated emission spectra from GaSe excited by picosecond laser pulses, the transition from exciton-carrier scattering emission to electron-hole plasma emission was observed at carrier density $\sim 3x10^{17}$ cm^{-3}.

Table of Contents Page

Chapter 1. Introduction.................................. 1

References.................................. 5

Chapter 2. Cadmium Chromium Selenide($CdCr_2Se_4$).... 7

2.1 The crystal structure and the calculated electronic energy diagrams of $CdCr_2Se_4$. 7

2.2 The determination of the fundamental energy gap of $CdCr_2Se_4$............................ 10

2.2.1 The steady state photoluminescence of $CdCr_2Se_4$........................ 10

2.2.2 The relaxation decay time of the photoluminescence from $CdCr_2Se_4$. 13

2.3 The determination of the exchange constant between the S-conduction electrons and the local magnetic moments of Cr ions in $CdCr_2Se_4$...............................17

2.3.1 The conduction band structure of a ferromagnetic semiconductor..........17

2.3.2 The two emission bands of the steady state photoluminescence at low temperatures.........................20

2.3.3 The exchange constant between the S-electrons and the local magnetic moments 24

2.4 The temperature dependences of the decay time and the steady state integrated intensity of the photoluminescence from $CdCr_2Se_4$.... 27

2.5 The determination of the direct energy gap of $CdCr_2Se_4$..............................30

References.................................36

Chapter 3 Gallium Selenide(GaSe).......................64

3.1 The determination of the dominant relaxation process for the hot photogenerated carriers in GaSe..................................64

3.1.1 The crystal structure and the calculated electronic energy diagrams...........64

3.1.2 Time resolved absorption spectroscopy of GaSe...............................65

3.1.3 The hot carrier relaxation process in GaSe...............................70

3.2 The transition from exciton-carrier scattering emission to the electron-hole plasma emission in GaSe..................................74

3.2.1 Introduction.........................74

3.2.2 Time integrated emission spectra from GaSe excited by picosecond laser pulses 75

3.2.3 Theoretical analysis of the time integrated emission spectra from GaSe 77

3.3 The screening of nonpolar optical phonon-hole interaction by high density photogenerated carriers in GaSe........................... 84

3.3.1 Introduction........................ 84

3.3.2 Time resolved emission spectra from GaSe 84

3.3.3 Theoretical analysis of the time resolved emission spectra from GaSe.. 86

References................................ 94

Chapter 4 Conclusion.................................121

References.................................123

Chapter 5 Future Work................................124

Appendix 1 The intensity dependence of exciton emission, exciton-exciton scattering emission, exciton-carrier scattering emission, and electron-hole recombination emission with respect to the excitation intensity........................126

Appendix 2 The computer programming to calculate eq.(3.1.2) 129

Appendix 3 The derivation of eq.(3.1.5)................136

Appendix 4 The computer programming to calculate eq.(3.1.6) 138

Appendix 5 The computer programming to calculate eq.(3.2.1) 140

Appendix 6 The computer programming to calculate eq.(3.2.2) 142

Appendix 7 The derivation of eq.(3.3.2)................144
Appendix 8 The derivation of eq.(3.1.2)................147
Appendix 9 The concepts of the exchange and correlation energies in electron-hole plasma............148
Appendix 10 The concept of screening on the carrier-nonpolar optical phonon interaction..................150

List of Figures

Chapter 2: $CdCr_2Se_4$

Figure number	Description	Page
2.1.1	Crystal structure of $CdCr_2Se_4$.........	39
2.1.2	Electronic energy structure of $CdCr_2Se_4$ for paramagnetic phase by Kambara et al...	40
2.1.3	Electronic energy structure of $CdCr_2Se_4$ for ferromagnetic phase by Kambara et al.(ref.1)................................	41
2.1.4	Electronic energy structures of $CdCr_2Se_4$ for up and down spins of ferromagnetic phase by T. Oguchi et al.(ref.2)................	42
2.2.1	Steady state photoluminescence measurement setup....................................	43
2.2.2	The carrier temperature from high energy side of spectra of $CdCr_2Se_4$ compared with the sample temperature. The inset shows the steady state photoluminescence spectra at two different temperatures....................	44
2.2.3	The high energy tail of steady state emission spectra of $CdCr_2Se_4$ can be fitted by $\exp(-h\nu/kT_e)$..........................	45
2.2.4	The experimental setup for decay time measurement...............................	46
2.2.5	The relaxation decay time of $CdCr_2Se_4$	47

Chapter 2: $CdCr_2Se_4$

Figure number	Description	Page
2.2.6	The optical absorption edge of $CdCr_2Se_4$ as a function of temperature..............	48
2.2.7	The fundamental electronic energy diagram of $CdCr_2Se_4$.............................	49
2.3.1	The splitting of conduction band in a ferromagnetic semiconductor as proposed by Haas(ref.10)..............................	50
2.3.2	The conduction band structure of a ferromagnetic semiconductor as proposed by Nolting et al.(ref.7)...............................	51
2.3.3	The conduction band structure of a ferromagnetic semiconductor as proposed by Kubo(ref.11)..............................	52
2.3.4	The steady state photoluminescence spectra of $CdCr_2Se_4$ from 4K to 70K...............	53
2.3.5	The separation of the two emission bands of $CdCr_2Se_4$ at low temperatures..........	54
2.3.6	The ratio of the half intensity of the second emission peak to that of the first emission peak of $CdCr_2Se_4$ as a function of the electronic temperature....................	55
2.4.1	The photoluminescence intensity of $CdCr_2Se_4$ as a function of the excitation intensity................................	56

Chapter 2: $CdCr_2Se_4$

Figure number	Description	Page
2.4.2	The integrated photoluminescence intensity of $CdCr_2Se_4$ as a function of temperature from 4K to 220K	57
2.5.1	A series of time integrated spectra of $CdCr_2Se_4$ at 80K as a function of the picosecond laser pulse intensity	58
2.5.2	The linewidth of picosecond time integrated spectra from $CdCr_2Se_4$ as a function of the excitation intensity	59
2.5.3	The peak energy of picosecond time integrated spectra from $CdCr_2Se_4$ as a function of the excitation intesity	60
2.5.4	The integrated intensity of $CdCr_2Se_4$ at 80K excited by picosecond laser pulse as a function of the excitation intensity	61
2.5.5	The theoretical curve for K-selection(direct gap transition) fits the experimental data of the time integrated picosecond photoluminescence of $CdCr_2Se_4$	62
2.5.6	a) The reduced band gap of $CdCr_2Se_4$ as a function of the carrier density when $m_e=m_h=0.5m_o$.b) $E_g-\widetilde{E}_g$ as a function of the carrier density. E_g is the bandgap energy of $CdCr_2Se_4$ at 80K	63

Chapter 3: GaSe

Figure number	Description	Page
3.1.1	The crystal structure of GaSe.............	97
3.1.2	Three different modifications of GaSe structure................................	98
3.1.3	The electronic energy bands of GaSe by Schlueter................................	99
3.1.4	The charge densities of highest valence band of GaSe..................................	100
3.1.5	The time resolved absorption spectroscopy measurement setup.........................	101
3.1.6	The absorption spectra of GaSe at different time delay................................	102
3.1.7	The carrier temperature T_e of GaSe as a function of the time delay................	103
3.2.1	A series of time integrated photoluminescence spectra from GaSe at 77K at different excitation intensities....................	104
3.2.2	A series of time integrated photoluminescence spectra from GaSe at 300K at different excitation intensities....................	105
3.2.3	The integrated emission intensity of GaSe as a function of the excitation intensity of picosecond laser pulse at 77K............	106
3.2.4	The integrated emission intensity of GaSe as a function of the excitation intensity of	

Chapter 3: GaSe

Figure number	Description	Page
	picosecond laser pulse at 300K	107
3.2.5	The peak energies of higher and lower energy bands of GaSe excited by picosecond laser pulse	108
3.2.6	The mechanism of exciton-electron(hole) scattering emission	109
3.2.7	The theoretical expression of exciton-electron (hole) scattering emission fits the high energy side of the experimental data of GaSe at 77K	110
3.2.8	The theoretical expression of exciton-electron (hole) scattering emission fits the high energy side of the experimental data of GaSe at 300K	111
3.2.9	The theoretical expression of exciton-exciton scattering emission does not fit the high energy side of the experimental data of GaSe at 77K	112
3.2.10	The theoretical expression of exciton-exciton scattering emission does not fit the high energy side of the experimental data of GaSe at 300K	113
3.2.11	The theoretical expression of electron-hole plasma emission fits the high energy side of	

Chapter 3: GaSe

Figure number	Description	Page
	the experimental data of GaSe at 300K.....	114
3.2.12	The reduced bandgap $\tilde{E}_g$ as a function of the photogenerated carrier density for GaSe...	115
3.3.1	A series of time resolved spontaneous emission from 610 to 630 nm of GaSe excited by picosecond laser pulse at 300K........	116-7
3.3.2	A series of time resolved stimulated emission with wavelength larger than 640 nm of GaSe excited by picosecond laser pulse at 300K	118
3.3.3	The rise times at different carrier densities for both a) spontaneous and b) stimulated emissions from GaSe at 300K...............	119
3.3.4	The inverse of the risetime of the spontaneous emission from GaSe as a function of the photogenerated carrier density.....	120

Chapter 1: Introduction

In recent years, ferromagnetic semiconductors and layered semiconductors have been studied by many physicists. These semiconductors have many interesting phenomena. Ferromagnetic semiconductors have anomalous resistance peaks at their Curie temperatures[1,2] due to the existence of narrow d or f conduction bands[3]. They also show red shifts in their optical absorption spectra when the temperature is below their Curie temperatures[4]. This is because the optical absorption is between the P valence band and the local d or f bands which broaden below their Curie temperatures[5]. This is different from nonmagnetic semiconductors. For nonmagnetic semiconductors, the optical absorption edges have blue shifts with decreased temperature because there is no d or f band and the optical absorption is between P valence and S conduction bands[6]. Layered semiconductors have exciton optical emission[7] and absorption[8] even at room temperature due to the resonance effect between the direct exciton and the indirect conduction band[7,8]. For nonlayered semiconductors, the exciton emission and absorption usually disappear at room temperature because of the dissociation of excitons.

Chalcogenide semiconductors are important because some of them are ferromagnetic and some are layered semiconductors. In this thesis, two chalcogenide semiconductors: cadmium chromium selenide($CdCr_2Se_4$) and gallium selenide(GaSe)

were studied by investigating their optical emission and absorption spectroscopies. The spectral analyses of these spectroscopies can determine the electronic energy structures and the dynamical processes of hot carriers in these semiconductors.

$CdCr_2Se_4$ is a ferromagnetic semiconductor with a Curie temperature[2] at 130K. The optical absorption edge[4] is at 1.2ev and shows red shift below 130K. For the last fifteen years, many researchers have tried to determine the complete electronic energy diagram of $CdCr_2Se_4$. However, their results are confusing with one another. In addition, the locations of the d bands of the Cr ions make the energy diagram more complicated than that of nonmagnetic semiconductors because these d bands can be inside either the two wide bands or the energy gap. Recently, a rather complete energy diagram had been calculated by Kambara et al.[9,10]. This energy diagram was confirmed by the photoluminescence spectra[11] in this thesis and by the photoemission method of Miniscalco et al.[12] .

$CdCr_2Se_4$ is a good sample to study the exchange effects between the itinerant conduction electrons and the local magnetic moments of Cr ions because the band to band luminescence has two peaks at low temperatures. The conduction band of a ferromagnetic semiconductor is split by the local magnetic moments into subbands. According to Hass theory[13], the conduction band consists of two purely

spin-polarized subbands(spin up and down). Recently, this model has been questioned by Nolting and Oleś[5] who believe that the conduction band in a ferromagnetic semiconductor consists of multi-mixed-spin subbands. The photoluminescence spectra of $CdCr_2Se_4$ below 70K were observed to consist of two emission bands in this thesis. The splitting was attributed to the splitting of S conduction band and the two split bands were found to be not purely spin-polarized using steady state photoluminescence method.

GaSe is a layered semiconductor. It can be used to study the strong hole-phonon interactions[14] due to its layered structure. In each layer of this semiconductor, both gallium and selenium atoms are covalently bonded together. Between two layers, only van der Waals forces exist. Schlueter[14] calculated that the toppest valence electrons are distributed around the two gallium ions and the conduction electrons are more diffusely distributed. Schmid et al.[15] concluded experimentally that holes strongly interact with nonpolar optical phonons $A_1'^{(1)}$ which are vibrating between two gallium ions. This leads us to ask whether hot carriers lose their kinetic energy by emitting these nonpolar optical phonons from holes and whether this emission rate of phonons from holes will be screened by high density of carriers as predicted by Yoffa's theory[16]. Using time resolved picosecond spectroscopy, these questions were answered in this thesis.

In semiconductors, an interesting transition from exciton state to electron-hole plasma state can occur due to high density free carriers. This theory was originally proposed by Mott[17] who believed that the transition from insulator to metal is possible when the distances between atoms are close enough. This exciton -plasma transition was observed in Si by Shah et al.[18]. In this thesis, the transition from exciton-carrier scattering emission to electron-hole plasma emission was apparently observed from the analysis of the time integrated picosecond photoluminescence spectra of GaSe.

Using steady state and time resolved spectroscopy, many physical processes can be observed in ferromagnetic semiconductor $CdCr_2Se_4$ and layered semiconductor GaSe. The detailed theories, experimental procedures, and results will be described in the following chapters.

References of Chapter 1:

1. S. von Molnar and S. Methfessel, J. of Appl. Phys. 38,959 (1967).

2. H. W. Lehman, Phys. Rev. 163,488(1967).

3. M. D. Coutinho and I. Balberg, J. Appl. Phys. 50,1920(1979)

4. G. Busch, B. Magyar, and P. Wachter, Phys. Lett. 23,438 (1966).

5. W. Nolting and A. M. Oleś, Phys. Rev. B22, 6184(1980).

6. G. D. Mahan, J. Phys. Chem. Solids, 26, 751(1965).

7. J. P. Voitchovsky and A. Mercier, Nuovo Cimento, 22B,273 (1974).

8. A. Bosacchi, B. Bosacchi, and S. Franchi, Phys. Rev. Lett. 36,1086(1976).

9. T. Kambara, T. Oguchi, and K. I. Gondaira, J. Phys. C13,1493(1980).

10 T. Oguchi, T. Kambara, and K. I. Gondaira, Phys. Rev. B22, 872(1980).

11. S. S. Yao, F. Pellegrino, R. R. Alfano, W. J. Miniscalco, and A. Lempicki, Phys. Rev. Lett. 46,558(1981).

12. W. J. Miniscalco, B. C. McCollum, N. G. Stoffel, and G. Margaritondo, Phys. Rev. B25,2947(1982).

13. C. Hass, Phys. Rev. 168,531(1968).

14. M. Schlueter, Nuovo Cimento, 13B,313(1973).

15. Ph. Schmid and J. P. Voitchovsky, Phys. Stat. Sol.

(b)65,249(1974).

16. E. J. Yoffa, Phys. Rev. B23,1909(1981).

17. N. F. Mott, Rev. Mod. Phys. 40,677(1968).

18. J. Shah, M. Combescot, and A. H. Dayem, Phys. Rev. Lett. 38,1497(1977).

Chapter 2: Cadmium Chromium Selenide($CdCr_2Se_4$)

2.1 The crystal structure and the calculated electronic energy diagram of $CdCr_2Se_4$

The crystal structure[1] of $CdCr_2Se_4$ is a spinel as shown in Fig.2.1.1. Both chromium and selenium ions are on the octahedral sites. The cadmium ions are close to the selenium ions. The unit lattice cell is ~10 Å on each dimension. Most recently, Kambara et al.[1] calculated by the use of the extended Hückel method the electronic energy diagram which is shown in Fig.2.1.2 for paramagnetic phase and in Fig.2.1.3 for ferromagnetic phase. The atomic orbitals of Cr(4S), Cr($d\epsilon$), Cr($d\gamma$), and Se(4P) are denoted in both figures. The energy gap between the lowest S conduction band and the highest P valence band is 1.9 ev in paramagnetic phase and each band splits into two subbands in ferromagnetic phase. The energy difference between two split S conduction bands is ~ 500 mev, and that between two split P valence bands is 50 mev. The two d bands($d\epsilon$ and $d\gamma$) lie in the energy gap for the majority spins and above the lowest conduction band for the minority spins. They also found $Cd^{+1.94}(Cr^{+1.82})_2(Se^{-1.39})_4$ for each ionic charge, therefore the bonds are not pure ionic but with some covalency. In their calculation, an exchange constant of 250mev between the Cr(4S) orbitals and the local magnetic moments of Cr ions was assumed. Oguchi et al.[2] also calculated the electronic energy diagram of $CdCr_2Se_4$

using the discrete variational $X\alpha$ method in the ferromagnetic phase as shown in Fig.2.1.4. The energy gap is 2.35 ev for the majority spin and 3.05 ev for the minority spin. Some of the d bands are in the energy gap and the others are in either the conduction or valence bands. The atomic orbitals of Cr(4S), Cr($d\epsilon$), Cr($d\gamma$), and Se(4P) are denoted in this figure.

In the later sections, the steady state and time integrated picosecond photoluminescence spectra from $CdCr_2Se_4$ will be presented to justify the above calculated electronic energy diagram. Except some quantitative disagreements, the above diagram are agreeable to the experimental results. The fundamental energy gap was determined experimentally to be 1.8ev instead of 1.9ev and the splitting of S-conduction band was determined experimentally to be $\sim$3.5mev instead of 500mev. This big difference in splitting energy is because a very large exchange constant of $\sim$250mev was assumed in the theoretical calculation by Kambara et al.. The splitting of P valence band was determined to be very small in this thesis compared with the splitting of S conduction band.

The above theoretical calculations have a common assumption that the two split S conduction bands and the two split P valence bands are purely spin-polarized. This contradicts the experimental result that the two split bands are not purely spin-polarized which will be shown in the

section 2.3. Therefore the theoretical calculation of the splitting of bands calculated by Kambara et al. is not significant.

2.2 The determination of the fundamental energy gap of $CdCr_2Se_4$

2.2.1 The steady state photoluminescence of $CdCr_2Se_4$

Veslago et al.[3] reported the first photoluminescence spectra at 1.8 ev of $CdCr_2Se_4$ excited by a pulsed laser. The emission was attributed to the radiative transition betwen two crystal -field-split levels($d\epsilon$ and $d\gamma$) of chromium ions. In this section, the steady state photoluminescence spectra at 1.8 ev from $CdCr_2Se_4$ will be reported, and this emission will be proved to arise from a band to band transition.

The steady state photoluminescence was measured using the setup shown in Fig.2.2.1. A pure single crystal $CdCr_2Se_4$ sample with the courtesy of Dr. Miniscalco was placed on a cold finger in an optical dewar. The temperature of the sample was measured by a copper-constantan thermocouple or by a silicon diode. The sample of $1mm^3$ volume was excited by an argon laser at 488 nm which was chopped at 100cps before the sample. The luminescence was collected by a Spex 1/2m spectrometer, a RCA 7265 photomultiplier, and analyzed by a lock-in amplifier and a recorder.

The inset of Fig.2.2.2 shows the emission spectra of $CdCr_2Se_4$ at two different temperatures(100K and 161K). The peak energies are around 1.8ev. The slope of the high energy tail of each curve is dependent on the sample temperature T_s.

For a direct band to band transition (or K-selection

$$I(\hbar\omega) \propto \int \frac{d\vec{K}_h}{(2\pi)^3} \int \frac{d\vec{K}_e}{(2\pi)^3} |M(\vec{K}_e, \vec{K}_h)|^2 f_h(\vec{K}_h) f_e(\vec{K}_e) \delta(\vec{K}_e - \vec{K}_h) \delta(\hbar\omega - E_g - E_e - E_h)$$

$$I(\hbar\omega) \propto \int \frac{d\vec{K}_h}{(2\pi)^3} \int \frac{d\vec{K}_e}{(2\pi)^3} |M(\vec{K}_e, \vec{K}_h)| f_h(\vec{K}_h) f_e(\vec{K}_e) \delta(\vec{K}_e - \vec{K}_h) \delta(\hbar\omega - E_g - E_e - E_h)$$

where K_e and K_h are the momenta of electrons and holes, $M(\vec{K}_e, \vec{K}_h)$ is the transition matrix, f_e and f_h are the Fermi distributions of electrons and holes, $\hbar w$ is the emission energy, E_g, E_e, and E_h are the band gap energy, electronic kinetic energy and hole's kinetic energy.

$$E_h = \hbar^2 K_h^2 / 2m_h = \hbar^2 K_e^2 / 2m_h = m_e E_e / m_h$$

$$I(\hbar\omega) \propto \int d\vec{K}_e |M(\vec{K}_e, \vec{K}_h)|^2 f_h(\vec{K}_e) f_e(\vec{K}_e) \delta(\hbar\omega - E_g - E_e - E_h)$$

$$\hbar^2 K^2 / 2m = E, \quad 2\hbar^2 K dK / 2m = dE$$

$$d\vec{k} = 4\pi K^2 dK \propto 4\pi K^2 dE / K \propto 4\pi E dE / E^{1/2} \propto E^{1/2} dE$$

$$I(\hbar\omega) \propto \int E_e^{1/2} dE_e |M|^2 f_e(K_e) f_h(K_e) \delta(\hbar\omega - E_g - E_e - E_e m_e / m_h)$$

$$\hbar w - E_g - E_e - E_h = hw - E_g - E_e(1 + m_e/m_h) \cong hw - E_g - E_e$$

$$I(\hbar w) \propto \exp(-(\hbar w - E_g)/kT_c)(\hbar w - E_g)^{1/2} \qquad (2.2.1)$$

where T_c is the carrier temperature. The Maxwellian distribution for electrons and holes is assumed. The peak energy of the emission intensity is at $\hbar w = E_g + 1/2 kT_c$.

For an indirect band to band transition (or non-K-selection transition), the emission intensity is

$$I(\hbar\omega) \propto \int |M|^2 f_e f_h \rho_e \rho_h \delta(E_e + E_h + E_g - \hbar\omega) dE_e dE_h$$

where ρ_e, ρ_h are the density of states. For allowed transition, $|M|^2$ is a constant. For free carriers, $\rho \propto E^{1/2}$,

$$I(\hbar w) \propto \exp(-(\hbar w - E_g)/kT_c) \int_0^{\hbar\omega - E_g} E_e^{1/2} (\hbar\omega - E_g - E_e)^{1/2} dE_e$$

$$I(\hbar w) \propto \exp(-(\hbar w - E_g)/kT_c)(\hbar w - E_g)^2 \qquad (2.2.2)$$

The peak energy of the emission intensity is at $\hbar w = E_g + 2kT_c$.

In Fig.2.2.2, the carrier temperature T_c extracted from the high energy tail[4] by assuming the intensity I(hv) $\exp(-hv/kT_c)$ as shown in Fig.2.2.3 is compared with the sample temperature T_s, where hv is the emission energy. This is because the carriers in a wide band will have Maxwellian distribution when the carrier temperature is high. In Fig.2.2.3, the intensity of the high energy tail is fitted well by a straight line in a semilog scale. The slope of the straight line is $-1/kT_c$. Over the whole temperature range(80K to 200K), both T_c and T_s are the same within experimental error. This indicates that the emission involves with at least a wideband(either conduction of valence band) because the high energy tails of the emissions have Maxwellian distribution. The low energy tail of each curve in Fig.2.2.2 is independent of the temperature and is due to the transition involved with imperfect band tails or impurity states. Measuring the area under the photoluminescence curve over the whole wavelength regime, the quantum yield of this emission at 77K was measured to be $\sim 10^{-4}$ which will be used later to find the radiative transition rate of this emission. The quantum yield of Rhodamine 6G is assumed to be 1 under the same experimental conditions.

Miniscalco and Lempicki at GTE Research Labs. also

observed this emission at 1.8 ev from $CdCr_2Se_4$ excited by dye laser with excitation wavelength from 560 nm to 640 nm which is 40 mev to 400 mev above the emission energy. This near resonance excitation indicates that deep levels are not involved with this transition. This photoluminescence can involve with a transition between a shallow donor or acceptor state and a wide band. The single crystal $CdCr_2Se_4$ can be n type by doping In or p type by doping Ag. These dopants replace the Cd positions. The binding energies for donor and acceptor states are unknown at this time.

2.2.2 The relaxation decay time of the photoluminescence from $CdCr_2Se_4$

Since the d bands from Cr ions in $CdCr_2Se_4$ lie either in the energy gap, in the conduction or valence bands[1,2], it is necessary to prove that the emission at 1.8 ev is not due to the transition between two d bands. In this section, the results of the relaxation decay times will help to solve the above question .

The experimental setup for the measurement of the decay time is shown in Fig.2.2.4. The Nd:glass laser emits a train of laser pulse at 1054nm with about 6 ps duration in the beginning of the pulse train. One of these pulses is selected and amplified. The second harmonic (527 nm) of this pulse is generated by a KDP crystal. This 527nm pulse is

used to excite the sample $CdCr_2Se_4$. The kinetics of the photoluminescence is measured by a Hamamatsu streak camera of 10 ps resolution time and analyzed by a temporal analyzer and a PDP 11 computer.

As shown in Fig.2.2.5, the measured relaxation decay times from 10K to 250K decrease from ~50 ps to ~10 ps without any deconvolution of the decay times. When the temperature increases, the decay time decreases. This is because the thermal effect inhances the decay rate of carriers. The solid line is a fit which will be explained later from the steady state integrated intensity of the photoluminescence of $CdCr_2Se_4$. The decay time is scattered at each temperature due to the uncertainty of the excitation intensity of the laser pulse. The Auger effect predicts that the recombination time of carriers will be shorter when the carrer density is higher. The decay time at 77K is ~25 ps which gives $\sim 4x10^{10}$ sec^{-1} of the transition rate. Because the quantum yield mentioned in the previous sention is $\sim 10^{-4}$ at 77K, the radiative transition rate will be $\sim 4x10^{6}$ sec^{-1}. This is too large for a parity forbidden transition and precludes the possibility of the transition being between crystal-field-split $3d^3$ states of Cr. In this material the Cr sites hame octahedral symmetry and in the many-electron representation[5] the ground state of Cr^{3+} has $^4A_{2g}$ symmetry while the first excited state is either ^2E_g or $^4T_{2g}$. In the

high-crystal-field limit the former is lower making the transition to the ground state both spin and parity forbidden with typical radiative transition rates of $\cong 10^2$ sec^{-1}. In the low-field limit the $^4T_{2g}$ is the lowest excited state making the transition spin allowed with radiative rates$\cong 10^3$ sec^{-1}, still three orders of magnitude smaller than in $CdCr_2Se_4$. Therefore, the $4x10^6$ sec^{-1} rate for this material requires that the emission result from transitions between bands of opposite parity(P band to S band , or P band to d band).

As shown in Fig.2.2.6, the absorption edge[6] has a red shift of about 200mev when the temperature decreases from 180K. This red shift of the absorption edge is probably due to the broadening[7] of the dγ band of Cr ions in $CdCr_2Se_4$. The optical absorption edge of $CdCr_2Se_4$ is at 1.2 ev which is lower in energy than the photoluminescence emission at 1.8 ev when the temperature is at 77K. The simplest interpretation for this difference requires a 1.8 ev valence-band to conduction-band gap with d band in the gap which causes the optical absorption edge. The octahedral symmetry splits the Cr $3d^3$ states into two components with the Fermi level between them and one or both components in the gap as shown in Fig.2.1.2, 2.1.3, and 2.1.4. The absorption edge results from transitions between either occupied d bands in the gap and the conduction band or unoccupied d bands in the gap and the valence band.

Emission results from conduction-band to valence-band transition.

Recently, Miniscalco et al.[8] determined that the filled d bands lie below the highest valence by 1.45 ev in $CdCr_2Se_4$ using photoemission method. This indicates that the unfilled d bands are 1.2 ev above the highest valence band and the absorption edge is from the transition between the highest valence band and the unfilled d bands.

To conclude this section, the fundamental electronic energy diagram is drawn in Fig.2.2.7 from both the photoluminescence results in this section and the photoemission results by Miniscalco et al.[8]. The valence band is at 0 ev, the conduction band is at 1.8 ev, the filled d bands are at -1.45 ev, and the unfilled d bands are at 1.2 ev.

2.3 The determination of the exchange constant between the S conduction electrons and local magnetic moments of Cr ions in $CdCr_2Se_4$

2.3.1 The conduction band structure of a ferromagnetic semiconductor

There have been many theories to describe the conduction band structure of a ferromagnetic semiconductor. The first one is given by Rys et al.[9] and Haas[10]. They claimed that both conduction band and valence band split into two subbands below the Curie temperature of a ferromagnetic semiconductor. One of the subbands is spin up and the other is spin down. This is shown in Fig.2.3.1. The splitting is caused by the exchange interaction between the free charge carriers in a broad band and localized magnetic moments. The first order energy change is

$$\Delta\epsilon^{1,\pm} = \mp \tfrac{1}{2} S J (M/M_0) \qquad (2.3.1)$$

where $M_0 = -Ng\mu_B S$, S is the local magnetic quantum number, μ_B is the Bohr magneton, g is the Lande factor, N is the number of magnetic atoms per unit volume, J is the exchange interaction between the free carriers and the local magnetic moments, M is the total magnetization per unit volume, $M = -g\mu_B \sum_n \langle S_n \rangle$.

The second theory given by Nolting and Olés[7] states that conduction band consists of multi-mixed-spin subbands at all temperatures. This theory was derived using the methods of spectral densities and spectral moments. As shown

in Fig.2.3.2, the conduction band of a ferromagnetic semiconductor is split into two subbands as a consequence of the exchange interaction between conduction electrons and localized magnetic moments. This splitting takes place in principle for all temperatures, ie, it is not at all due to the onset of ferromagnetism. The conduction band of a ferromagnetic semiconductor splits for each spin direction into two quasiparticle subbands. It is important to stress that the spin index(↑ or ↓) of the quasiparticle energies denotes the spin of the electron before its excitation into such a quasiparticle subband; after the excitation the spin is generally uncertain. These subbands do not at all consist of pure spin states, but rather complicated mixed-spin-states. The experimentally observed red shift of the optical absorption edge for a suitable electronic transition into the conduction band is explained by a broadening of a lower ↑ subband with decreasing temperature in this theory given by Nolting and Oleś. This theory is valid when the exchange constant between two local magnetic moments is several order smaller than the coupling constant between the free carriers and the local magnetic moments.

The third theory on the conduction band structure by Kubo[11] indicates that conduction band in a ferromagnetic semiconductor splits into subbands which exist at all temperatures, however these subbands are neither purely spin-polarized nor totally spin-depolarized. Kubo[11]

calculated the electronic structure in magnetic semiconductors by the coherent potential approximation. The density of states for down and up states is calculated in the paramagnetic and completely ferromagnetic states for various values of interaction strength. This is shown in Fig.2.3.3.

In the following section, the steady state photoluminescence spectra with two emission bands at very low temperatures will be presented and attributed to the splitting of S conduction band in $CdCr_2Se_4$. The subbands will be proved to be totally spin-depolarized.

2.3.2 The two emission bands of the steady state photoluminescence at low temperatures(4K to 70K)

The steady state photoluminescence of $CdCr_2Se_4$ excited by a 10 mw argon laser were measured from 4K to 70K The spectra are shown in Fig.2.3.4. Both sample temperature T_s and electronic temperature T_e were denoted for each curve. At a sample temperature of $\sim$4K, a small second peak on the high energy side of the luminescence peak exists. When the sample temperature T_s increases, the second peak on the high energy side increases in intensity. The electronic temperature T_e extracted from the high energy tail of the second peak assuming $I(hv) \propto \exp(-hv/kT_e)$ is larger than the sample temperature by $\sim$10K when T_s is smaller than 20K. This higher carrier temperature than the sample temperature by more than 10K was observed in GaAs by Shah and Leite[4] and was attributed to the reduced emission rate of phonons from carriers at very low sample temperature. In GaAs, the power $P(T_e)$ transfered per electron from the hot-electron system to the lattice is $P(T_e) \propto \exp(-T_o/T_e)$ with T_o=33mev. The rate of loss of energy via optical-phonon scattering decreases drastically with the reduction in electron temperature. The electronic temperature is the same as the sample temperature when T_s is above 20K for $CdCr_2Se_4$. Above 70K, the two peaks can not be resolved. The energy difference between these two peaks is a constant of 3.5 mev from 4K to 70K.

These two emission bands arise from two split conduction bands separated by an energy ΔE. The electronic density at the bottom of higher energy band is equal to $\exp(-\Delta E/kT_e)$ times that at the bottom of lower energy band. This is because the electronic distribution is Maxwellian when the semiconductor is nondegenerate due to small photogenerated carrier density created by 10 mw argon laser. The steady state photogenerated carrier density(S conduction electrons and P valence electrons) is equal to I/KV, when I is the laser power(10mw), K is the recombination rate of carriers(the decay time is $\sim$50 ps at 4K), and V is the volume where the photogenerated carriers occupy and equals A.d($10^{-5}cm^{-3}$), where A is the excitation area($10^{-2}cm^{2}$) and d is the absorption depth(10^{-3}cm), therefore about $10^{11} \sim 10^{12}$ cm^{-3} carrier density are generated. This value is too small compared with the ion density($\sim 10^{21}$ cm^{-3}), therefore the semiconductor is nondegenerate.

Since both the higher energy sides of these two emission bands are superimposed each other for each curve in Fig.2.3.4, the following separation method is needed to analyze the spectral shape. The intensity of the higher energy side of the lower energy emission band was obtained by dividing equally the intensity of the higher energy side of the higher energy emission band as can be seen in Fig.2.3.5. This is because the density of states is assumed

to be the same for both split bands at the same energy level and this assumption will be justified. The lower energy side of the higher energy emission band was assumed to contribute nothing to the lower energy emission band. Any other method of separating these two emission bands fails because the spectral profiles of these separated emission bands can not be represented by the same formula. The high energy sides of both emission bands at various temperatueres were analyzed. Both bands can be fitted approximately to $\exp(-(h\nu-E_{gi})/kT_e)$, $i=1,2$, $h\nu$ is the emission energy. Compared with eq.(2.2.1), this indicates that the density of states are close to a constant value within 20 mev from the bandedge. The ratio of the half intensity of the second peak to that of the first peak is plotted as a function the electronic temperature T_e in Fig.2.3.6. The density of states at ΔE above the bottom of the lower energy band is assumed to be the same as that at the bottom of the higher energy band, therefore the intensity at the second peak is twice the intensity from the bottom of the higher energy band. The solid line is equal to $\exp(-\Delta E/kT_e)$, where ΔE $=3.5$ mev. The experimental data(cross dots) are fitted by the solid line. This indicates that the two emission bands are from the split bands separated by $\Delta E=3.5$ mev.

The S conduction electrons[1] are more localized around the Cr ions in $CdCr_2Se_4$, and the P valence electrons(or holes) are around the selenium ions which are about 3 Å away

from the Cr ions, therefore, the exchange effect between the P valence electrons (or holes) and the Cr ions can be neglected. This is also justified by the theory of Nolting and Oleś[7] who did not claim any splitting of the P valence band in a ferromagnetic semiconductor.

The reason that two split emission bands are not resolved above 70K is that the thermal distribution energy kT is ~6 mev at 70K and the intensity of the second peak(higher energy) is higher than that of the first peak(lower energy) due to the superposition of two emission bands.

It is important to know whether the main peak at 4K is due to a band to band transition in order to conclude that these two emission bands are from two split S-conduction bands. The intensity of the photoluminescence was measured to increase quadratically with the excitation intensity as shown in Fig.2.4.1. This excludes that these two emission bands are both exciton emissions or both impurity emissions because both exciton emission and impurity emission increase linearly with the excitation intensity[12,13]. It may be argued that the lower energy band could be either exciton or impurity emission and the higher energy band is an electron-hole recombination; however, this can be excluded because the intensity ratio between these two bands remains the same at fixed temperature over a wide range of excitation intensity. Furthermore, excitons would be dissociated when the temperature is 40K(~3.5 mev) which is

the energy difference between these two bands. Therefore, the two emission bands are from S band to P band transition.

2.3.3 The exchange constant between the S conduction electrons and the local magnetic moments of $CdCr_2Se_4$

As mentioned in the previous section, there have been different theories to describe the spin polarities of the subbands in a ferromagnetic semiconductor. In order to test whether these subbands are purely spin-polarized, the intensities of the right -circular-polarized and left-circular-polarized light emitted from $CdCr_2Se_4$ should be measured. The transition probabilities[14] from spin-up state and spin-down state of conduction band to the valence band are different; therefore, the emission intensity from the spin-up conduction state to the valence band will not be the same as that from the spin-down conduction state to the valence band.

The method of measuring the intensity of the right or left circular polarized light is as follow: a quarter wave plate, a linear polarizer, and a depolarizer are placed orderly in the luminescence path between the sample and the spectrometer shown in Fig.2.2.1. When the polarity of the linear polarizer is in perpendicular or horizontal direction, the intensity of the right or left circular polarized light is measured. The measurement of the right or

left circular polarized light from $CdCr_2Se_4$ at 20K shows no change on the intensity ratio between two emission bands of the photoluminescence within experimental accuracy. This proves that the split conduction bands are not purely spin-polarized. The photoluminescence was also measured at 10K when an external magnetic field of 4 Kgauss was applied to the sample $CdCr_2Se_4$. The spectra of both right and left circular polarized emissions are the same with or without the external magnetic field applied on the sample. The energy difference between two peaks remains 3.5 mev. This indicates that the two emision bands are independent of the external magnetic field up to 4 Kgauss . According to Haas theory, the splitting between two subbands is dependent on the local magnetic moment which can be increased by external magnetic field as shown by eq.(2.3.1), however no increase of the splitting in energy was observed with external magnetic field applied on the sample. Therefore, the theory developed by Nolting and Olés can be used to find the exchange constant between the S conduction electrons and the local magnetic moments of Cr ions in $CdCr_2Se_4$ because the two split S-conduction bands are totally spin-depolarized and the energy difference between these two peaks are independent of the external magnetic field up to 4 Kgauss.

The theory of Nolting and Olés states that the centers of gravity for two different spin states are at $-1/2g\langle S_z\rangle$ and

$+1/2g\langle S_z\rangle$, respectively, if the conduction band of a ferromagnetic semiconductor is weakly occupied. The constant g is the exchange constant between S conduction electrons and Cr ions, and the thermodynamic average $\langle S_z\rangle=S=3/2$ at T=0 for $CdCr_2Se_4$. As mentioned in the previous section, the 10 mw argon laser can only generate carriers of $10^{11}\sim 10^{12}$ cm^{-3} which is very small compared with the ion density($\sim 10^{21}$ cm^{-3}). Therefore the energy difference $\Delta E=3.5$ mev between two emission bands should be equal to $g\langle S_z\rangle=gS=3/2g$, and g is estimated to be $\sim$2.3 mev if the energy difference between the centers of gravity for two different spin states at T=0 is assumed to be the same as that between two lower edges of the conduction bands.

The exchange constant of S-d model in ferromagnetic metal is $\sim$0.6 ev or more due to strong overlapping of these bands[15]. Yanase and Kasuya[16] estimated that the exchange constant between the S electrons and the local magnetic ions in doped EuSe is in the range of 1 to 10 mev using magnetic impurity model. The energy difference between these two bands is $\sim$1.78 ev in EuSe. However, the energy difference between the S band and the filled d band in $CdCr_2Se_4$ is 1.8+1.45=3.25 ev which is much larger than 1.78 ev, therefore 2.3 mev is a reasonable value for the exchange constant between the S electrons and the local magnetic moments in $CdCr_2Se_4$ due to larger energy difference and being lack of overlapping between the two bands.

2.4 The temperature dependence of the decay time and the steady state integrated intensity of the photoluminescence from $CdCr_2Se_4$

In this section, the relationship between the decay time and the steady state integrated intensity of the photoluminescence at 1.8 ev from $CdCr_2Se_4$ will be described. This relationship is obtained based on the fact that the emission at 1.8 ev is from a band to band transition and that the steady state photoluminescence intensity is proportional to the square of the free carrier density.

As shown in Fig.2.2.4, the decay times were measured assuming exponential decay. The quantum yield was measured to be $\sim 10^{-4}$ at 77K for the steady state photoluminescence from $CdCr_2Se_4$, this suggests that the nonradiative decay dominates the decay of free carriers. The decay rate equation of free carriers can be written as

$$dn/dt = KI - K_{NR} \cdot n \qquad (2.4.1)$$

where n is the electron density, K is a proportion factor, I is the excitation, and K_{NR} is the nonradiative decay rate of free carriers. At steady state case, dn/dt=0 implies that

$$KI = K_{NR} \cdot n \qquad (2.4.2)$$

Since the emission is from the transition between two bands, the radiative decay rate of free carriers should be proportional to $K_{RAD} \cdot n \cdot p$, where K_{RAD} is the radiative decay rate, p is the hole density. The radiative intensity

I_F of the photoluminescence should also be proportional to $K_{RAD}.n.p$, ie

$$I_F=K_{RAD}.n.p=K_{RAD}.(KI/K_{NR})^2 \qquad (2.4.3)$$

In order to test whether this is correct, the steady state photoluminescence intensity I_F is measured at different excitation intensity I, and the result is shown in Fig.2.4.1. The photoluminescence intensity I_F is nearly proportional to the square power of the excitation intensity(1.85 within experimental error). This confirms that $I_F=K_{RAD}(KI/K_{NR})^2$ is a correct relationship.

Another method to check the relationship $I_F=K_{RAD}(KI/K_{NR})^2$ is to check whether $I_F \propto \tau_{NR}^2$ holds at various temperatures, where $\tau_{NR}=1/K_{NR}$.Since

$$I_F(t) \propto n(t)p(t) \propto (e^{-t/\tau_{NR}})(e^{-t/\tau_{NR}})=e^{-2t/\tau_{NR}}=e^{-t/\tau}. \qquad (2.4.4)$$

This leads to $\tau=\tau_{NR}/2$. Therefore

$$I_F=K_{RAD}(I/K_{NR})^2=K_{RAD}.I^2.\tau_{NR}^2 \propto \tau^2 \qquad (2.4.5)$$

where K_{RAD} and I are assumed constant at all temperatures. In Fig.2.4.2, the steady state integrated intensity over the whole wavelength regime decreases when the temperature increases from 4K to 220K. The square root value of the solid line in Fig.2.4.2 is plotted in Fig.2.2.5, and compared with the experimental data. The experimental data in Fig.2.2.5 are fitted by this solid line within experimental accuracy. This proves that $I_F \propto \tau^2$ is a

correct relationship between the decay time and the steady state integrated intensity of the photoluminescence from $CdCr_2Se_4$.

The above analysis gives another evidence to prove that the photoluminescence at 1.8 ev is from a band to band transition.

2.5 The determination of the direct energy gap of $CdCr_2Se_4$

The steady state photoluminescence from the ferromagnetic semiconductor $CdCr_2Se_4$ was mentioned in the earlier section[17]. The emission centered at 1.81 ev was ascribed to the transition from fundamental gap. It was not possible to determine whether the transition was direct or indirect. One way to determine whether the bandgap is direct or indirect is to measure the photoluminescence spectra from $CdCr_2Se_4$ excited by high power picosecond laser pulses. Using well known expressions of electron-hole plasma emission for the transitions from direct and indirect band gaps as shown in eq.(2.2.1) and eq.(2.2.2), the spectral profiles can be analyzed and the bandgap can be determined to be either direct or indirect.

A 6 ps 0.53 μ laser pulse was used to excite the pure sample $CdCr_2Se_4$ of 1 mm^3 on the front surface. The excitation area on the sample was 0.5x0.6 mm^2. The sample was placed in an optical dewar at 80K. The luminescence emitted from the front surface of $CdCr_2Se_4$ was detected and analyzed using a 1/4m Spex spectrometer coupled to a PAR SIT camera and an optical multichannel analyzer(OMA)II.

As shown in Fig.2.5.1, a series of time integrated spectra for $CdCr_2Se_4$ at 80K as a function of the picosecond laser pulse intensity from 0.3 to 20 $GWcm^{-2}$ are displayed. With increasing excitation intensity the peak of

the luminescence shifts to lower energy and the spectral linewidth becomes broader. As shown in Fig.2.5.2 and Fig.2.5.3, the linewidth increases from 10 mw to 30 mw and the peak energy shifts to red from 1.79 ev to 1.76 ev as the pumping intensity increases from 0.3 to 20 $GWcm^{-2}$. Fig.2.5.4 shows that the integrated emission intensity increases linearly with the excitation intensity.

From the results shown in Fig.2.5.1, the lowest excitation intensity used is $(3.5 \pm 0.5)10^8$ Wcm^{-2}. The peak energy of the photoluminescence at this excitation intensity is 1.789 ev(693 nm) which is 18 mev smaller than the peak energy of 1.807 ev(686 nm) measured by the low power steady state luminescence work. Since the exciton state in $CdCr_2Se_4$ has not been observed at 80K, the effect of exciton emission and other exciton effects are not possible either. The red shifts of the peak energy in Fig.2.5.3 points to stimulated emission of exciton-exciton collisions because it also has a red shift as the excitation increases[18]. We can still exclude this possibility because of the intensity dependence shown in Fig.2.5.4 for $CdCr_2Se_4$. Spontaneous exciton-exciton scattering emission increases quadratically[19] with the exciton density and a stimulated emission should have more than square dependence of the exciton density. At high excitation intensities, the densities of electrons and holes are proportional to the square root of excitation[20](see

Appendix 1). Therefore the luminescence intensity from electron-hole plasma should be linearly proportional to the excitation intensity which is shown in Fig.2.5.4.

The spontaneous emission spectrum of electron-hole plasma from eq.(2.2.1) is described[21] by either

$$I(h\nu) \propto (h\nu-\tilde{E}_g)^{1/2} \cdot f_e((h\nu-\tilde{E}_g)m_h/(m_e+m_h)) \times f_h((h\nu-\tilde{E}_g)m_e/(m_e+m_h)) \qquad (2.5.1)$$

for K-selection(direct gap transition), or from eq.(2.2.2) by

$$I(h\nu) \propto \int_0^{h\nu-\tilde{E}_g} E^{1/2}(h\nu-\tilde{E}_g-E)^{1/2} f_e(E) f_h(h\nu-\tilde{E}_g-E)\,dE \qquad (2.5.2)$$

for non-K-selection(indirect transition) for the degenerate distributions(the carrier temperature is 80K). $m_e=m_h=0.5m_0$ is assumed at present time. The carrier temperatures were extracted from the high energy tails of the emission curves when the excitation is less than 17 $GWcm^{-2}$,assuming that the carrier distributions are Maxwellian[4] and $I(h\nu) \propto \exp(-h\nu/kT_e)$. The distribution was nondegenerate below $10^{18}cm^{-3}$ for input power density of 17 $GWcm^{-2}$. For all the emission spectra of $CdCr_2Se_4$ for the high excitation intensity, the carrier temperatures were all close to the lattice temperature 80K. This is expected because of ultrafast recombination time of carriers $\leq$ 20 ps. The carrier density at highest excitation intensity($20GWcm^{-2}$) was chosen to be $\sim 1.25\times10^{18}cm^{-3}$ to fit the experimental data, the lower carrier density at

lower excitation intensity were accordingly determined. As shown in Fig.2.5.5, the theoretical curve for K-selection(direct gap transition) fits the experimental data well from 0.4 to 20 $GWcm^{-2}$ and the theoretical curve without K-selection(indirect transition) does not fit the data. The low energy side of the experimental data is not fitted by the curves because a perfect parabolic band without impurities is assumed for the theoretical curve. Therefore, $CdCr_2Se_4$ is a direct band gap semiconductor. Below 0.4 $GWcm^{-2}$, the high energy tails can be fitted by simple exponential $\propto \exp((h\nu-\tilde{E}_g)/kT_{carrier})$, indicating constant density of states within 20 mev from bandedge.

The reduced bandgap $\tilde{E}_g$, obtained by subtracting 0.0 $kT_{carrier}$ to 0.9 $kT_{carrier}$ from the peak energy of the emission spectrum[22], is plotted as a function of the carrier pair density n in Fig.2.5.6a. The error bar for $\tilde{E}_g$ is $\pm$ 4 mev. In Fig.2.5.6b, $E_g-\tilde{E}_g$ is plotted as a function $n^{1/3}$, where E_g is the gap energy of $CdCr_2Se_4$ at 80K and is equal to 1.804 ± 0.002 ev. $E_g-\tilde{E}_g$ increases linearly with $n^{1/3}$. The reduced gap $\tilde{E}_g$ is

$$\tilde{E}_g=E_g-(48\pm 4)10^{-6}(\text{mev.cm})n^{1/3}(\text{cm}^{-1}) \qquad (2.5.3)$$

The many body Coulomb effect[23-25] among photogenerated free carriers causes the red shift of the luminescence from $CdCr_2Se_4$. According to the theory of Rice[26], the lowering of the bandgap is equal to

(in unit of $\mu e^4/2k^2\hbar^2$):

$$E_{exchange}+E_{correlation}+n\frac{\partial}{\partial n}(E_{exchange}+E_{correlation}) \quad (2.5.4)$$

For an ideal parabolic band shape, the reduction of bandgap is

$$E_g-\widetilde{E}_g=+1.6e^2/k.n^{1/3}=+21.8/k.10^{-5}(mev.cm)x \; n^{1/3}(cm^{-1}) \quad (2.5.5)$$

where k is the static dielectric constant of the semiconductor, $E_{exchange}=-1.832/r_s$, and $E_{correlation}=0.497lnr_s-0.33$ for equal masses of electrons and holes, $n=3/(4\pi r_s^3 a_x^3)$, a_x is the exciton Bohr radius($=kh^2/\mu e^2$), and μ is the reduced mass. If $CdCr_2Se_4$ has an ideal parabolic band, then $k=(4.8\pm0.4)$. This value is about two times smaller than the calculation by Itoh et al[27]. for the real part $\varepsilon_1(\sim9)$ of dielectric constant at 1.8 ev. This difference may be due to the assumption of $m_e=m_h=0.5m_0$. When the values of m_e and m_h change, the carrier density will change and the k value will be adjusted. The correlation energy $E_{correlation}$ can be different from the above value and can affect the result of $E_g-\widetilde{E}_g$, this also may account for the difference in k.

As discussed by Rice[26], the temperature dependence of the reduced bandgap energy can be neglected as long as the thermal erergy is small compared with the plasma energy. The thermal energy is $\sim$ 7 mev at 80K which is much smaller than

the plasmon energy($\sim$20 mev) at $\sim 10^{18}cm^{-3}$ for $m_e=m_h=0.5m_0$. Therefore the temperature effect on the reduced bandgap is small for the carrier temperature(80K) and the carrier density($\sim 10^{18}cm^{-3}$). However the thermal effect on the reduced bandgap could be finite at low carrier density($\leq 3x10^{17}$ cm^{-3}) and $\tilde{E}_g$ becomes smaller compared with that at lower temperature than 80K.

Brinkman and Rice theory[28,29] for the electron-hole plasma in GaAs estimated the reduced bandgap energy $\tilde{E}_g$ as

$$\tilde{E}_g=E_g-0.01ev(n/10^{17})^{1/3}=E_g-21x10^{-6}(mev.cm)x \; n^{1/3}(cm^{-1}) \quad (2.5.6)$$

for $n \geq 5x10^{16}cm^{-3}$. Comparing with GaAs, $CdCr_2Se_4$ gives similar experimental results to GaAs. From the above analysis, it is obvious that the reduction of the bandgap is related to the optically generated electron-hole plasma.

In conclusion of this section, the electron-hole plasma can be generated in $CdCr_2Se_4$ under high power picosecond laser excitations which affects the band structures. The bandgap renormalizes as a function of the photogenerated carrier density. The good fitting of the spectral shape by a theoretical expression for electron-hole plasma indicates that $CdCr_2Se_4$ is a direct gap semiconductor.

References of Chapter 2:

1. T. Kambara, T. Oguchi, and K. I. Gondaira, J. of Phys. c13,1493(1980).
2. T. Oguchi, T. Kambara, and K. I. Gondaira, Phys. Rev. B22,872(1980).
3. V. G. Veselago, I. A. Damaskin, S. L. Pyshkin, S. I. Radautsan, and V. E. Tezlevan, JETP Lett. 20,149(1975).
4. J. Shah and R. C. C. Leite, Phys. Rev. Lett. 24,1304(1969).
5. S. Sugano, Y. Tanabe, H. Kamimura, Multiplets of Transition Metal Ions in Crystals(Academic Press, New York, 1970).
6. G. Harbeke and H. Pinch, Phys. Rev. Lett. 17,1090(1966).
7. W. Nolting and A. M. Olés, Phys. Rev. B22, 6184(1980).
8. W. J. Miniscalco , B. C. McCollum, N. G. Stoffel and G. Margaritondo, Phys. Rev. B25, 2947(1982).
9. Rys, J. S. Helman, and W. Baltensperger, Physik Kondensierten Materie, 6,105(1967).
10. C. Haas, Phys. Rev. 168,531(1968).
11. K. Kubo, J. of the Phys. Soc. of Japan, 36,32(1974).
12. J. F. Figueria and H. Mahr, Phys. Rev. B7,4520(1973).
13. A. Mooradian and H.Y. Fan, Phys. Rev. 147,873(1966).
14. L. M. Roth, B. Lax, and S. Zwerdling, Phys. Rev. 114, 90 (1959).
15. K. Kubo and N. Ohata, J. Phys. Soc. of Japan,33,21(1972).
16. A. Yanase and T. Kasuya, J. Phys. Soc. of Japan, 25,1025

(1968).

17. S. S. Yao, F. Pellegrino, R. R.Alfano, W. J. Miniscalco, and A. Lempicki, Phys. Rev. Lett. 46,558(1981).

18. T. Moriya and T. Kushida, J. Phys. Soc. of Japan, 40,1676 (1976).

19. T. Moriya and T. Kushida, J. Phys. Soc. Japan, 40,1668 (1976).

20. C. Benoit a La Guillaume, J. M. Debever, and F. Salvan, Phys. Rev. 177,567(1969).

21. Y, Yoshikumi, H. Saito, and S. Shionoya, Sol. St. Comm. 24,833(1977).

22. Since $I(h\nu) \propto (h\nu-\tilde{E}_g)^{1/2} \cdot f_e \cdot f_h$, $dI(h\nu)/d(h\nu)=0$ and $m_e=m_h=0.5m_0$ implies that $1+\exp(1/2x-\mu)-2x.\exp(1/2x-\mu)=0$, where $x=(h\nu-\tilde{E}_g)/kT_{carrier}$, and $\mu=\mu_e/kT_{carrier}=\mu_h/kT_{carrier}$, μ_e and μ_h are the chemical potentials of electrons and holes, respectively. At highest density $n=1.25\times10^{18}cm^{-3}$, $\mu=0.4$ and $x=0.9$. At lower density $\leq 10^{18}cm^{-3}$, x is close to 0.5.

23. M. Hayashi, H. Saito, and S. Shionoya, Sol. St. Comm. 24, 833(1977).

24. O. Hildebrand, E. O. Groebel, K. M. Romanack, H. Weber, and G. Mahler, Phys. Rev. B17,4775(1978).

25. K. Arya and W. Hanke, Phys. Rev. B23,2988(1981).

26. T. M. Rice, The Electron-Hole Liquid in Semiconductors,

Theoretical Aspects, p37 and p44, in Solid State Physics, Vol.32, edited by H. Ehrenreich, F. Seitz, and D. Turnbull(Academic Press, NY, 1977).

27. T. Itoh, N. Miyata, and S. Narita, Japan. J. Appl. Phys. 12, 1265(1975).
28. W. F. Brinkman and T. M. Rice, Phys. Rev. B7,1508(1973).
29. J. Shah, R. F. Leheny, and C. Lin, Sol. St. Comm. 18,1035 (1976).

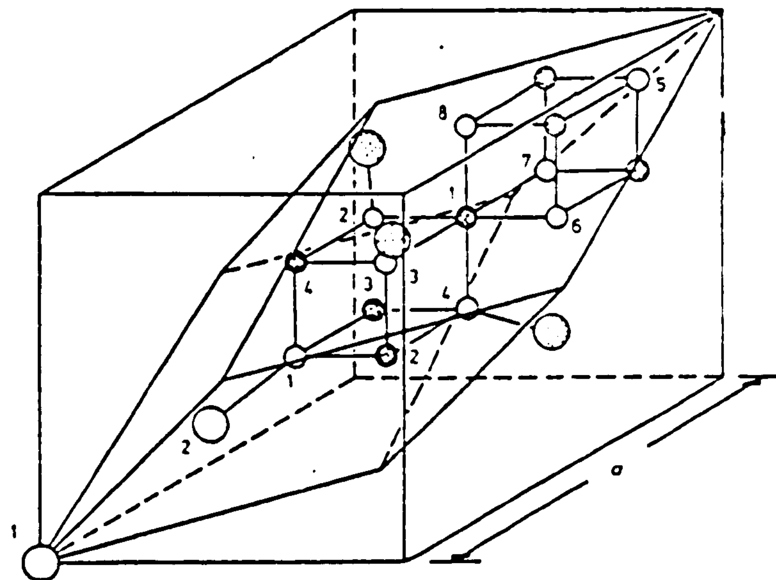

Crystal structure of spinel. Large open and large flecked circles are Cd, full and small flecked circles are Cr and small open circles are S or Se. The numbers on the circles represents the site numbers in table 3. The flecked circles are outside the primitive unit cell.

(ref. 1)

Fig. 2.1.1

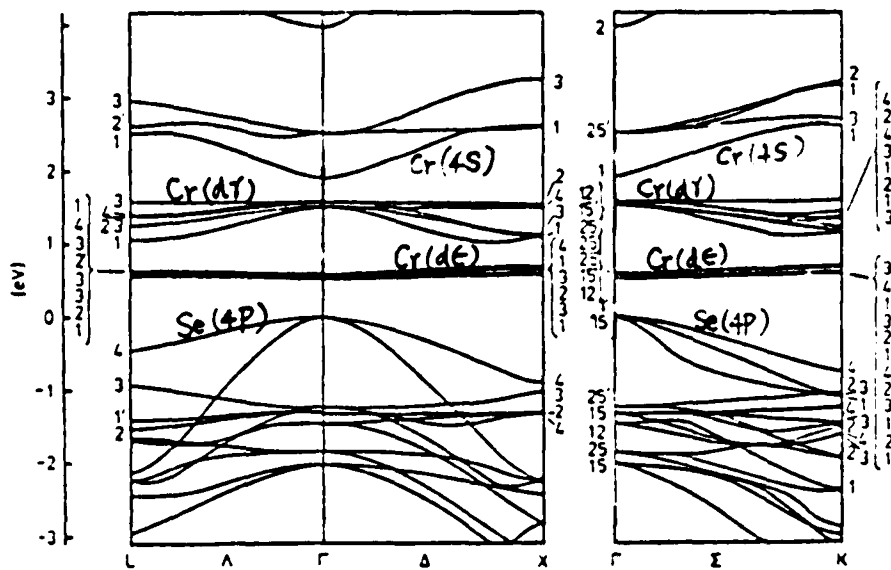

Calculated band structure of the paramagnetic $CdCr_2Se_4$ on the symmetry lines Γ-Λ-L, Γ-Δ-X and Γ-Σ-K. (ref. 1)

Fig.2.1.2

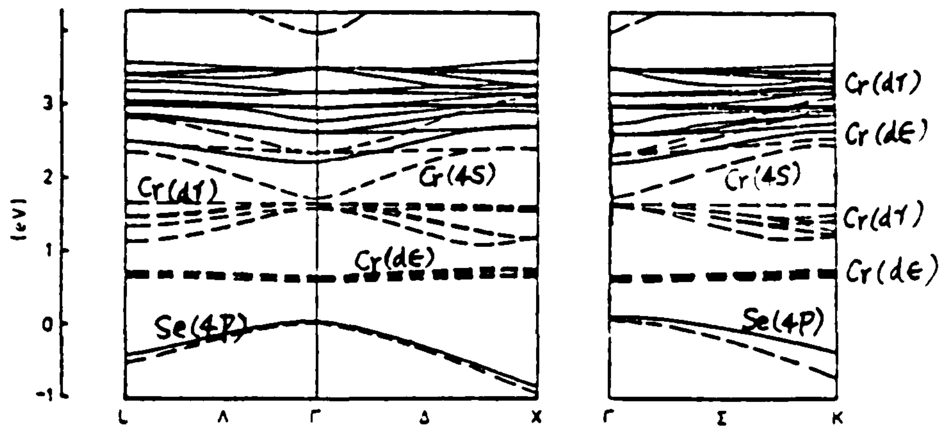

Calculated band structure of the ferromagnetic $CdCr_2Se_4$ on the symmetry lines Γ-Λ-L, Γ-Δ-X and Γ-Σ-K. The broken and full curves represent the energy band for the majority and minority spins respectively. The valence bands, except for the top band, are omitted. (ref.1)

Fig.2.1.3

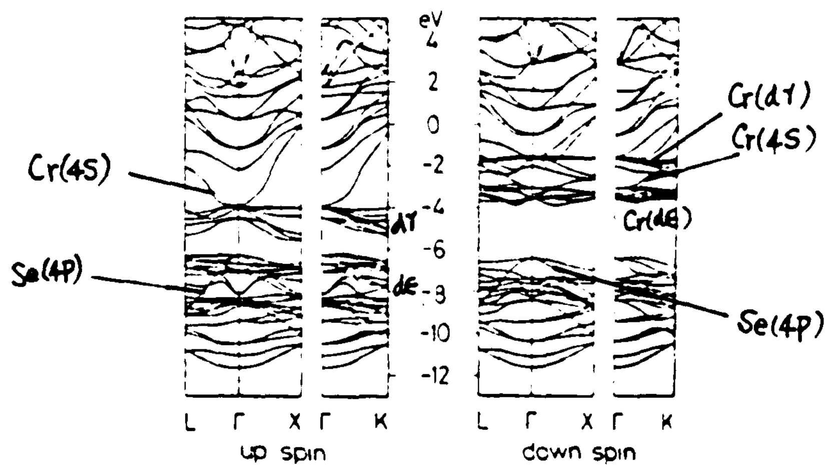

Calculated band structure of $CdCr_2Se_4$.

(ref.2)

Fig.2.1.4

LUMINESCENCE SETUP

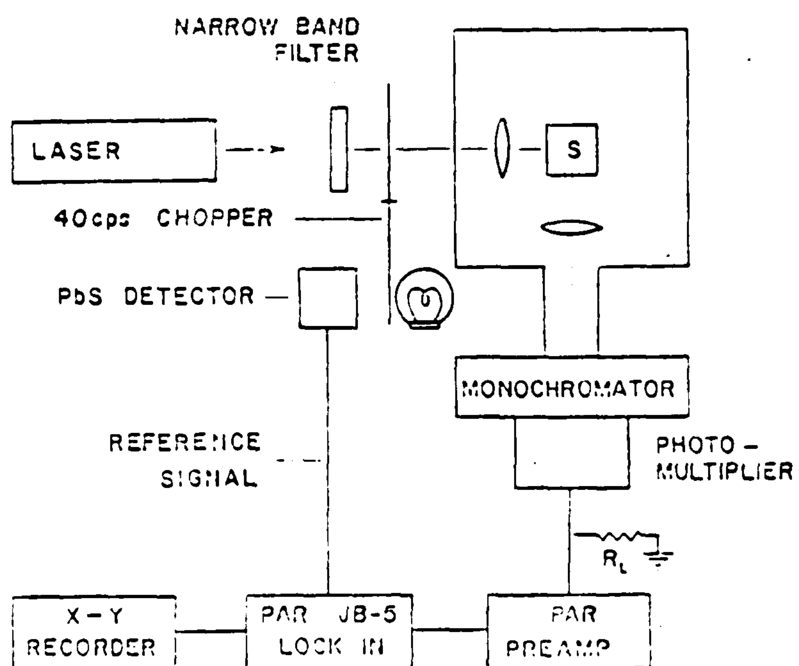

Fig.2.2.1

Fig.2.2.2

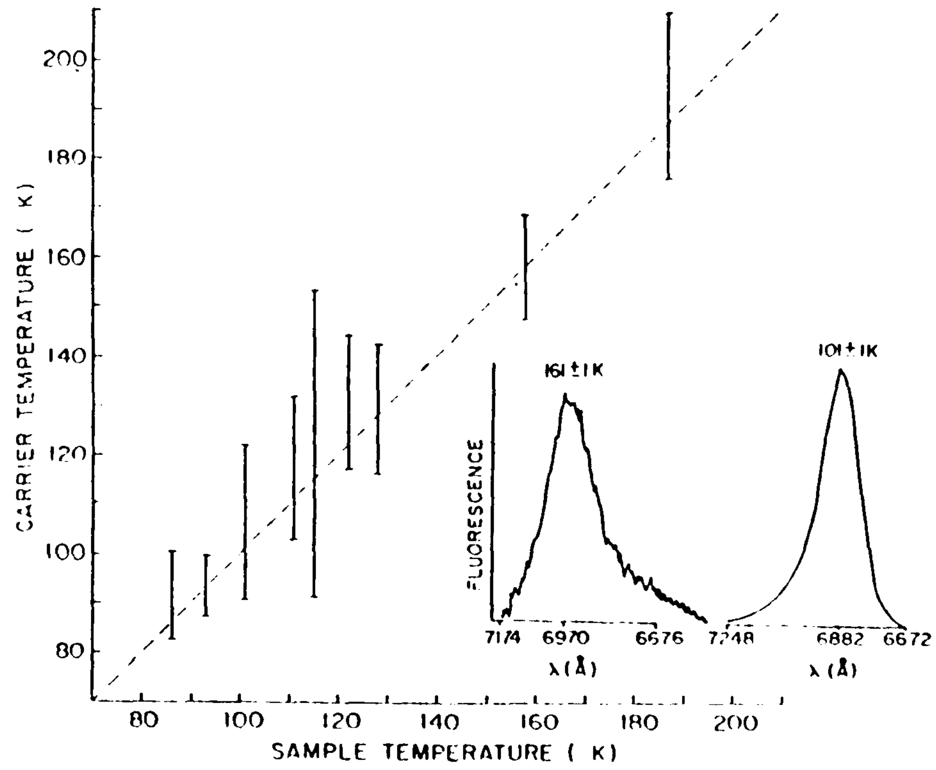

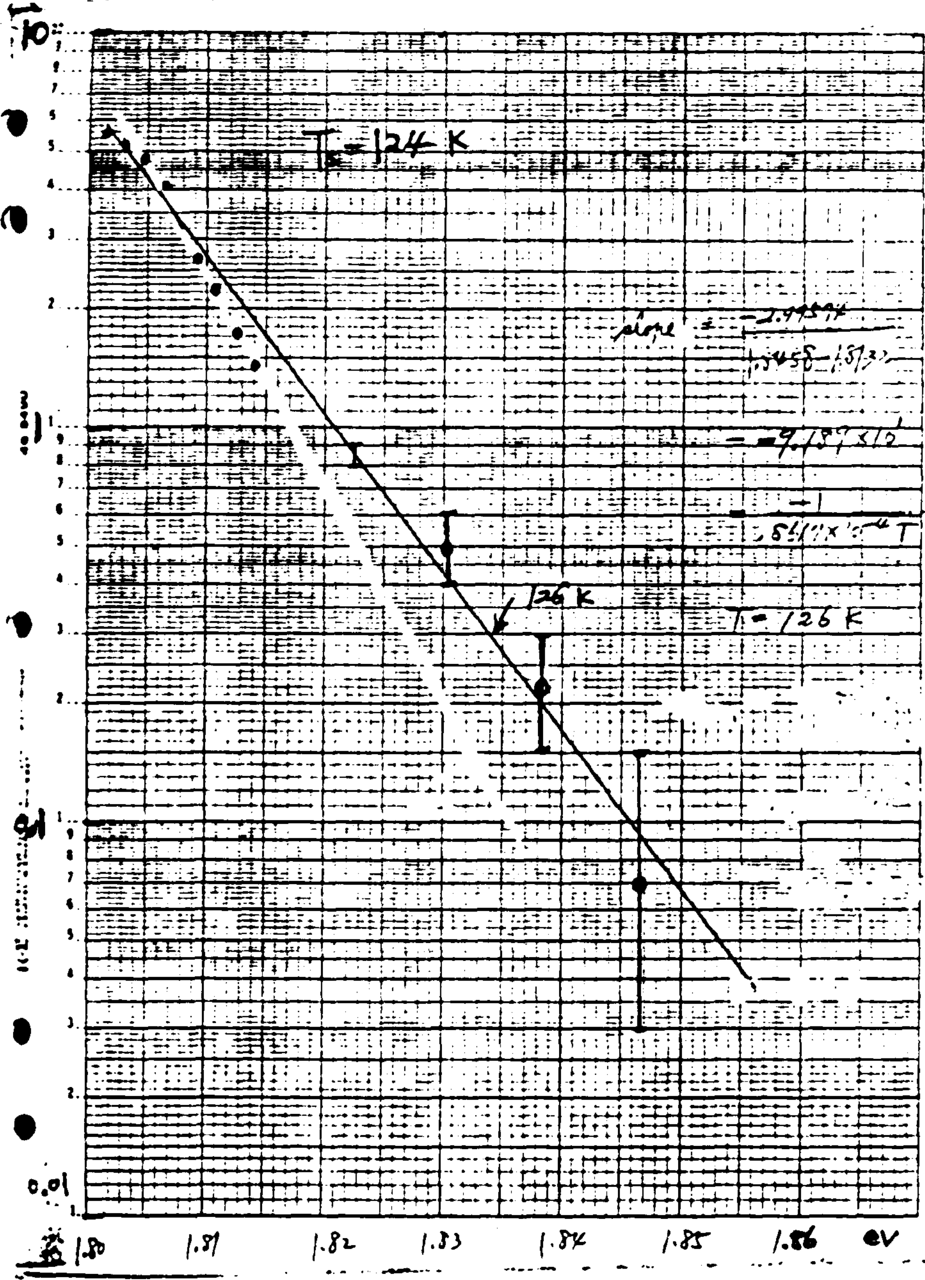

Fig.2.2.3

Fig.2.2.4

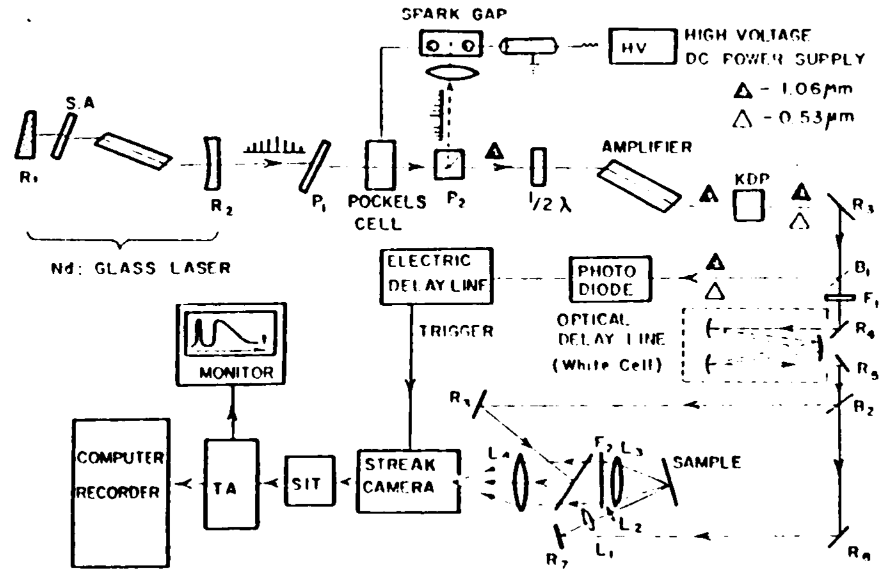

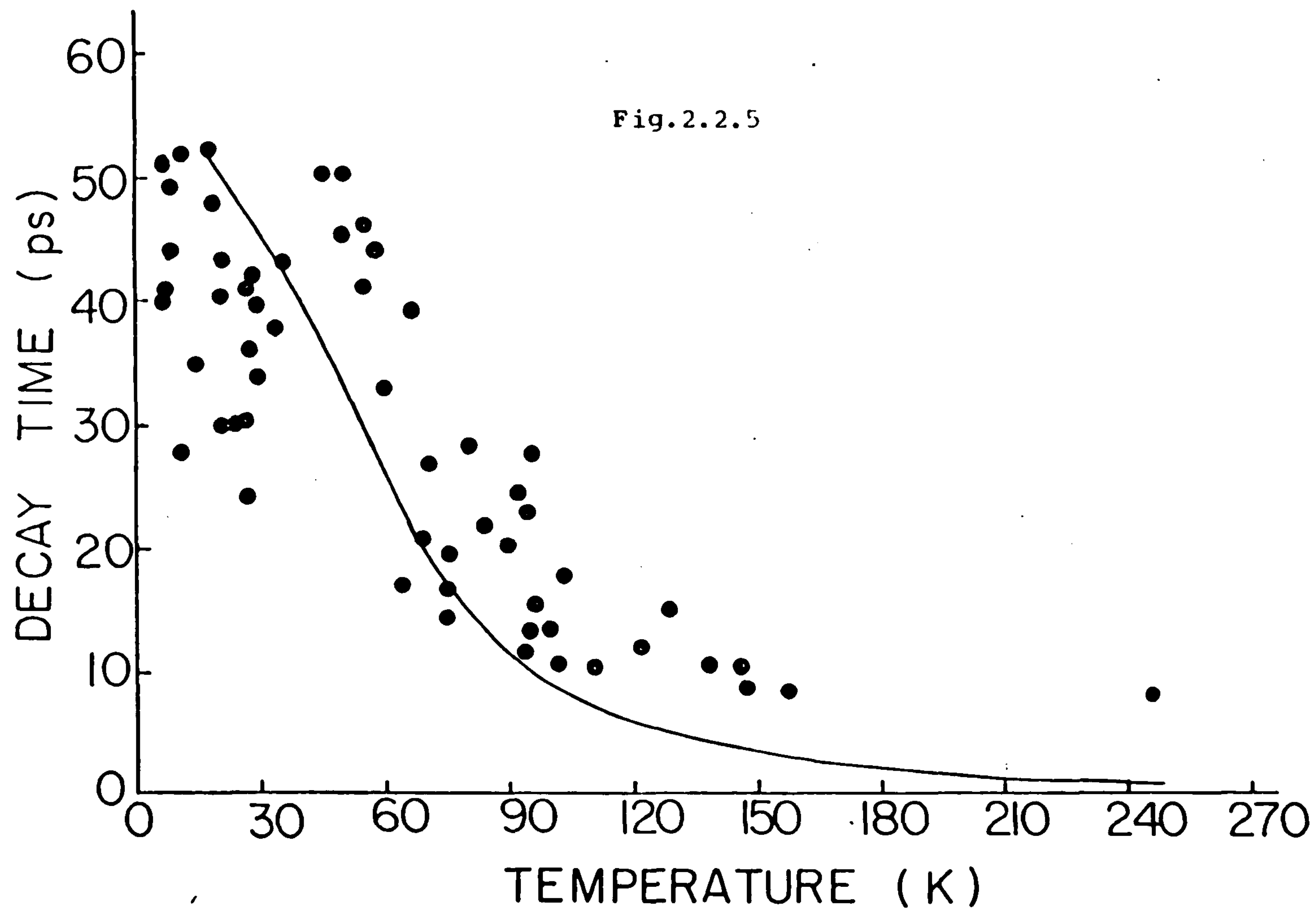
Fig.2.2.5
DECAY TIME (ps)
TEMPERATURE (K)
0
10
20
30
40
50
60
0
30
60
90
120
150
180
210
240
270

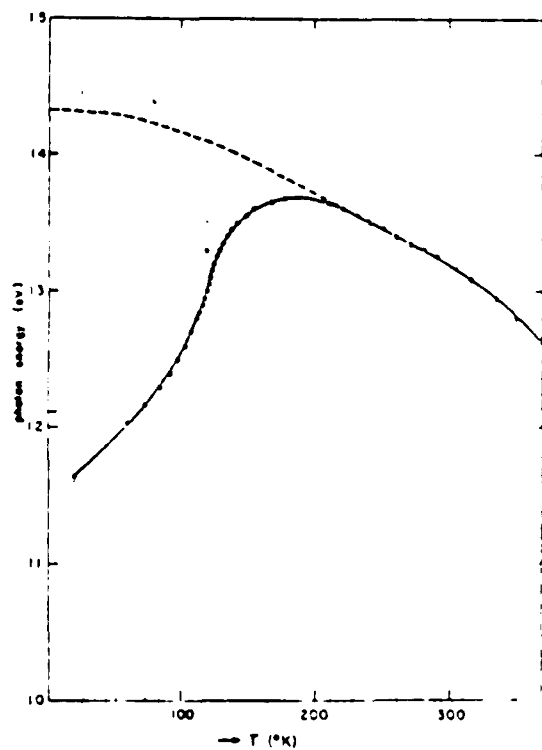

Absorp. edge of $CdCr_2Se_4$ versus temperature.
Dashed line: assumed extrapolation for paramagnetic state.

(**ref.6**)

Fig.2.2.6

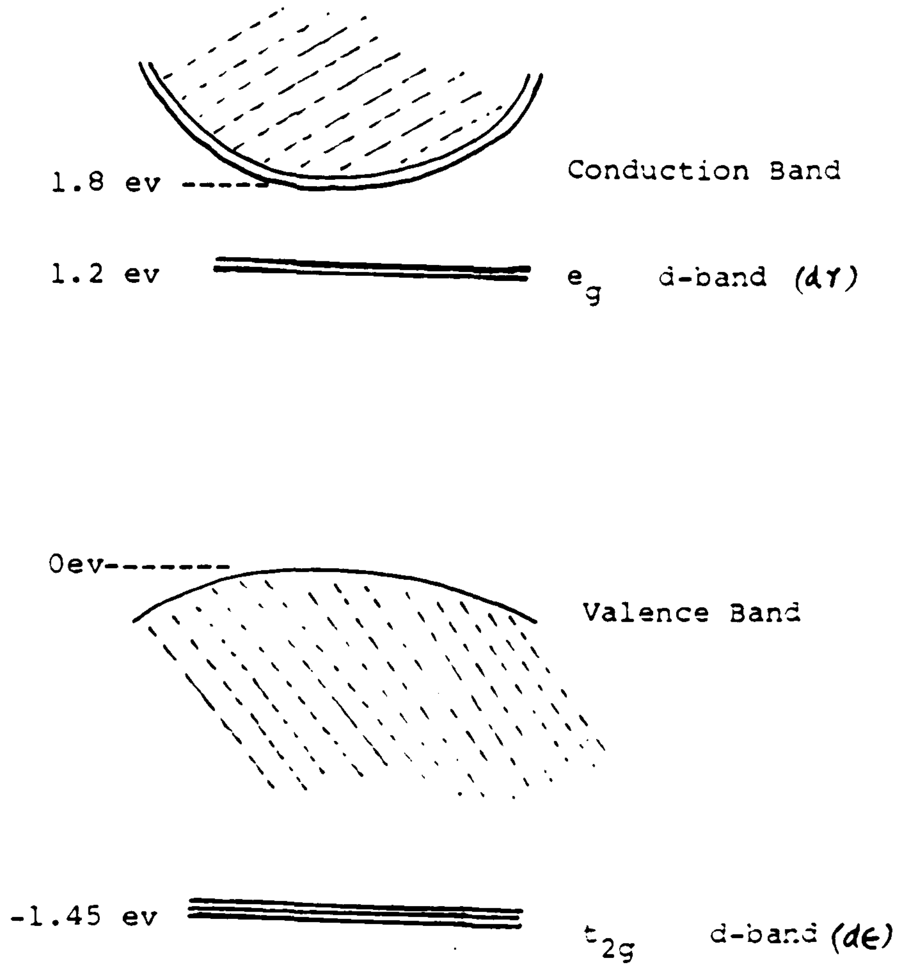

Fig.2.2.7

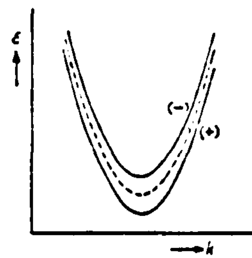

Splitting of the conduction band into sub-bands for spin parallel (+) and antiparallel (−) to the magnetization. - - -, band in paramagnetic region; ——, sub-bands in ferromagnetic region.
(ref. 10)

Fig.2.3.1

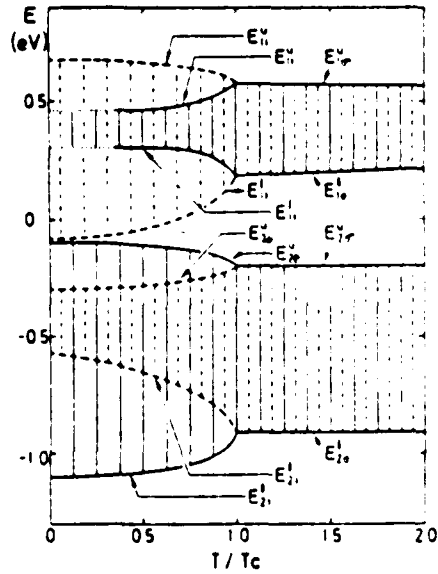

Lower (l) and upper (u) edges of the quasi-particle subbands as functions of the reduced temperature T/T_c; parameters from Eq. (4.1); solid lines for ↑ subbands and broken lines for ↓ subbands.

(ref.7)

Fig.2.3.2

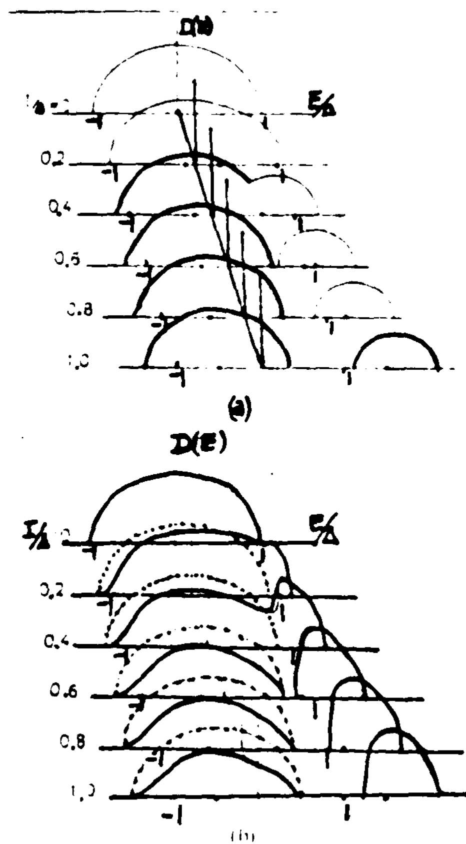

(a) The density of states curves in the paramagnetic state for $S=1/2$. The points on the energy axes indicate $-IS$ and $I(S+1)$, the energy levels of an electron coupled with a localized spin.
(b) The density of states curves in the completely ferromagnetic states for $S=1/2$. The solid lines show down-spin states and the dashed ones up-spin states.

Δ is the width of conduction band.

Fig.2.3.3

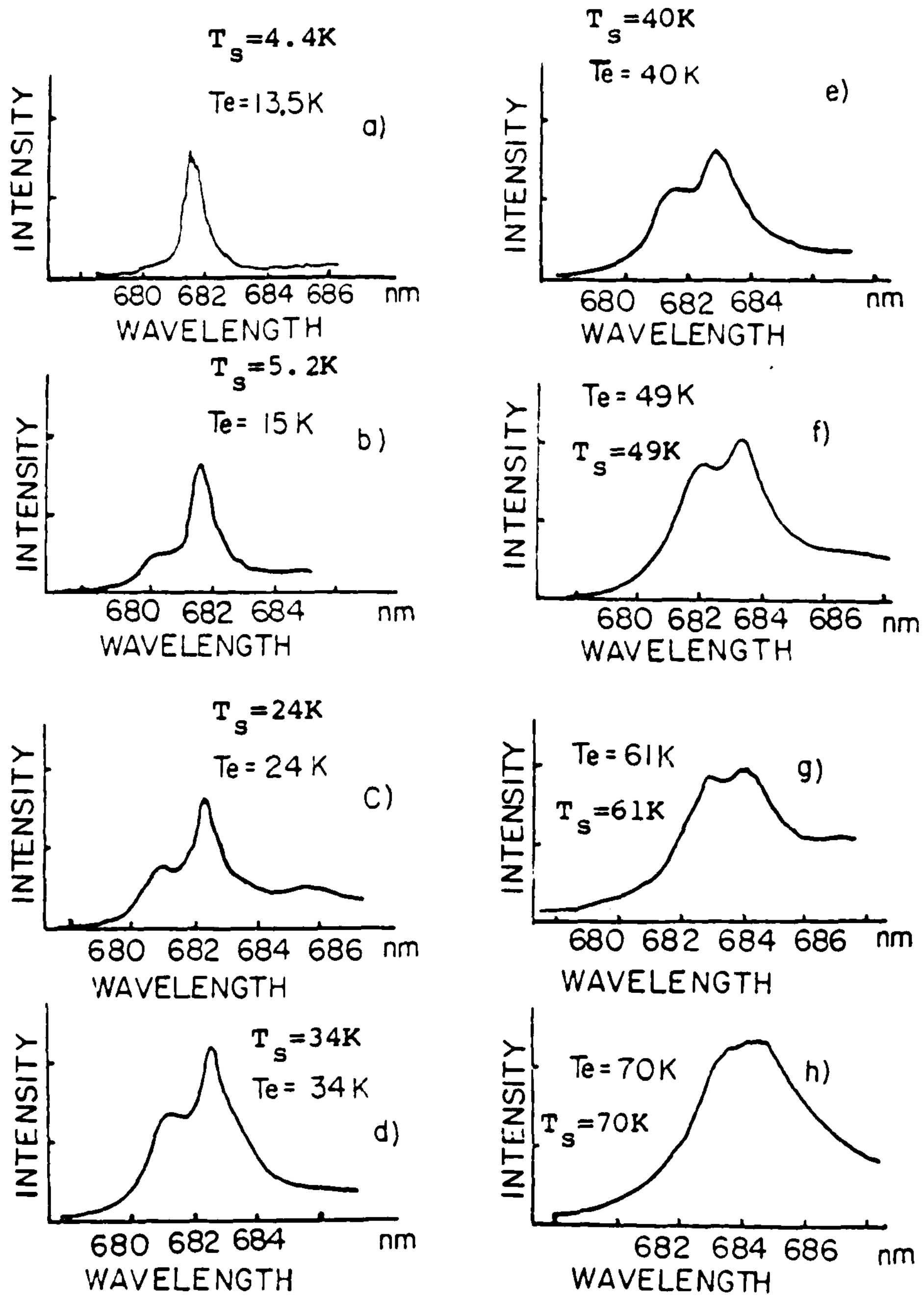

Fig.2.3.4

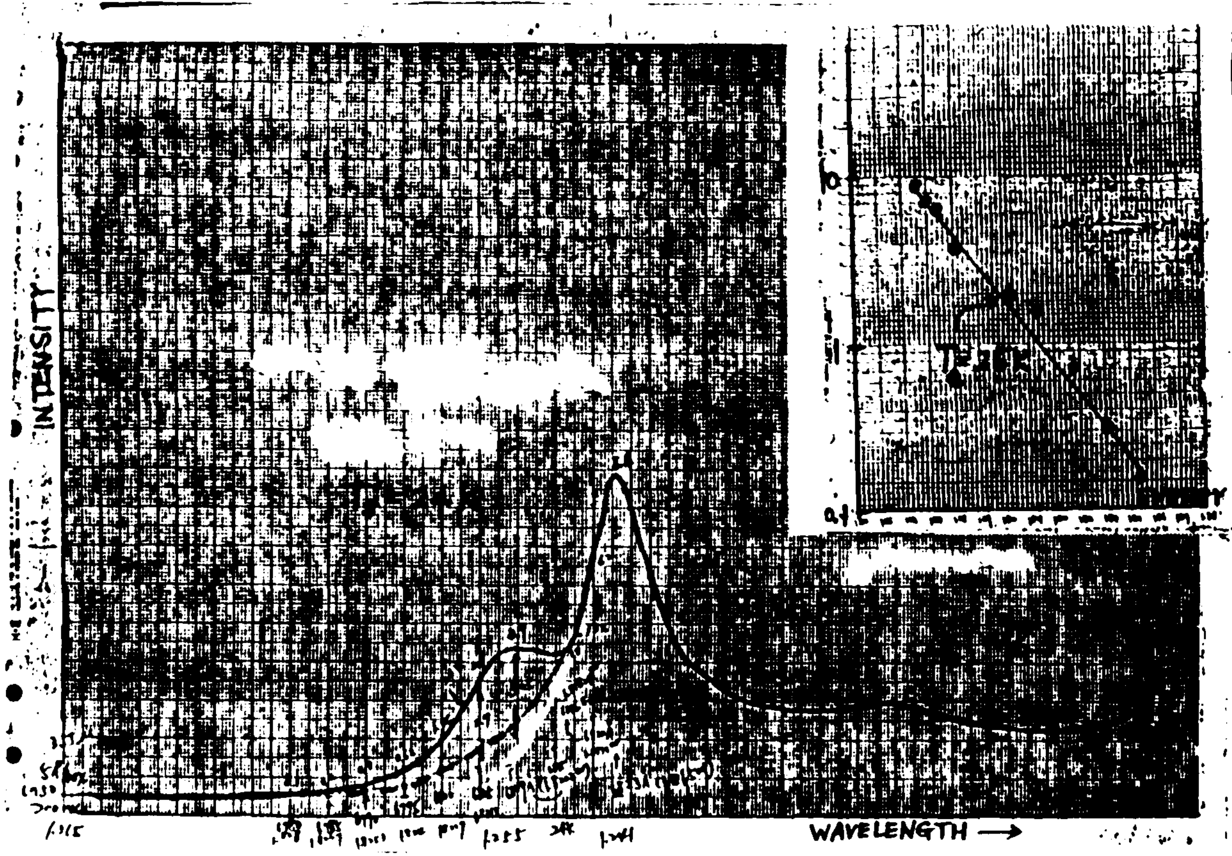

Fig.2.3.5

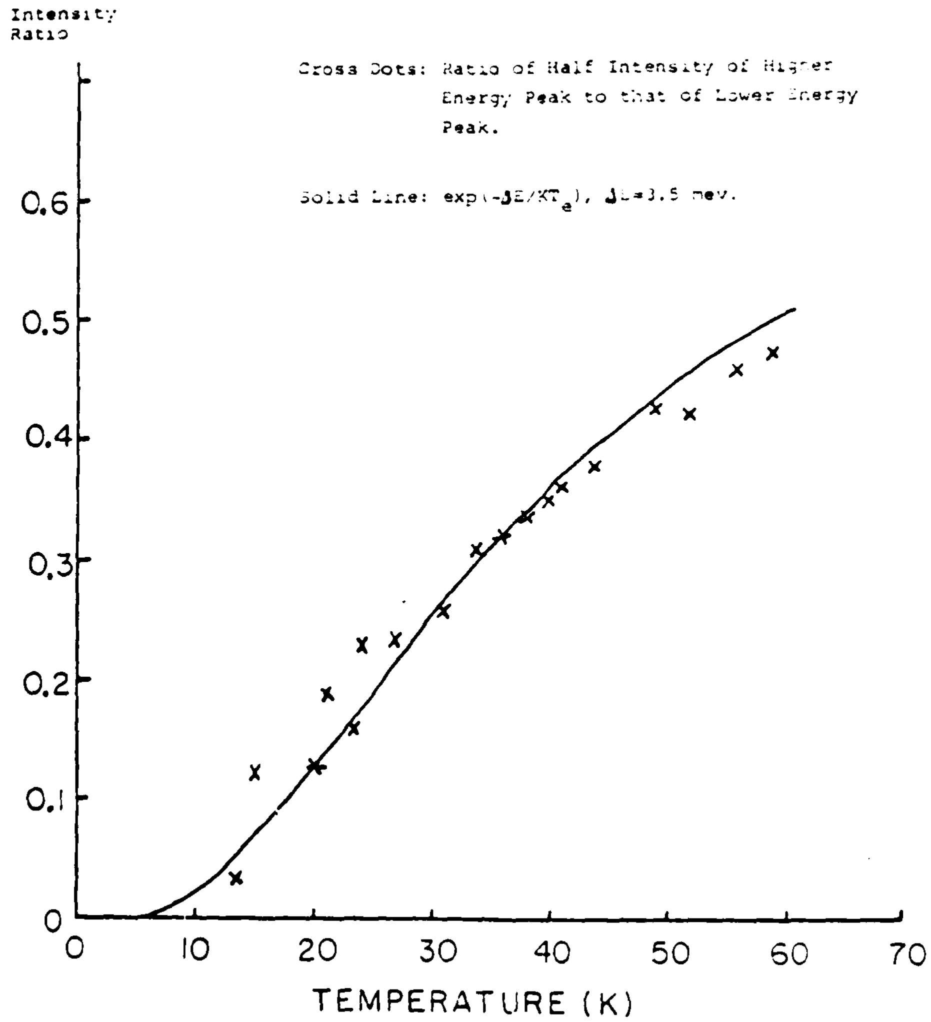

Fig.2.3.6

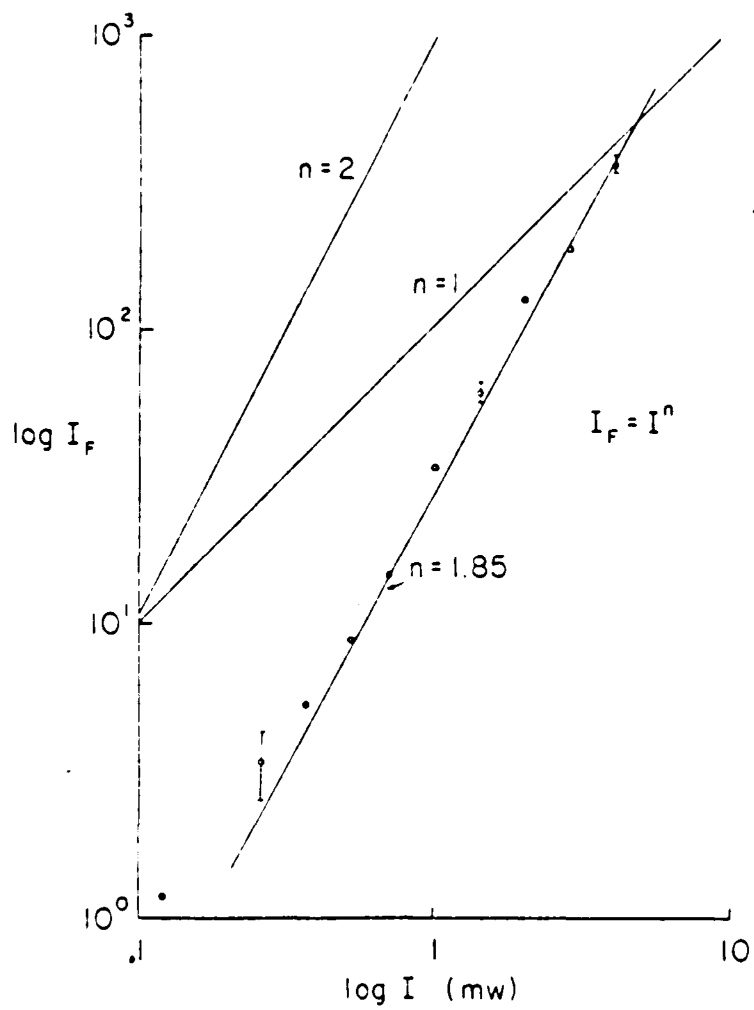

Fig.2.4.1

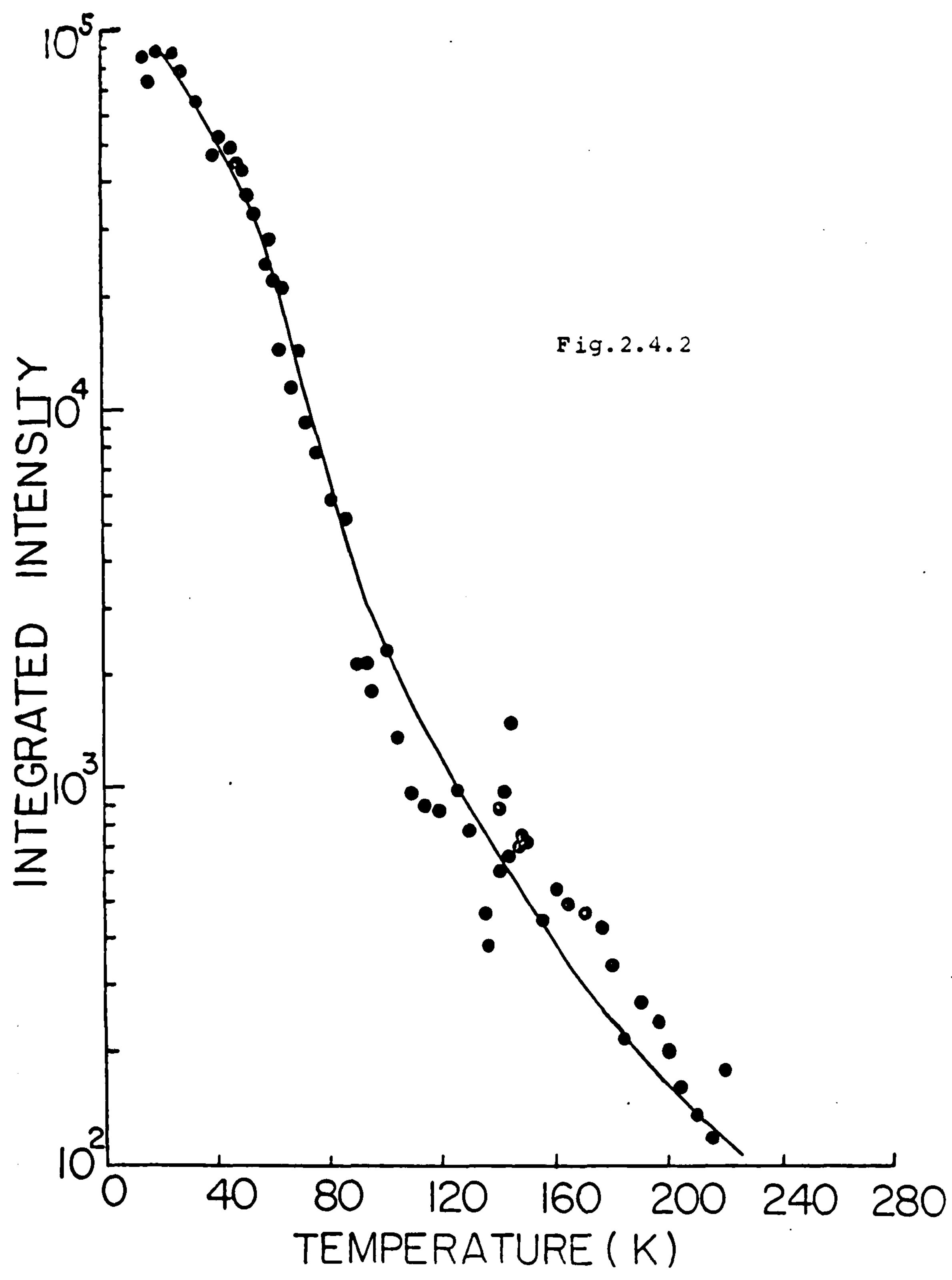

Fig.2.4.2

Fig.2.5.1

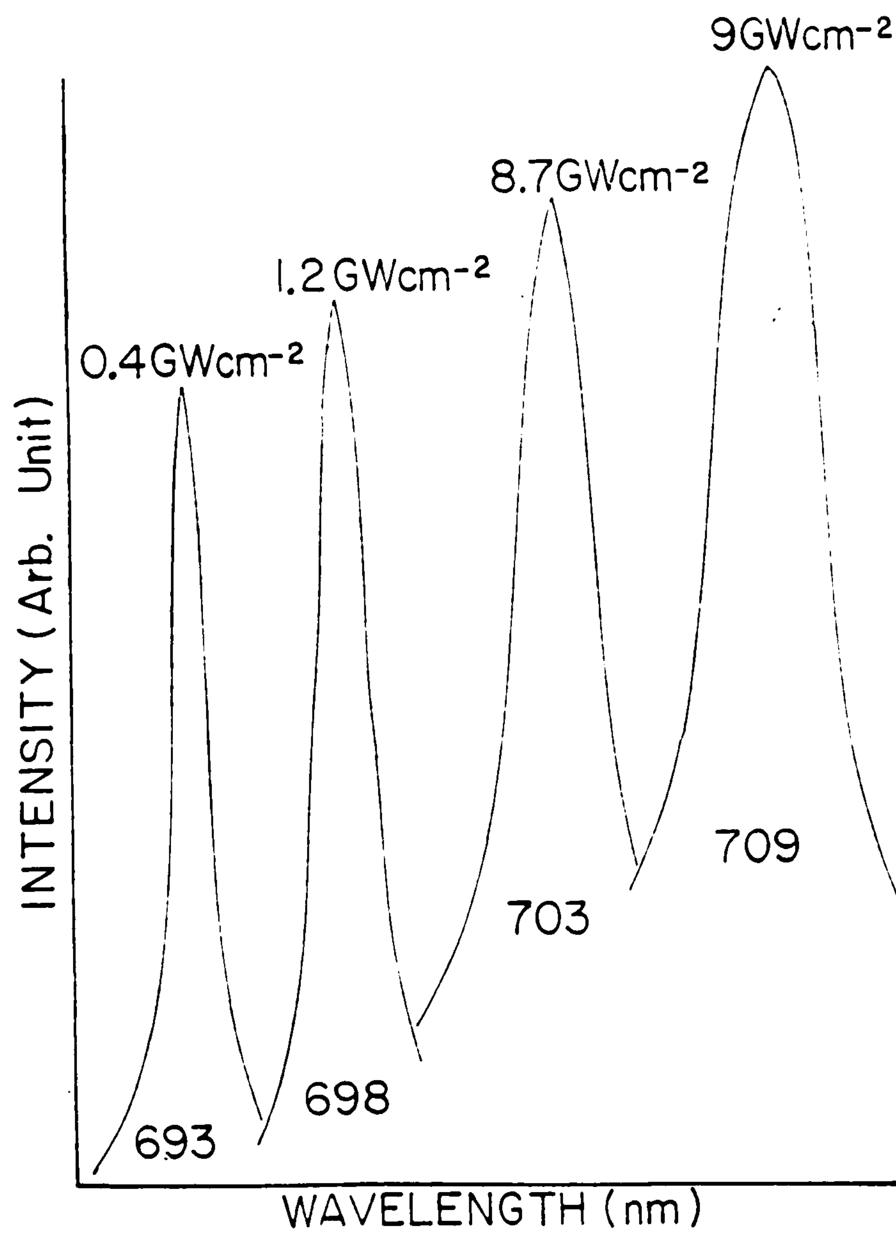

Fig.2.5.2

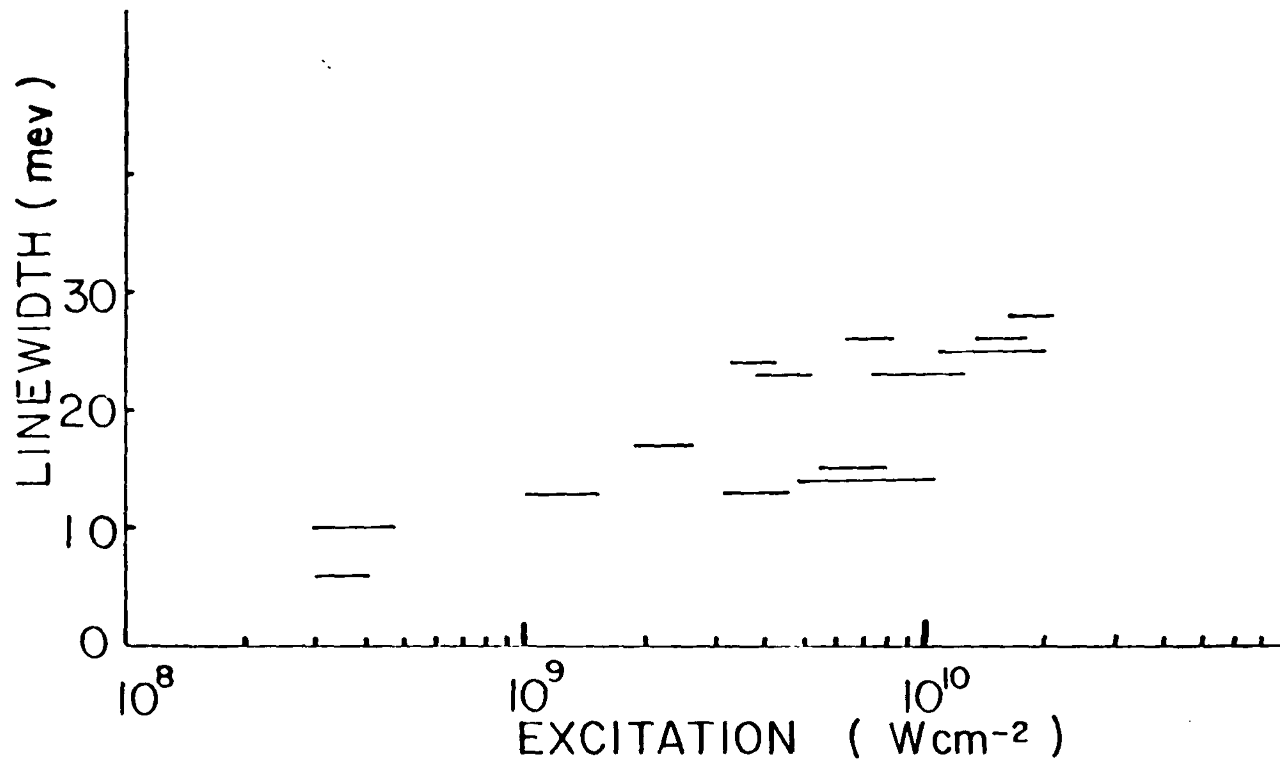

Fig.2.5.3

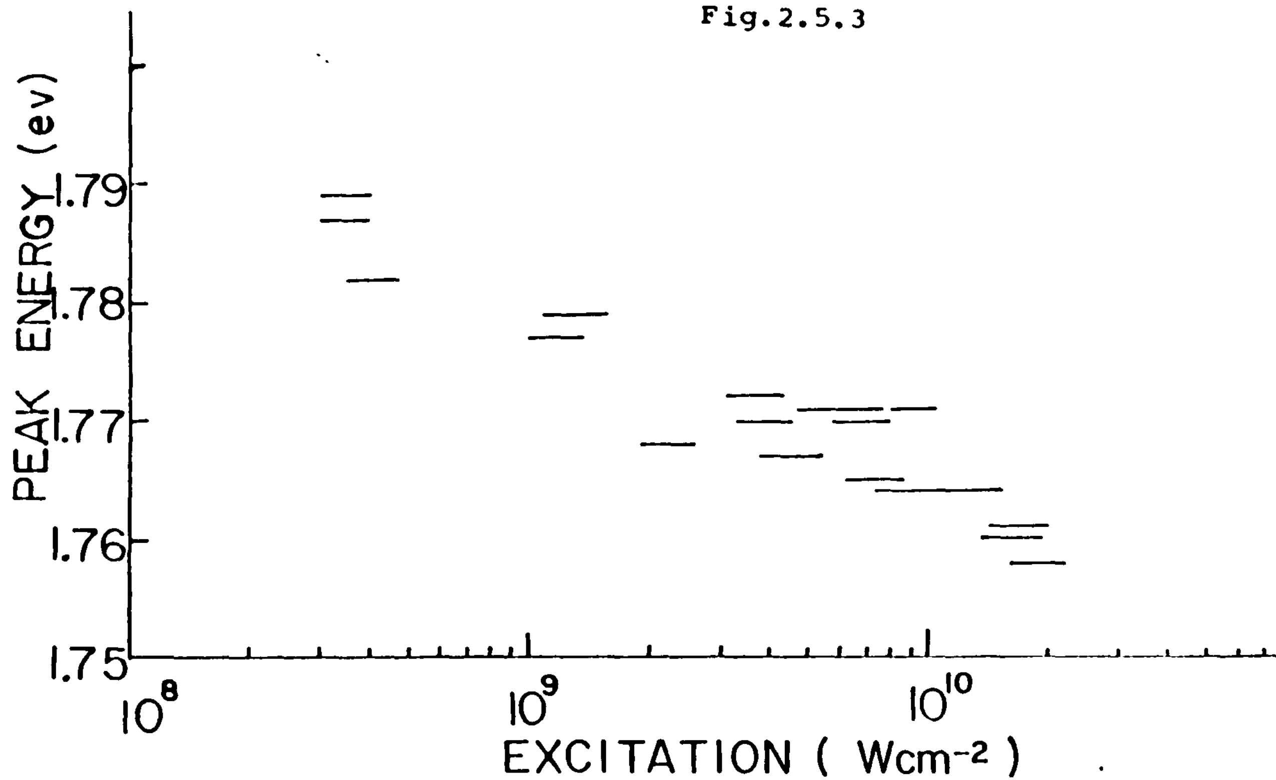

Fig.2.5.4

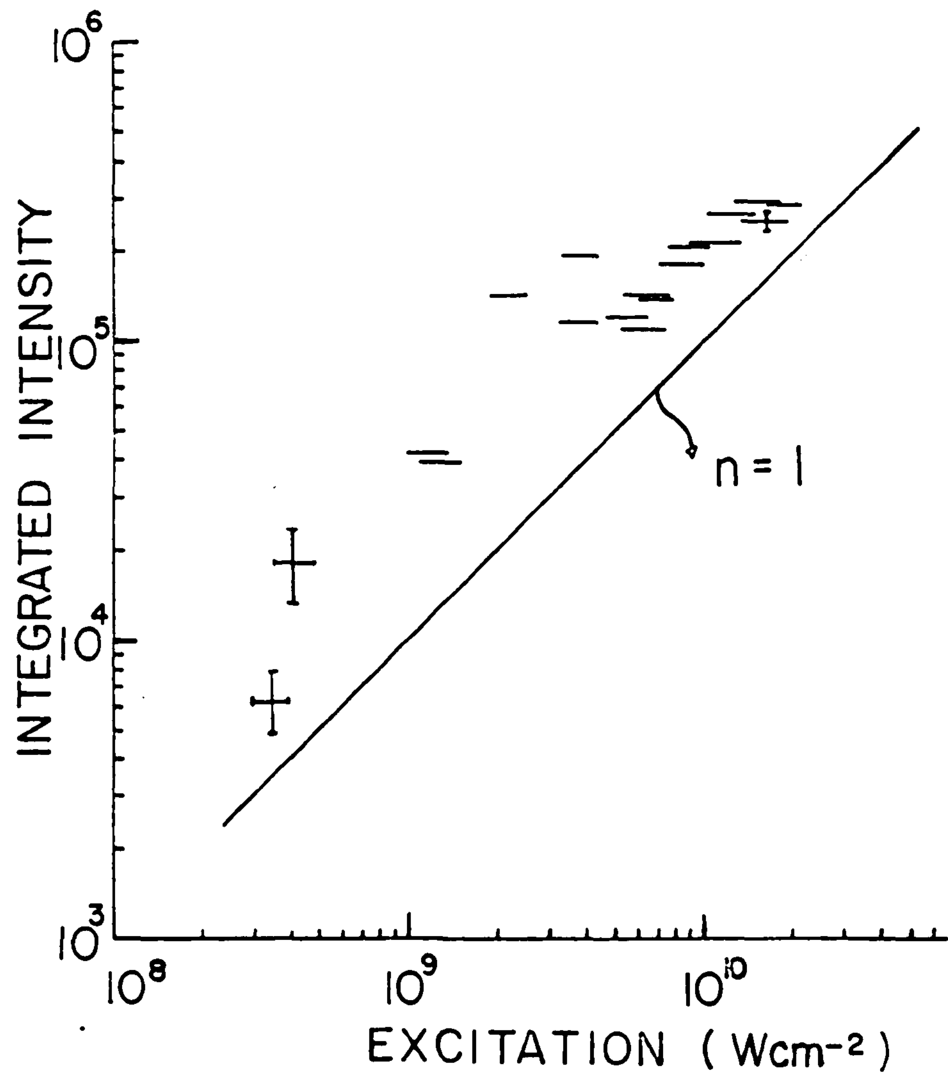

Fig.2.5.5

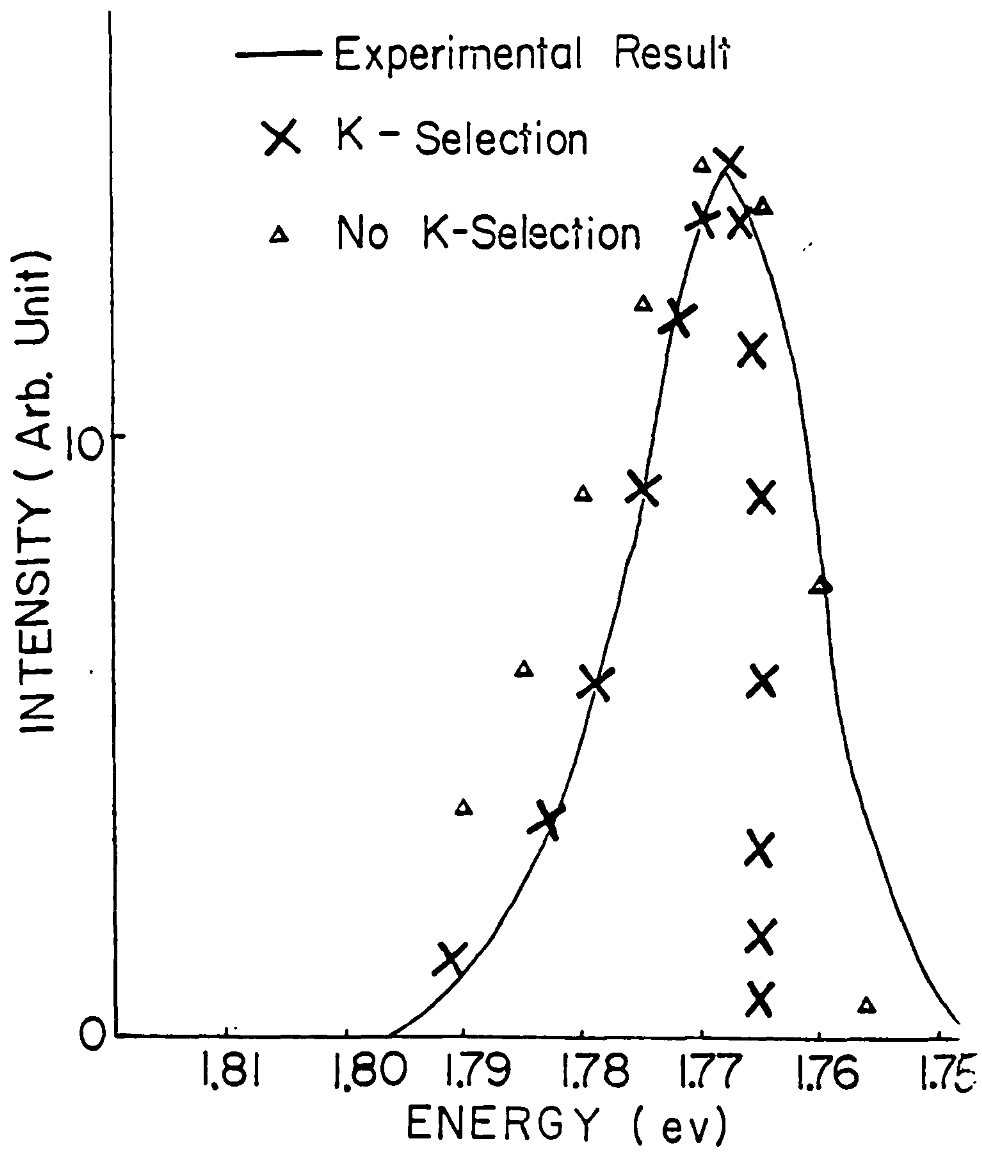

Fig.2.5.6

a)

REDUCED BANDGAP (ev)

1.75
1.76
1.77
1.78
1.79

10^{16}
10^{17}
10^{18}

CARRIER DENSITY (cm^{-3})

b)

$E_g - \tilde{E}_g$ (mev)

0
10
20
30
40
50

0
5
10
X10^5

$n^{1/3}$ (cm^{-1})

Chapter 3: Gallium Selenide(GaSe)

3.1 The determination of the dominant relaxation process for the hot photogenerated carriers in GaSe.

3.1.1 The crystal structure and the calculated electronic energy diagrams.

The sample GaSe is a layered semiconductor. The crystal structure[1] is shown in Fig.3.1.1. The layers in GaSe consist of four close-packed monoatomic sheets, each in the sequence Se-Ga-Ga-Se. The bonding between adjacent layers is predominantly of the van der Waals type; the intralayer bonding is covalent with some ionic contribution. Three different modifications β, ϵ, and γ are known to exist. They are characterized by different stacking sequences[2] of the fourfold layers as shown in Fig.3.1.2. The distance between two intralayer Ga ions is ~ 2 Å, that between the intralayer Ga-Se ions is 2.5 Å. Each unit cell extends over two layers and consists of four Se and four Ga atoms.

Schlueter[1] had calculated the electronic energy bands of β-GaSe. The sample used in this experiment is ϵ-GaSe under the X-ray test by Dr. J. C. Irwin. The simplified structure of the lowest conduction band and the highest valence band is shown in Fig.3.1.3. The lowest conduction band lies at M point, and the highest valence band is at Γ point and it is nondegenerate. Therefore this semiconductor is an indirect gap semiconductor. However some physicists believed that the direct conduction band at Γ point is lower

than the indirect conduction at M point by ~ 20 mev.

From the calculation by Schlueter, the charge densities of highest valence band electrons are near the two Ga atoms and each Se atom as shown in Fig.3.1.4. For nonlayered semiconductors, the valence electrons(or holes) are more localized around the anions(or negative ions). For this layered semiconductor GaSe, the valence electrons are not only around each Se ion(or anion) but also around the two Ga ions(or cations). The charge distribution of this band suggests that holes in the valence band will strongly couple to phonons involving vibrations which change the Ga-Ga bond length[2,3].

3.1.2 Time resolved absorption spectroscopy of GaSe

It will be interesting to know how the hot photogenerated carriers relax to the sample temperature after they are generated in a layered semiconductor. The emissions of nonpolar optical phonons $A_1'^{(1)}$ which are vibrating [3] between the two Ga atoms from hot carriers are expected to be the dominant relaxation process due to the strong interaction between $A_1'^{(1)}$ phonons and holes in GaSe. The deformation potential between holes and polar optical phonons[1] is calculated to be 0.8 ev/Å which is much smaller than that(5.8 ev/Å) between holes and nonpolar optical phonons $A_1'^{(1)}$. In order to test the above assumption, the following time resolved absorption was measured.

As shown in Fig.3.1.5, the second harmonic at 530 nm of a Nd:glass laser pulse of 10 ps duration at 1.06 μ is used as a pump pulse, the laser pulse of continuous wavelength from 400 nm to 800 nm is used as a probe pulse. This probe pulse is generated by passing a Nd:glass laser pulse at 1.06μ through a CCl_4 cell and the intensity of this probe pulse is about 100 times smaller than that of the pump pulse(800 μj). The relative time difference between the pump and probe pulse is controlled by a prism. The probe pulse is divided into two beams: one is above the sample and the other is through the sample. The probe beams are collected by a spectrometer, detected by a TV system, and analyzed by a Hamamatsu temporal analyzer and a PDP 10 computer.

The absorption spectra at different time delays from -30 ps to 250 ps are displayed in Fig.3.1.6. Each curve was obtained from the average of three curves at the same excitation intensity. The absorption constant at 620 nm which is near the direct bandgap energy decreases from 2.1 OD to ~1.6 OD when the delay time changes from -30 ps to 150 ps, and increases back to the original value 2.1 OD after 150 ps. The background absorption above 630 nm which is below the bandgap energy is 1.5 OD(~97%). This indicates that only 3 % of the incident light intensity can be absorbed to create the electron-hole pairs. The absorption is mainly from the transition between the highest valence

band and the direct conduction band, the transition to the indirect conduction band is weak and can be neglected compared with the direct bandgap transition[4]. The carrier density generated optically can be estimated to be $\sim 7\times10^{18}$ cm^{-3} using the pulse energy($\sim$800μj), the absorption percentage($\sim$3%), the absorption constant($2\times10^{3}cm^{-1}$ when $\vec{E}\perp$C axis)[5], and the excitation area($\sim$1x2 mm^2). According to the calculations of Ugumori et al[6]., the Mott transition in GaSe from the exciton state to the plasma state occurs at the carrier density $n=4.8\times10^{17}cm^{-3}$. Thus electron -hole plasma is generated and the bandgap is renormalized.

The absorbance at a given delay time between the exciting and probe pulses is obtained from the equation:

$$OD(\lambda,t) = -\log_{10}\left[\left(\frac{I_1(\lambda,t) - I_{1,emission}}{I_2(\lambda,t) - I_{2,emission}}\right) \times \frac{I_{20}(\lambda,t)}{I_{10}(\lambda,t)}\right] \tag{3.1.1}$$

where $I_{10}(\lambda,t)$ and $I_{20}(\lambda,t)$ are the incident intensities of the probe pulses; $I_1(\lambda,t)$ and $I_2(\lambda,t)$ are the transmitted intensities of the probe pulses; $I_{1,emission}$ and $I_{2,emission}$ are the emission intensities from the sample excited by the pump pulses at a fixed intensity.

As shown in Fig.3.1.6, the changed absorptions at different time delays can be fitted by solid lines using the equation[7](The computer programming is in Appendix 2):

$$\alpha = \alpha_0(1-f_e)(1-f_h) \tag{3.1.2}$$

where α_0 is the absorption of the sample without

excitation, f_e and f_h are the Fermi distributions of electrons and holes in the conduction and valence bands,

$$f_i=(1+\exp(\epsilon_i-\mu_i)/kT_i))^{-1} \quad i=e,h \qquad (3.1.3)$$

The reason for eq.(3.1.2) is that the probability for the optical absorption from valence band to conduction band decreases from 1 to $(1-f_e)(1-f_h)$ due to the reduction of the available states for absorption. When the sample is excited by the pump pulse, some of the electrons in the valence band are excited into the conduction band. Therefore the probability for valence electrons to be excited into the conduction band by the probe pulse is $(1-f_h)$ where f_h represents the probability of vacant electron states in the valence band, and the probability for the excited electrons to occupy the conduction band is $(1-f_e)$ where f_e represents the probability of occupied electrons states in the conduction band. The absorption constant α is linearly proportional to the optical density(OD). In order to fit the experimental data in Fig.3.1.6, 1.5 OD is subtracted from α_0. The electrons and holes were assumed to be thermalized among themselves immediately after they were generated optically via carrier collisions and have a common temperature, $T_e=T_h$. This assumption is reasonable because the electron-electron scattering can redistribute the momenta and the energies of free carriers in a very short time so that the quasi Fermi distributions can be reached by the free carriers. This was observed in GaAs

under intense excitations[8]. In eq.(3.1.3), ϵ_e and ϵ_h are the energies of the electrons and holes in the conduction and valence bands, and μ_e and μ_h are the chemical potentials for electrons and holes, respectively. The carrier density for degenerate distribution[9] is:

$$n=2(2\pi m_i kT_i/h^2)^{3/2}F_{1/2}(\mu_i/kT_i),\ i=e,h \tag{3.1.4}$$

where $\epsilon_e=(\hbar w-\widetilde{E}_g)m_h/(m_e+m_h)$,

$\epsilon_h=(\hbar w-\widetilde{E}_g)m_e/(m_e+m_h)$,

and $F_{1/2}(\mu_i/kT_i)=$

$2\pi^{-1/2}\int_0^\infty E^{1/2}dE/(1+\exp(E-\mu_i/kT_i)$.

The effective masses[10] of electrons and holes in the direct band of GaSe are $m_e(=0.2m_0)$, $m_h(0.5m_0)$, where $m_i=(m_{i\perp}^2\cdot m_{i\parallel})^{1/3}$, and $m_{i\perp}$ and $m_{i\parallel}$ are the effective masses of carriers i(=e,h) normal or parallel to the C-axis of GaSe. The reduced bandgap is $\widetilde{E}_g$ and $\hbar w$ is the probe pulse wavelength.

In Fig.3.1.6(b), the best fit to the experimental result from eq.(3.1.2) is that $T_e=T_h=2000K$, $n=10^{19}cm^{-3}$ and $\widetilde{E}_g=1.950\pm0.01$ ev for 0 ps delay. Other sets of parameters T_e, n and $\widetilde{E}_g$ have been tried to fit the experimental data, however they do not fit the data as well as the above set does. For example, $T_e=T_h=2000K$, $n=2x10^{19}cm^{-3}$ and $\widetilde{E}_g=1.950$ ev does not fit the experimental data.

In Fig.3.1.6(c), $T_e=T_h=1700K$, $n=9x10^{18}cm^{-3}$, and $\widetilde{E}_g=1.950\pm0.01$ ev for 10 ps delay; In Fig.3.1.6(d),

$T_e=T_h=1000K$, $n=8x10^{18}cm^{-3}$, and $\widetilde{E}_g=1.950\pm0.01$ ev for 30 ps delay; In Fig.3.1.6(e), $T_e=T_h=600K$, $n=7x10^{18}cm^{-3}$, and $\widetilde{E}_g=1.955\pm0.01$ ev for 50 ps delay; In Fig.3.1.6(f), $T_e=T_h=320K$, $n=6.5x10^{18}cm^{-3}$, and $\widetilde{E}_g=1.955\pm0.01$ ev for 100 ps delay; In Fig.3.1.6(g), $T_e=T_h=300K$, $n=3x10^{18}cm^{-3}$, and $\widetilde{E}_g=1.960\pm0.01$ ev for 150 ps delay; and in Fig.3.1.6(h), $T_e=T_h=300K$, $n=7x10^{17}cm^{-3}$, and $\widetilde{E}_g=1.965\pm0.01$ ev for 250 ps delay.

The carrier density $n=10^{19}cm^{-3}$ at 0 ps delay is close to the estimated value calculated earlier. The reduced bandgap $\widetilde{E}_g=1.950$ ev to 1.965 ev are obtained from the photoluminescence spectra which will be observed in the following sections. The theoretical fit to the experimental results shown in Fig.3.1.6 by $\alpha=\alpha_0(1-f_e)(1-f_h)$ is sensitive to the change of the carrier density but not to the change of reduced bandgap $\widetilde{E}_g$.

Fig.3.1.7, the carrier temperature T_e as a function of the time delay is drawn. The lattice temperature of GaSe is 300K. The carriers cooled down to 300K less than 100 ps. The solid line will be stated in the following section.

3.1.3 The hot carrier relaxation process in GaSe

The hot carrier relaxation mechanism occurs from the emissions of optical and accoustical phonons. When the rate of change of carrier energy due to the nonpolar-optical phonon scattering is assumed to be equal to the phonon

energy times the difference between the phonon absorption rate and the phonon emission rate, the average rate of change of carrier energy due to nonpolar optical phonon interactions is[11] (see Appendix 3):

$$\left\langle \frac{d\varepsilon}{dt} \right\rangle = -\left(\frac{2}{\pi}\right)^{1/2} \frac{D^2 m_t m_\ell^{1/2}}{\pi \hbar^2 MN} (kT_e)^{1/2} \left[\frac{e^{(x_0 - x_e)} - 1}{e^{x_0} - 1}\right] \frac{x_e}{2} e^{x_e/2} K_1(x_e/2)$$

(3.1.5)

where K_1 is a Bessel function of the second kind, $x_0 = \hbar w_0/kT$, $x_e = \hbar w_0/kT_e$, T and T_e are the temperatures of the lattice and the carriers, $\hbar w_0$ is the energy of the nonpolar optical phonon. D is the interaction constant having the dimensions of energy/length, M is the reduced ionic mass in GaSe because each unit cell is treated as an independent oscillator[12], N is the number of cells per unit volume, the crystal density ρ in (3.1.5) was replaced by MN , m_t and m_ℓ are the transverse and longitudinal masses of the holes. In GaSe, $m_t = m_\perp$ and $m_\ell = m_\parallel$.

Since the electrons and holes are Fermi gas, the average energy $\langle E \rangle$ for each pair of electron and hole is $\sim 3\ kT_e$. It is reasonable to write

$\langle dE/dt \rangle \sim d\langle E \rangle/dt \sim 3k dT_e/dt$

and when $x_e/2 \ll 1$, ie $\hbar w_0 \ll 2kT_e$, $K_1(x_e/2) \sim 2/x_e$,

Therefore

$$3k \frac{dT_e}{dt} \simeq -\left(\frac{2}{\pi}\right)^{1/2} \frac{D^2 m_\perp m_\parallel^{1/2}}{\pi \hbar^2 MN} (kT_e)^{1/2} \frac{e^{(x_0 - x_e)} - 1}{e^{x_0} - 1} e^{x_e/2}$$

(3.1.6)

Equation (3.1.6) was used to fit the experimental data in Fig.3.1.7. Eq.(3.1.6) was rearranged so that the left hand side is a function of time and the right hand side is a function of carrier temperature, then integrations were made on both sides. Given a delay time, the carrier temperature can be found. The computer programming is listed in Appendix 4. When

$$(2/\pi)^{1/2}(D^2 m_\perp m_{//}^{1/2}/\pi\hbar^2 MN)(k)^{-1/2} 1/3 = 1.11\times10^{12},$$

and $\hbar w_0 = 16.7$ mev, the experimental data in Fig.3.1.7 can be fitted well by eq.(3.1.6). Using known parameters and the coefficient 1.11×10^{12}, the interaction constant between the holes and the nonpolar optical phonons is ~ 1.3 ev/Å. In Fig.3.1.7, the dots with error bars represent the experimental results and the solid line represents the results from eq.(3.1.6). Therefore the dominant relaxation mechanism of the photogenerated hot carriers is the emission of nonpolar optical phonons $A_1'^{(1)}$ with energy 16.7 mev.

Using known parameters and the coefficient 1.11×10^{12} the interaction constant D between the holes and the nonpolar optical phonons is calculated to be about 1.3 ev/Å. The value of D=1.3 ev/Å is about five times smaller than the result measured by Schmid et al[3] (6.6 ev/Å). The value of D deduced by Schmid was from the Hall mobility of holes parallel to the layers in ϵ-GaSe when the impurity hole density is of the order of $3\times10^{17}cm^{-3}$. A reasonable explanation for the difference between the value of D(1.3

ev/Å) and Schmid's value is that the interaction strength between the holes and the nonpolar optical phonons is screened by the photogenerated carrier density which in this experiment is thirty times larger than Schmid's thermal hole density[13].

As will be seen in a later section, the slower risetimes of the time resolved luminescence from GaSe at higher excitation intensities will support the speculation that the emissions of nonpolar optical phonons from holes are screened due to high carrier density.

3.2 The transition from exciton-carrier scattering emission to electron-hole plasma emission in GaSe

3.2.1 Introduction

In order to measure the time resolved emission spectroscopy, the time integrated emission spectroscopy from GaSe excited by picosecond laser pulse should be measured because there may be different emission modes in the photoluminescence spectra.

Over the years, many studies have been performed on the photoluminescence spectra of GaSe. Nahory, et al[14]. reported the measurements of stimulated emission in single crystal ε-GaSe, and showed that the emission arises from a recombination across a direct bandgap. Ugumori, et al[15]. investigated the emission spectra from GaSe under nitrogen laser excitation at 4.2K and 77K. He observed two emission bands ascribed to the recombination of the exciton-exciton and exciton-electron collision process. Mercier et al[16]. observed four lines at high excitations where two were attributed to exciton-carrier scattering: one arising from spontaneous and the other from stimulated emission. The two other lines correspond to two different exciton-exciton scattering processes. The stimulated emission was observed by Kuroda, et al[17]. who attributed the emission mechanism to the Auger process between the direct and the indirect excitons. The electron-hole plasma emission was observed on the lower energy side of the exciton emission at both 77K

and 300K by Baltramiejunas, et al[18]. using the second harmonics of a neodymium glass laser. However they did not observe the transition from exciton state to plasma state. The electron-hole plasma was also observed at the low energy sides of the stimulated emission(S line) in the temperature range 77-300K by Cingolani, et al[19]. using a nitrogen pulse laser. This result is different from the experimental result in this section which shows that the electron-hole plasma emission is on the high energy side of the S line when the sample temperature is at 300K.

In this thesis, a single 6 ps pulse at 527 nm from Nd:glass laser was used to excite the sample GaSe on the front surface. The excitation area was $\sim$7 mm^2. The luminescence spectra emitted from the front surface was detected and analyzed using a 1/4m Spex spectrometer, a PAR SIT camera, and an optical multichannel analyzer(OMA). The polarization of the excitation pulse was perpendicular to C axis which is normal to the layer of GaSe.

3.2.2 Time integrated emission spectra from GaSe excited by picosecond laser pulses

Two series of time integrated photoluminescence from GaSe at different excitation intensities are shown in Fig.3.2.1 and Fig.3.2.2 at 77K and 300K, respectively. As the excitation intensity increases, the two emission bands change for both temperatures.

The integrated emission intensity as a function of the excitation intensity are plotted in Fig.3.2.3 and Fig.3.2.4 for the observed two bands at 77K and 300K, respectively. The intensity dependences for higher and lower energy bands at 77K are displayed in Fig.3.2.3a and Fig.3.2.3b, respectively. For the higher energy band, the luminescence intensity increases linearly with the excitation intensity. Beyond $2.5 \times 10^{7} Wcm^{-2}$, the higher energy band is very small as compared with the lower energy band. The luminescence intensity of the lower energy band increases very drastically with the excitation intensity. The intensity dependences for higher and lower energy bands at 300K are plotted in Fig.3.2.4a and Fig.3.2.4b, respectively. The luminescence of the higher energy band increases linearly with the excitation intensity. Above $4 \times 10^{8} Wcm^{-2}$, the higher energy band is no longer apparent as compared with the lower energy band which increases very drastically with the excitation intensity from 3×10^{8} to 8×10^{8} Wcm^{-2}.

The peak energies of higher and lower energy bands are plotted in Fig.3.2.5 for 300K and 77K as a function of excitation intensity. The error bars in the peak energies are determined from the spectral resolution of the measuring system. In Fig.3.2.5, curve(a), the peak energy of the higher energy band at 77K, is constant between 1.3×10^{7} and 2.5×10^{7} Wcm^{-2}; curve(b), the peak energy of lower energy

band at 77K, decreases continuously from 1.3×10^{7} to $6\times10^{8}\,Wcm^{-2}$; curve(c), the peak energy of the higher energy band at 300K, is constant($\sim$1.994 ev) below the excitation $1.6\times10^{8}\,Wcm^{-2}$ and starts to decrease above the excitation $1.7\times10^{8}\,Wcm^{-2}$; curve(d), the peak energy of the lower energy band at 300K, decreases continuously from 8×10^{7} to $8\times10^{8}\,Wcm^{-2}$.

3.2.3 Theoretical analysis of the time integrated emission spectra from GaSe

In this section, the shape of the high energy tail of the higher energy luminescence band will be analyzed using the theoretical expressions for exciton-electron(hole) scattering, exciton-exciton scattering emission, and electron-hole plasma emission process in the different intensity regions.

The theoretical expression for the luminescence shape arising from exciton-electron (hole) scattering emission is given by[20]:

$$P_S(h\nu) \propto \frac{1}{\beta_e} \frac{N_0 n_0}{(E_0-h\nu)^2+(\pi\gamma/\epsilon)E_0^2} \left(\frac{\alpha_2}{\alpha_1}\right)^{1/2} K_1\{2(\alpha_1\alpha_2)^{1/2}\} \exp\left\{\frac{m_{h(e)}}{2M}\beta_e(E_0-h\nu)\right\} \tag{3.2.1}$$

where $\alpha_1 \equiv \frac{\hbar^2\beta_e}{2M}\left|\frac{\beta_L}{\beta_e}+\frac{m_{h(e)}^2}{4m_{e(h)}M}\right|$, $\alpha_2 \equiv \frac{m_{e(h)}\beta_e}{2\hbar^2}(E_0-h\nu)^2$, E_0=exciton energy , $\beta_e \equiv 1/kT_e$, $\beta_L \equiv 1/kT_L$. The mechanism of the radiative annihilation of excitons in the exciton-electron(hole) scattering emission is shown in Fig.3.2.6. The electrons(or holes) gain kinetic energies and

the excitons lose the same amount of energies during the scattering processes with momenta conservation. The calculation by computer programming is shown in Appendix 5. The above symbols are defined as follows: T_e and T_L are the temperatures of carriers and lattice, respectively; N_0 and n_0 are the occupation number of excitons and electrons(holes) for a null wave vector; $K_1(x)$ is the first order modified Bessel function of the third kind; $M=m_e+m_h$ is the effective mass of the exciton; $\pi\gamma/\epsilon$ is the exciton-photon coupling which is not known for GaSe. The value of 2.5×10^{-4} for $\pi\gamma/\epsilon$ is chosen from CdS as a typical value; and $m_e=0.2\ m_0$, $m_h=0.5\ m_0$.

The theoretical expression for the luminescence shape arising from exciton-exciton scattering emission is as follows[21]:

$$P_s(h\nu) \propto \frac{h\nu\,\rho(h\nu)}{(E_0-h\nu)^2+(\pi\gamma/\epsilon)E_0^2}\,\frac{N_0^2}{kT_L}\int_0^\infty d\xi\int_0^\infty dt\,\frac{\xi^{1/2}}{(1+\xi/E_x^b)^4}\exp\left[-t-\frac{1}{4t}\left(\frac{E_g-E_x^b-h\nu-\xi}{kT_L}\right)^2\right] \tag{3.2.2}$$

where $\rho(h\nu)d\nu$ is the number of photon modes in the crystal between the frequency ν and $(\nu+d\nu)$; E_x^b is the binding energy of the exciton. The process of the exciton-exciton scattering emission is similar to the exciton-electron(hole) scattering emission: one of the excitons is excited into the dissociation state while the other traverses the crystal to leave as a luminescent photon. The calculation of the integrals can be found in Appendix 6 using computer

programming.

The theoretical expression for the shape of the luminescence arising from electron-hole plasma emission with K selection at high temperature as same as eq.(2.2.1) is given by[22]:

$$P_s \propto (h\nu-\widetilde{E}_g)^{1/2}\exp(-(h\nu-\widetilde{E}_g)/kT_e) \qquad (3.2.3)$$

where $\widetilde{E}_g+1/2kT_e$=peak energy of the emission band.

At 77K, the high energy side of the higher energy band can be fitted by the exciton-electron(hole) scattering process given by eq.(3.2.1) with $T_e=T_L=77K$, $E_0=2.098$ ev for Fig.3.2.1a and Fig.3.2.1b. In Fig.3.2.7, the dots with error bars are the experimental data while the solid line is the theoretical fit by eq.(3.2.1). As the excitation increases, the higher energy band of Fig.3.2.1c is very small in intensity relative to the lower energy band. At $2.5\times10^7 Wcm^{-2}$, the higher energy band does not grow as fast as the lower energy band as shown in Fig.3.2.1d and Fig.3.2.1e.

At room temperature, the higher energy bands from Fig.3.2.2a to Fig.3.2.2d can also be fitted by the eq.(3.2.1) on the high energy tails with $T_e=T_h=300K$, and $E_0=2.0$ ev. This is shown in Fig.3.2.8. These curves are for excitation intensities less than $1.77\times10^8 Wcm^{-2}$. For higher excitation intensities , the high energy tails of the higher energy bands can no longer be fitted by the eq.(3.2.1) with $T_e=T_L=300K$, and $E_0=2.0$ ev. The high

energy tail of the higher energy band of Fig.3.2.2e can be fitted by eq.(3.2.1) using T_e=2000K, T_L=300K, and E_0=1.979 ev. But higher carrier temperature and smaller exciton energy are unreasonable because the carrier temperature should not change from 300K to 2000K when the excitation changes from $1.6x10^8$ Wcm^{-2} of Fig.3.2.2d to $1.70x10^8Wcm^{-2}$ of Fig.3.2.2e. Aslo the exciton energy should not change at different excitation intensities. It has been shown by picosecond absorption spectroscopy on GaSe in the previous section that the hot photogenerated carriers thermalized within 100 ps to the lattice temperature. Since the photoluminescence recombination time (~300 ps) which will be obtained later is much larger than 100 ps, the time integrated emission will be from excitations thermalized with the lattice.

The peak energy of the theoretical formula for the exciton-exciton scattering emission would be at 2.078ev(2.0ev), with E_0=2.098 ev(2.0ev), and E_x^b=20mev, when the sample is at 77K(300K). As shown in Fig.3.2.9 and Fig.3.2.10, the theoretical expressions for the exciton-exciton scattering emissions at 77K and 300K are represented by solid lines and the experimental data from Fig.3.2.1a and Fig.3.2.2c are represented by dots with error bars. It is clear that eq.(3.2.2) can not fit the high energy tails of the higher energy bands of the photoluminescence spectra for both temperatures.

As shown by curve c in Fig.3.2.5, the peak energies of the higher energy bands shown in Fig.3.2.2e to Fig.3.2.2h for excitation intensity larger than $1.7 \times 10^8 Wcm^{-2}$ are smaller than the exciton energy(2.0 ev) by several tens of mev, it is reasonable to guess that these emissions are from the electron-hole plasma given by eq.(3.2.3). Using eq.(3.2.3), the high energy tails of the higher energy bands displayed from Fig.3.2.2.e to Fig.3.2.2h can be fitted with $T_e = 300K$ as shown in Fig.3.2.11. The solid line is from eq.(3.2.3) and the dots with error bars are the experimental data from Fig.3.2.2e. The value of $\tilde{E}_g$ as a function of the carrier density is plotted in Fig.3.2.12. The carrier density was calculated using the measured absorption coefficient, values of incident light energy, and loss of scattered light. For the excitation intensity $(1.70 \pm 0.25) 10^8 Wcm^{-2}$ of Fig.3.2.2e, the calculated density is $3 \times 10^{17} cm^{-3}$. The absorption constant at 530 nm is $2 \times 10^3 cm^{-1}$. Note that 97% of incident light is not absorbed due to the scattering of incident light as determined from the absorption measurement in the previous section. As shown in Fig.3.2.12, the reduced bandgap becomes smaller when the carrier density increases due to the many body effects of electrons and holes.

From the analysis of the high energy tails and the peak energies of the higher energy bands, the exciton-electron(hole) scattering emission disappears when

the excitation intensity reaches $(1.70 \pm 0.25) 10^8 Wcm^{-2}$ as shown in Fig.3.2.2e and Fig.3.2.5. Above this intensity the electron-hole plasma emission appears.

From the data displayed in Fig.3.2.4, the emission intensity is linearly proportional to the excitation intensity for both the exciton-electron(hole) scattering emission and the plasma emission regions. Since the exciton-electron(hole) scattering is proportional to the numbers of the excitons and electrons(holes) as shown in eq.(3.2.1), and the plasma emission is proportional to the numbers of electrons and holes. The number of excitons, electrons, and holes are all linearly proportional to the square root of excitation intensity at high excitations[20] as shown in Appendix 1, therefore the intensity dependences of both exciton-electron(hole) scattering emission and the plasma emission are linear with the excitation intensity.

Although the direct exciton binding energy is 20 mev, the exciton-electron(hole)scattering emission can still be observed at room temperature because of the existence of the excitons[23] due to the resonance effect of direct excitons and the indirect conduction band[24].

From the data displayed in Fig.3.2.3b and Fig.3.2.4b, the lower energy bands at both temperatures arise from stimulated emission. The peak energies of the lower energy bands are located about 50 mev or more below the higher energy bands. Many processes have been proposed earlier to

account for this stimulated emission: the exciton-carrier complex[25], the exciton-exciton scattering[6], the exciton-electron scattering[16], and the Auger process due to the direct and indirect excitons[17]. At room temperature, the excitation intensity required for stimulated emission is larger than $1.7 \times 10^{8} Wcm^{-2}$. Since the excitons disappear above this intensity, a possible mechanism for the stimulated emission process involves only free carriers of plasma. Since the electronic energy band diagram of GaSe is not complete at this time, it is difficult fo know the exact mechanism for the stimulated emission process.

3.3 The screening of nonpolar optical phonon-hole interaction by high density photogenerated carrier in GaSe

3.3.1 Introduction

In the previous section, the reduction of the deformation potential at $10^{19}cm^{-3}$ compared with that at $3x10^{17}cm^{-3}$ was attributed to the screening of nonpolar optical phonon-hole interaction by high density of photogenerated carrier density in GaSe. In this section, the measurements of time resolved emission spectroscopy will be reported. The increased risetime of the photoluminescence with increased excitation intensity will support the speculation that it is due to the screening effect of high density photogenerated carrier on the relaxation of hot carriers.

3.3.2 Time resolved emission spectra from GaSe

A second harmonic (530 nm) of Nd:glass laser pulse of 10 ps duration was used to excite a gallium selenide sample. The luminescence was collected by a streak camera with 100 μ slit, analyzed by a temporal analyzer and a computer. A narrow band filter at 620 nm with $\pm$10nm bandwidth, a cut off filter at 620nm, and a cut off filter at 640nm were used to select the spontaneous emission because the stimulated emission is much stronger than the spontaneous emission. A Hoya R-64 cut on filter was used to select the

stimulated emission above 640 nm. The excitation area on the sample is $\sim 2.6\ mm^2$. The polarization of the incident light is normal to the C axis of GaSe. The optical transmission of GaSe was measured to be $\sim$ 40% at 700 nm which is less than the direct bandgap energy. This means that only 40% of the incident light intensity will be absorbed to create the electron-hole pairs. The optical absorption constant at 530 nm is $\sim 2\times10^3 cm^{-1}$ at room temperature[5]. The carrier densities generated optically at different excitation intensities was estimated using the above parameters.

Fig.3.3.1 shows two time resolved photoluminescence spectra for spontaneous emission component with wavelength of 610 to 630 nm from GaSe at room temperature. The following equation is used to fit the time resolved emission spectra,

$$I(t)=A(\exp(-t/\tau_d)-\exp(-t/\tau_r)) \qquad (3.3.1)$$

where τ_d and τ_r are decay and rise times of the spectra, respectively. In Fig.3.3.1, various photoluminescence kinetics at different photogenerated carrier densities are plotted. The rise time increases and the decay time decreases with increasing carrier density.

As shown in Fig.3.3.2, two time resolved photoluminescence spectra for stimulated emission component with wavelength longer than 640 nm from GaSe at room temperature are presented. In Fig.3.3.2a, the carrier density is $\sim 6\times10^{18} cm^{-3}$, the laser pulse duration and

streak camera response is $\sim$20 ps, the risetime of the photoluminescence is $\leq$20 ps, and the decay time is $\sim$100 ps. In Fig.3.3.2b, the risetime is $\leq$20 ps, the decay time is $\sim$50 ps, and the photogenerated carrier density is $\sim$ $1.0\times10^{19}cm^{-3}$.

In Fig.3.3.3, the risetimes at different carrier densities for both spontaneous and stimulated emissions are plotted. The risetime of the spontaneous emission increases from 5 ps to 100 ps when the carrier density increases from $1.8\times10^{18}cm^{-3}$ to $\sim1.6\times10^{19}cm^{-3}$. However the risetime of the stimulated emission remains $\leq$ 20 ps from $1\times10^{18}cm^{-3}$ to $\sim1.1\times10^{19}cm^{-3}$.

3.3.3 Theoretical analysis of the time resolved emission spectra from GaSe

The photogenerated carrier density as shown in both Fig.3.3.1 and Fig.3.3.2 are from $\sim1\times10^{18}cm^{-3}$ to $\sim$ $1.6\times10^{19}cm^{-3}$ which is greater than $4.8\times10^{17}cm^{-3}$ for Mott transition[6]. The spontaneous emission arises from electron-hole plasma.

There have been two theories to describe the slowed relaxation processes of hot carriers in semiconductors. First, Yoffa[26] developed a screening theory about emissions of phonons from hot carriers for intravalley and intervalley scatterings inside polar direct-gap and nonpolar indirect-gap semiconductors. Her theory predicts important

difference between polar direct-gap and nonpolar indirect-gap semiconductors in the carrier density dependence of the hot carrier relaxation rate. The critical carrier density for the onset of screening in polar direct-gap semiconductors is found to increase with both effective mass and phonon energy. For the specific example of GaAs, it is shown that a reduction in the rate of phonon emission first occurs at an easily attainable carrier density, $N \sim 6 \times 10^{16} cm^{-3}$. By $N \sim 10^{18} cm^{-3}$, the intravalley transitions are screened and the cooling rates falls very rapidly to a value appropriate to emission of intervalley phonons. In contrast, screening of the energy relaxation rate in Si is negligible at densities less than $N \sim 10^{19} cm^{-3}$ and a significant reduction in this rate does not occur until $N \sim 10^{21} cm^{-3}$.

In her theory, the phonon absorption makes negligible contribution to the net energy relaxation rate of the carriers because the carrier temperature was assumed to greatly exceed the lattice temperature. Actual phonon emission rates depend strongly on the nature of the carrier-optical-phonon couplings. Energy relaxation via acoustic phonon emission is less efficient and dominates only when the carriers have already relaxed to within an optical-phonon energy of the band edge. In the case of nonpolar materials, matrix elements V for optical-phonon emission do not in general depend on the phonon wave vector

q, whereas for polar interactions, $V \sim 1/q$. In each case, large wave vector intervalley phonons remain unscreened until very high carrier density. The polar Frölich interaction which dominates small q intravalley transitions in GaAs is much less important for transitions between valleys, which proceed instead via a deformation coupling similar to that for intervalley transition in Si.

The second theory developed by van Driel[27] who claims that long energy relaxation time for dense electron-hole plasma through optical-phonon emission is due to a relaxation bottleneck produced by a buildup of optical-phonon population on a picosecond time scale. The lattice temperature has been in his theory replaced by the optical-phonon temperature. This reflects the fact that it is the optical-phonon reservoir with which the carriers are attempting to reach equilibrium. The relatively long phonon lifetimes have the effect of maintaining a high phonon temperature as the plasma cools. This results in a relaxation bottleneck for the hot carriers. The electron temperature initially decreases quite rapidly from its initial value. During this time the optical-phonon temperature rises to a maximum value. From then on the two temperatures cool at a relatively slow rate. In this model, the decrease in relaxation time with decreasing carrier density is due to a reduction in the amount of phonon heating, allowing the plasma to cool more quickly. Were it

not for phonon heating effects, the relaxation time should be independent of carrier density.

In this thesis, the first theory developed by Yoffa will be compared with the experimental result. It is impossible to compare with the second theory by van Driel at this time because it involves with carrier temperature, phonon temperature, and phonon density which can not be found simply from time resolved emission spectrum. The proposed research to test this second theory will be given in the chapter 5. Recently, Seymour et al.[29] observed slowed risetime of the near bandedge luminescence from GaAs, and attributed it to the screening of the electron-phonon interaction. They also observed that the slowing occurs at lower excitation densities in n-type material than in p-type material. This is as expected for the screening mechanism since background electrons in the central conduction band valley effectively contribute to the screening while the background holes in p-type material do not contribute to the screening[26]. They claimed that the conductivity type of the crystal would have no influence on the phonon build-up and thus one would expect the slowing to begin at the same excitation level in p- and n-type crystals. Therefore they suggested that the screening mechanism is dominant for the slowed relaxation process.

From Yoffa's theory, the emission rate v of nonpolar optical phonons from hot carriers for intravalley scattering

in semiconductors is (see Appendix 7)

$$v \propto (1+(N/N_c)^2)^{-1} \qquad (3.3.2)$$

where N is the carrier density and N_c is the critical carrier density which is equal to $\frac{\epsilon_0 \hbar}{8\pi e^2}\left(\frac{2 m_i^* \omega}{\hbar}\right)^{3/2}\left(\frac{1}{\beta m_i^*}\right)^{1/2}$. The emission rate v remains constant when the carrier density N is much smaller than the critical carrier density N_c and decreases when the carrier density is larger than N_c. In GaSe, ϵ_0, the static dielectric constant, is 10.6 when the polarization of the incident light is normal to C axis[5]; m_i^* is the effective mass of hole, which is 0.5 m_0 on the direct bandgap[16]; e is the electonic charge which is 4.8×10^{-10}esu; $\hbar w$ is the $A_1'^{(1)}$ phonon energy(16.7 mev); $\beta = 1/kT_e$, T_e is the carrier temperature. The critical density N_c is higher when the carrier temperature is higher. N_c is $\sim 4.8\times10^{18}$cm^{-3} when T_e is 2000K. During the rising period of the time resolved emission of the spontaneous component, the carrier temperature will drop from ~2000K to ~400K from time resolved absorption spectroscopy[13]. Both the carrier temperature and density decrease during the risetime period. Since it is difficult to extract the carrier temperature and density simply from the time resolved emission, the exact time rate of change was not included in the fitting process. According to the Yoffa's theory, the emission rate of phonons from relaxing holes is $v \propto 1/(1+(N(t)/N_c(t))^2)$. Because N_c is proportional to the square root of carrier temperature, both

$N(t)$ and $N_c(t)$ decrease monotonically with time. v will be close to a constant during the relaxation process of holes. This can be seen in the Figure 3.1.7 where the carrier temperature decreased at almost a constant rate(~30K/ps). Since the change rate of carrier temperature is linearly proportional to the phonon emission rate v from relaxing holes, v will be close to a constant for a given N(0). Therefore the inverse of the risetime of the spontaneous emission should be proportional to the emission rate v of phonons from relaxing holes. The initial carrier density was determined by the experimental parameters and the initial carrier temperature was estimated to be ~ 2000K when the sample was irradiated by a 530 nm light. In Fig.3.3.4, the inverse of the risetime at various density is plotted. The values of $v=A(1/(1+(N/N_c)^2))$ are also plotted when $N_c=4.8\times10^{18}cm^{-3}$ at $T_e=2000K$ with A=0.1. These values fit the experimental results well when the carrier density is above $5\times10^{18}cm^{-3}$.

The emission rate v at $10^{19}cm^{-3}$ and $T_e=2000K$ is about $(1+(10^{19}/4.8\times10^{18})^2)^{-1}=0.2$, or five times smaller than the unscreened value 1. From the time resolved absorption spectroscopy of GaSe, the deformation potential between the holes and the nonpolar optical phonons was found to be five times smaller when the initial photogenerated carrier density is ~ $10^{19}cm^{-3}$, and the energy of each pair of electron and hole decays at a rate proportional to

the square of the deformation potential[11] as shown in eq.(3.1.6). This energy decay rate would be about twenty-five times smaller than the unscreened value. Since the risetime is less than 20 ps which is the resolution of the measuring system when the carrier density is below $5x10^{18}cm^{-3}$, it is impossible to know experimentally whether the emission rate v at $10^{19}cm^{-3}$ will be twenty-five times smaller than the unscreened value. In Fig.3.3.4, the values of $v \propto 1/(1+(N/N_c)^2)$ are also plotted with $N_c=2x10^{18}cm^{-3}$ with A=0.45. In this case, the value of v at $10^{19}cm^{-3}$ would be twenty-five times smaller than the unscreened value. These values do not fit the experimental results as well as compared with that of $N_c=4.8x10^{18}cm^{-3}$ above $1.5x10^{19}cm^{-3}$.

There may be three reasons to account for the different values of emission rate at $10^{19}cm^{-3}$: one is that the carrier density of $10^{19}cm^{-3}$ and carrier temperature of 2000K from time resolved absorption spectroscopy measurements could be off from the exact values. The second reason is that this sample is a layered semiconductor, therefore the theory of Yoffa probably should be modified to account for this change to reduce the value of N_c by a factor 2. The third reason is that the unscreened deformation potential may be smaller than[3] 6.6 ev/Å by a factor 2, therefore emission rate v would be five times smaller than the unscreened value.

As shown in Fig.3.3.3b, the risetime of the time resolved stimulated emission remains within the time resolution of the measuring system with increasing photogenerated carrier density. This implies that the risetime is extremely fast in the stimulated emission.

In conclusion, the time resolved photoluminescence spectra of GaSe were measured at room temperature. The risetime of the spontaneous emission is within the resolution of the laser pulse when the photogenerated carrier density is below $5\times10^{18}cm^{-3}$ and increases above $5\times10^{18}cm^{-3}$ in agreement with Yoffa's theory. The risetime of the stimulated emission remains within the resolution of the laser pulse with increasing photogenerated carrier density.

References of Chapter 3:

1. M. Schlueter, Nuovo Cimento, B13,313(1973).

2. R. M. Hoff, J. C. Irwin, and R. M. A. Leite, Can. J. Phys. 53,1606(1975).

3. Ph. Schmid and J. P. Voitchovsky, Phys. Stat. Sol. (b)65, 249(1974).

4. B. L. Evans, Optical Properties of Layer Compound, in Optical and Electrical Properties, Vol.4(D. Reide Publishing Company, Boston, 1976).

5. R. Le Toullec, N, Piccioli, M. Mejatty, and M. Balkanskj, Nuovo Cimento, B38,159(1977).

6. T. Ugumori, K. Masuda, and S. Namba, J. Phys. Soc. of Japan, 41,199(1976).

7. J. Shah and R. F. Leheny, Phys. Rev. B16,1577(1977).

8. R. Ulbrich, Phys. Rev. B8,5719(1973).

9. J. S. Blakemore, Semiconductor Statistics, p79(Pergamon Press, NY, 1962).

10. G. Ottaviani, C. Canali, F. Nova, Ph. Schmid, D. Mooser, R. Minder, and I. Zschokke, Sol. St. Comm. 14,933(1974).

11. E. M. Conwell, in Solid State Physics, edited by F. Seitz, D. Turnbull, and H. Ehrenreich, p155(Academic Press, NY, 1967), Suppl. 9.

12. Ph. Schmid, Nuovo Cemento, 21B,258(1974).

13. S. S. Yao, J. Buchert, and R. R. Alfano, Phys. Rev. B 25,6534(1982).

14. R. E. Nahory, K. L. Shaklee, R. F. Leheny, and J. C.

Dewinter, Sol. St. Comm. 9,1107(1971).

15. T. Ugumori, K. Masuda, and S. Namba, Sol. State. Comm. 12,389(1973).
16. A. Mercier, and J. P. Voitchovsky, Phys. Rev. B11,2243 (1975).
17. N. Kuroda and Y. Nishina, J. of Luminescence, 12/13,623 (1976).
18. R. Baltramiejunas, V. Narkevicius, E. Skaistys, J. Vaitkus, and J. Viscakas, Nuovo Cimento, B38,603(1977).
19. A. Cingolani, M. Ferrara, and V. Lugara, Optic Comm. 32, 109(1980).
20. C. Benoit a La Guillaume, J. M. Debever, and F. Salvan, Phys. Rev. B177,567(1969).
21. T. Moriya and T. Kushida, J. Phys. Soc. of Japan, 40,1668 (1976).
22. Y. Yoshikuni, H. Saito, and S. Shionoya, Solid State Comm. 32,665(1979).
23. J. P. Voitchovsky and A. Mercier, Nuovo Cimento, B22,273 (1974).
24. A. Mercier, E. Mooser, and J. P. Voitchovsky, Phys. Rev. B12, 4307(1975).
25. R. C. C. Leite, E. A. Mineses, N. Jannuzzi, and J. G. P. Ramos, Solid State Comm. 11,1741(1972).
26. E. J. Yoffa, Phys. Rev. B23,1909(1981).
27. H. M. van Driel, Phys. Rev. B19, 5928(1979).
28. J. L. Staehli and A. Frova, Physica, 99B,299(1980).

29. R. J. Seymour, M. R. Junnarkar, and R. R. Alfano, Sol. St. Communication, 41,657(1982).

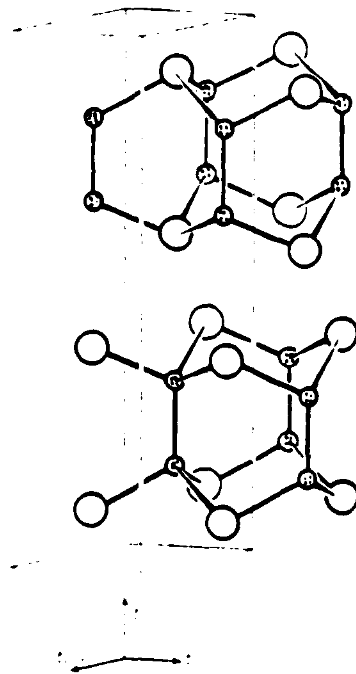

– Unit cell of β-GaSe. The Ga atoms are represented by the small shaded circles, the Se atoms by the large open circles. (ref.1)

Fig.3.1.1

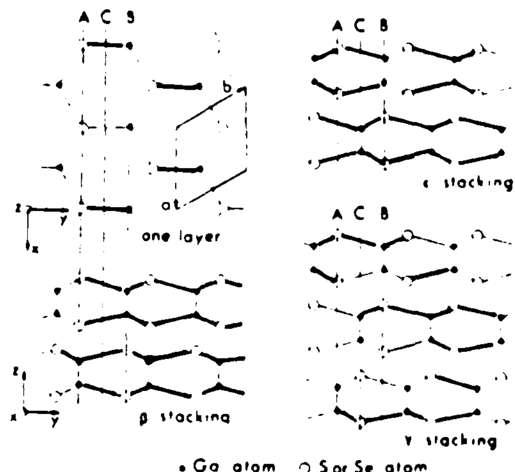

Stacking sequences for the β, ε, and γ polytypes of GaS and GaSe. (ref.2)

Fig.3.1.2

(From ref.28)

Fig.3.1.3

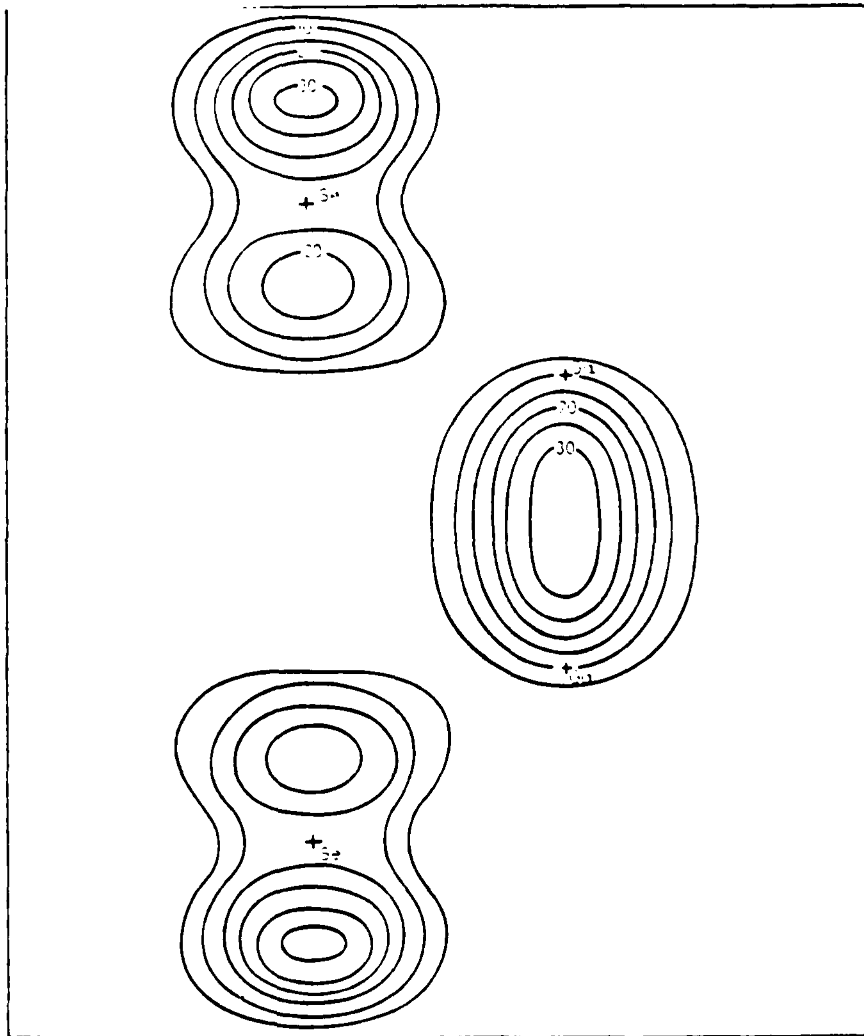

– Electron charge density for the fourth group of bands in GaSe including the uppermost valence band Γ_1. (ref.1)

Fig.3.1.4

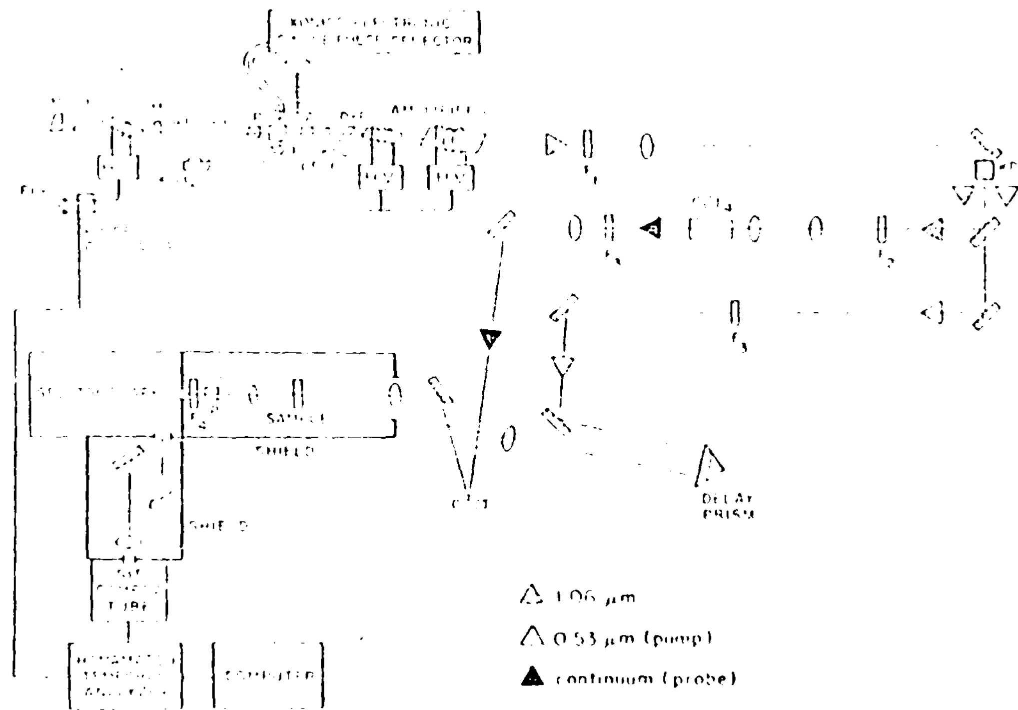

Fig.3.1.5

Fig.3.1.6

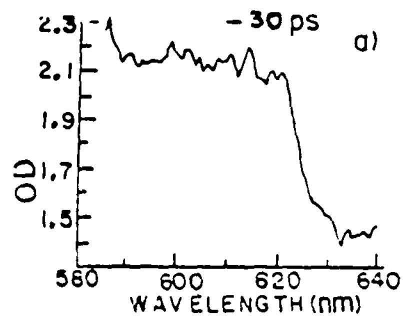

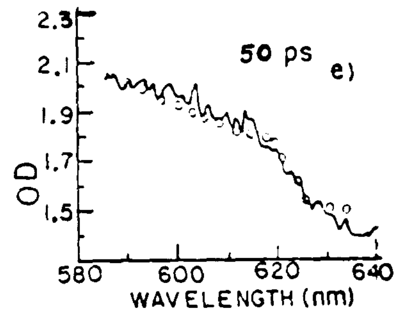

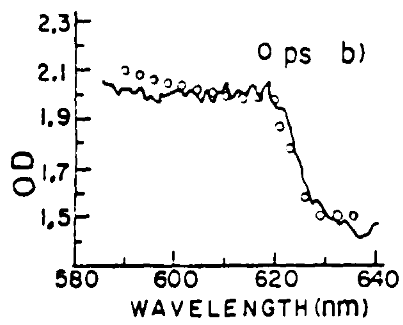

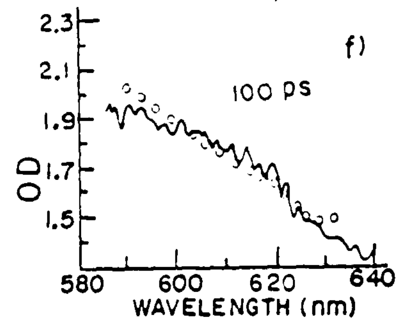

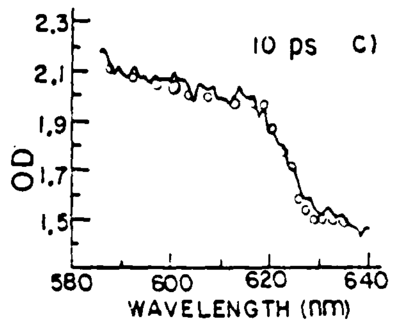

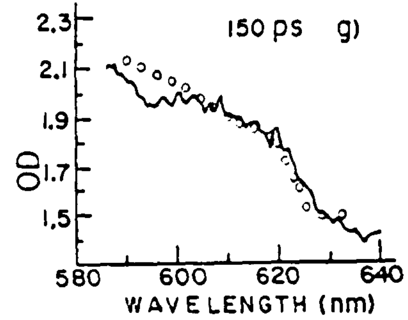

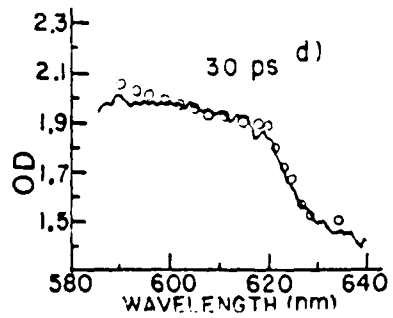

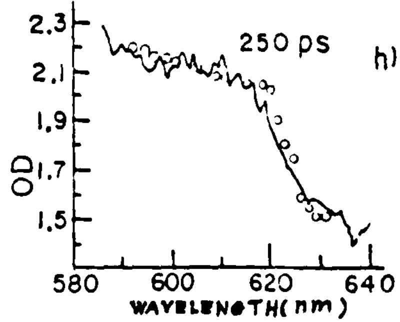

Fig.3.1.7

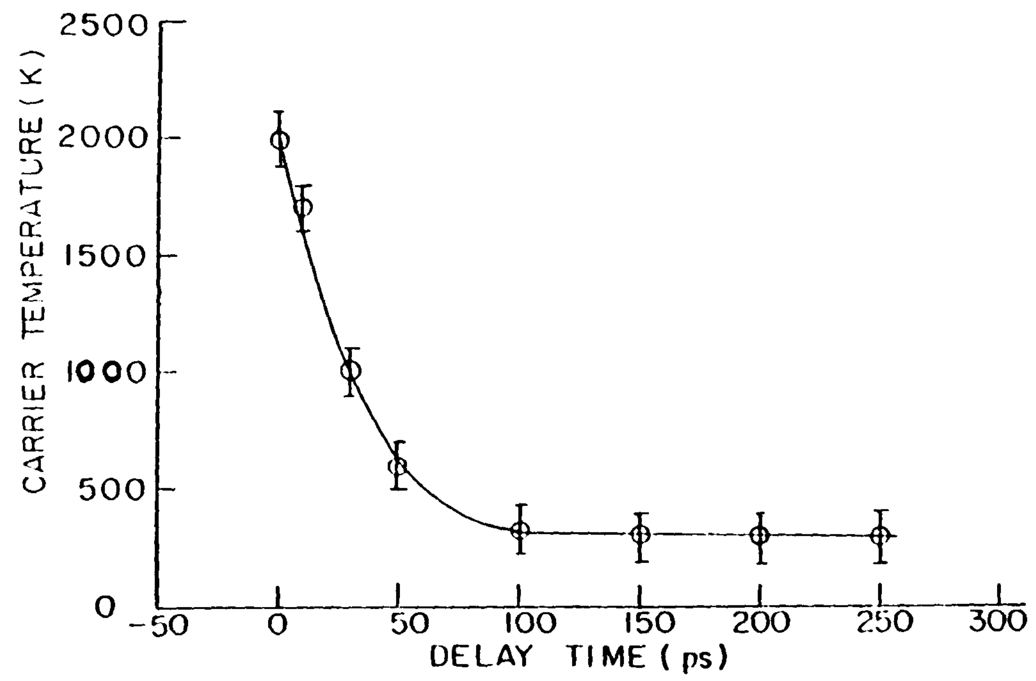

Fig.3.2.1

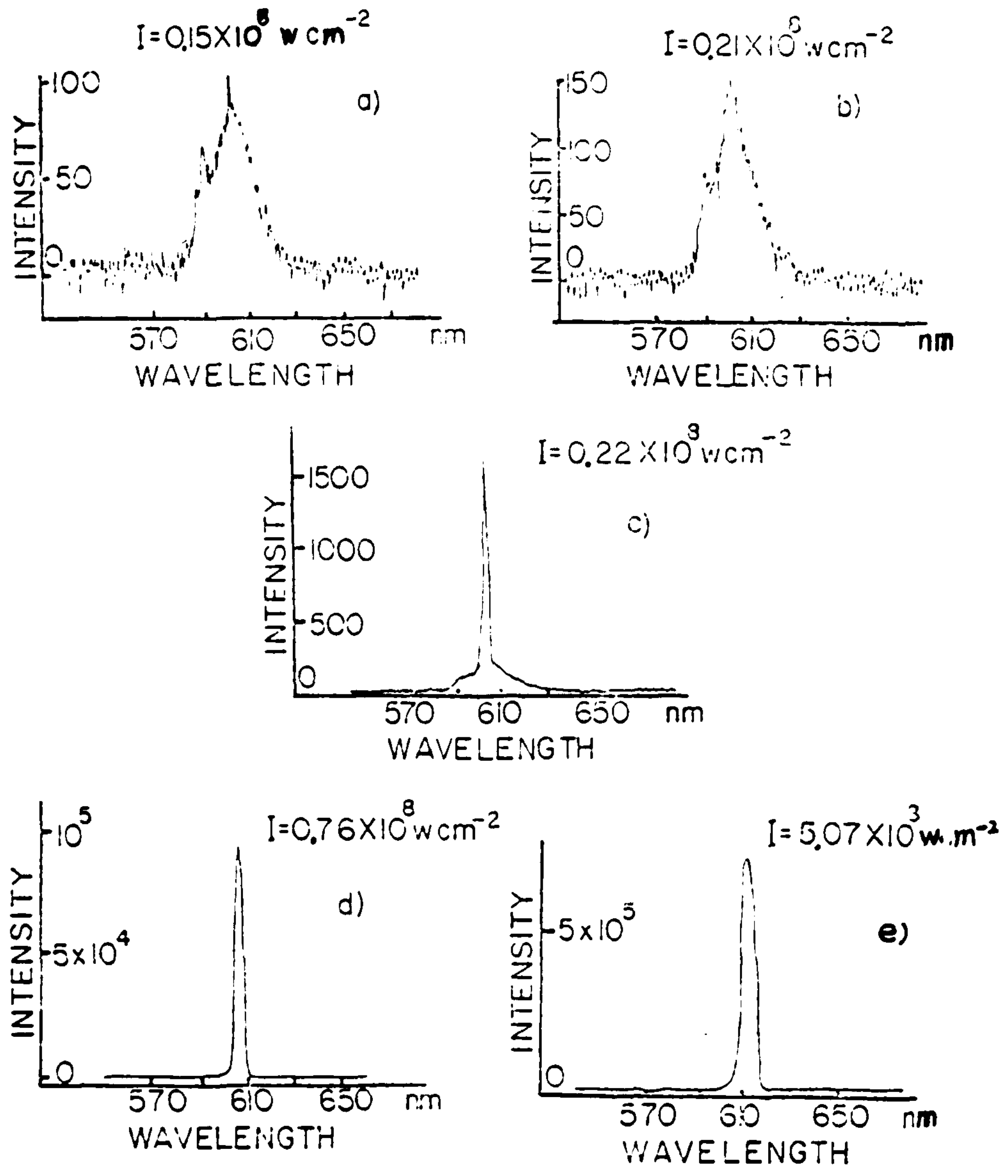

Fig.3.2.2

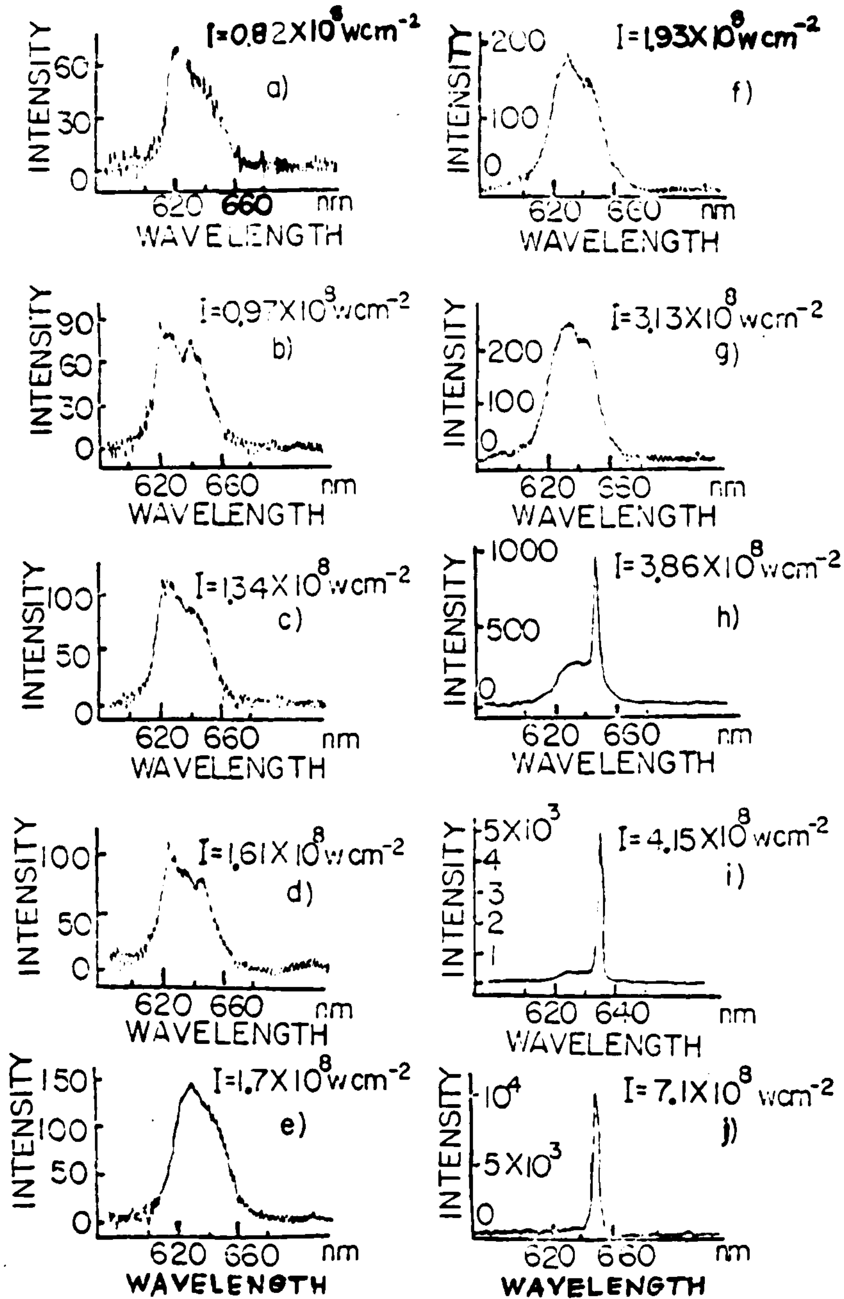

Fig.3.2.3

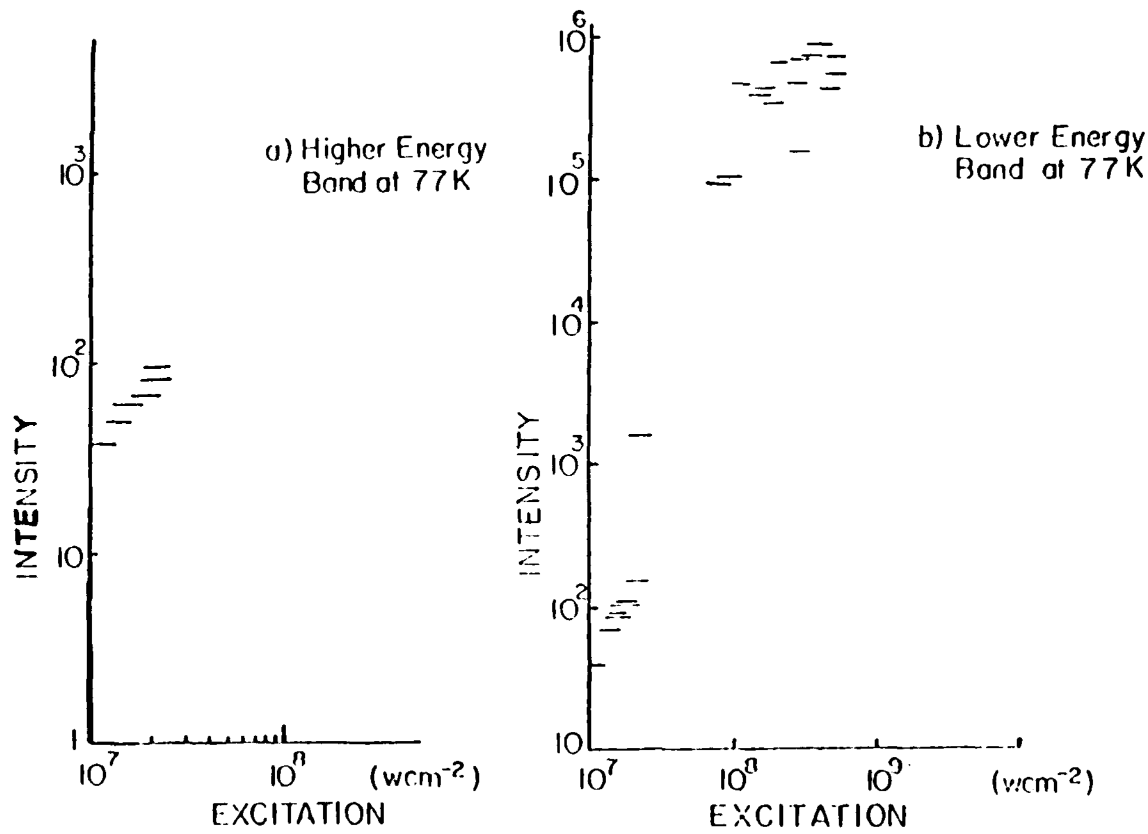

Fig.3.2.4

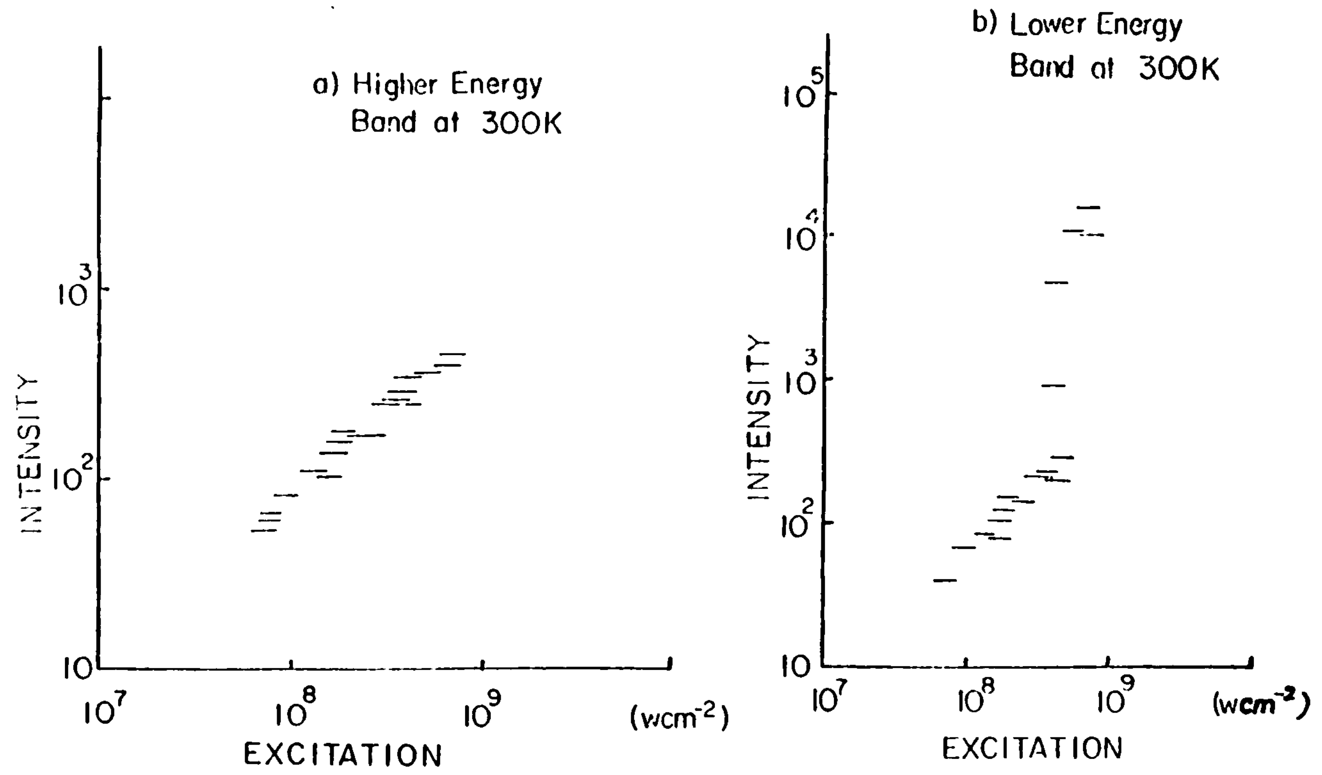

Fig.3.2.5

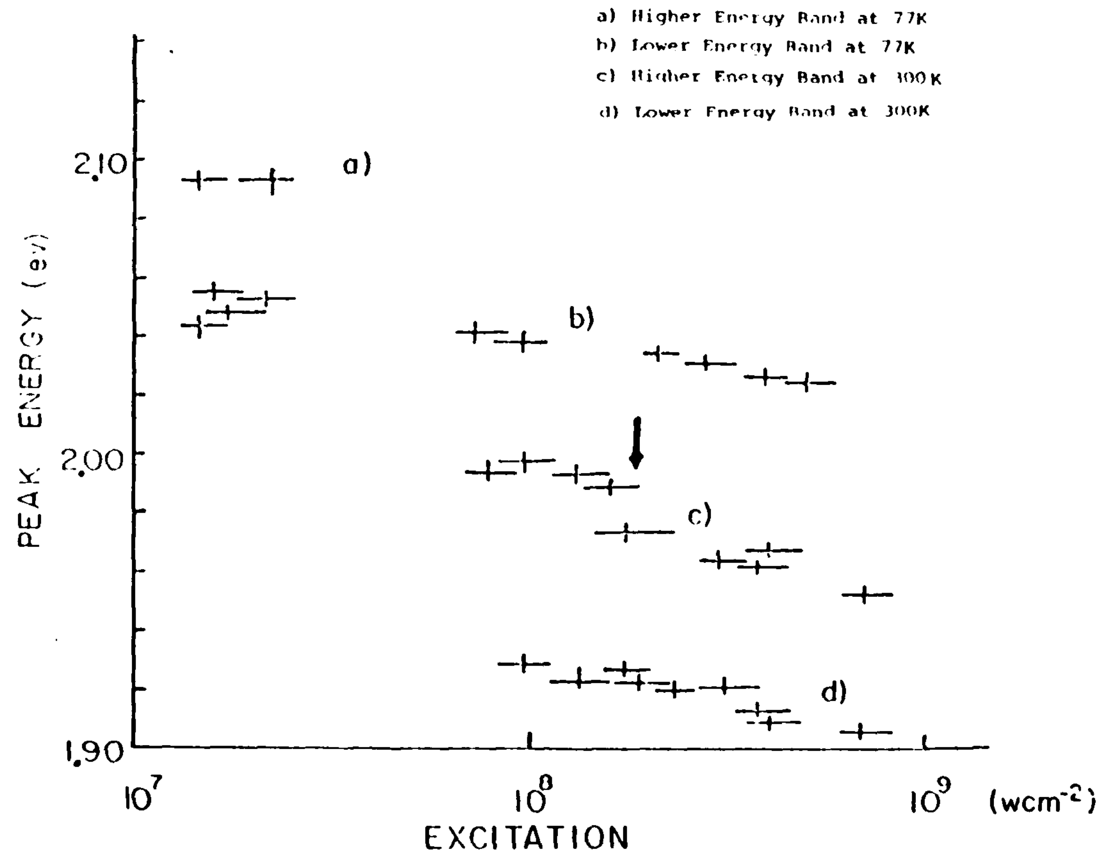

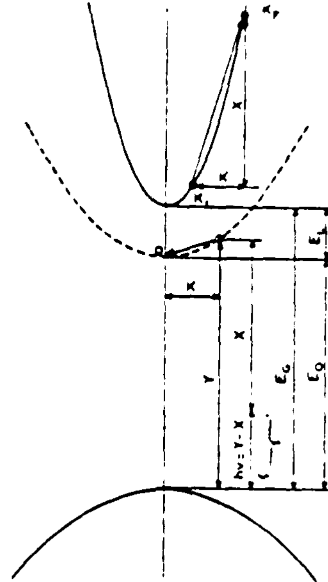

Sketch of the radiative recombination of an exciton giving its momentum to a free electron.

Fig.3.2.6

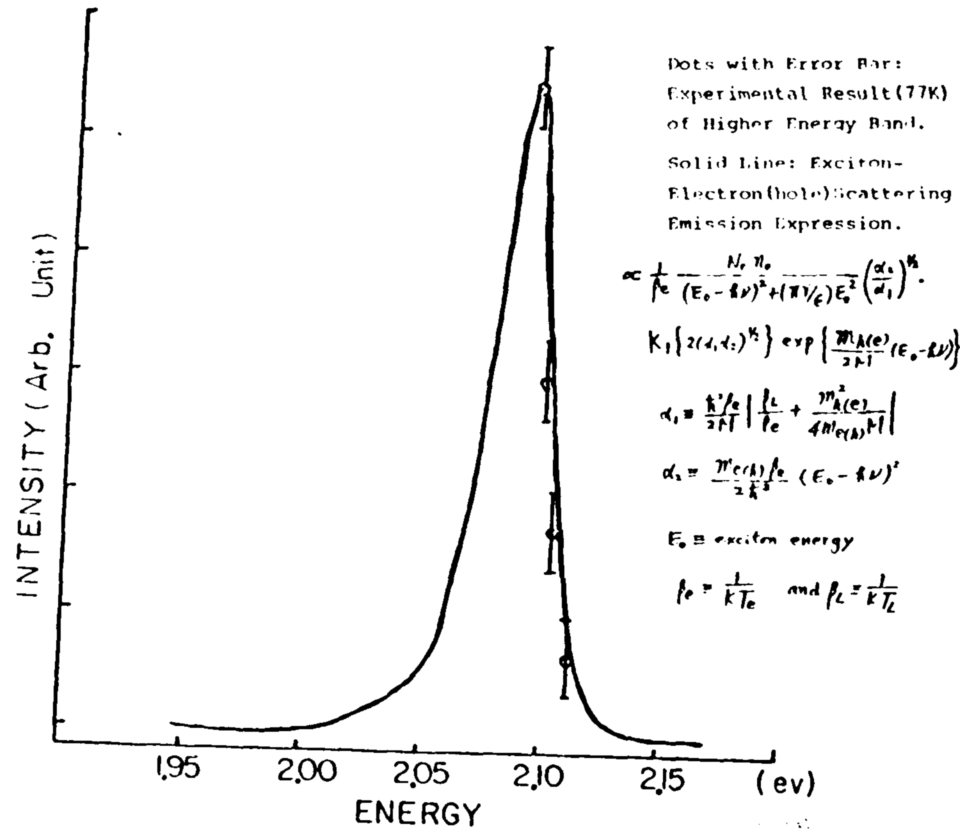

Fig.3.2.7

Fig.3.2.8

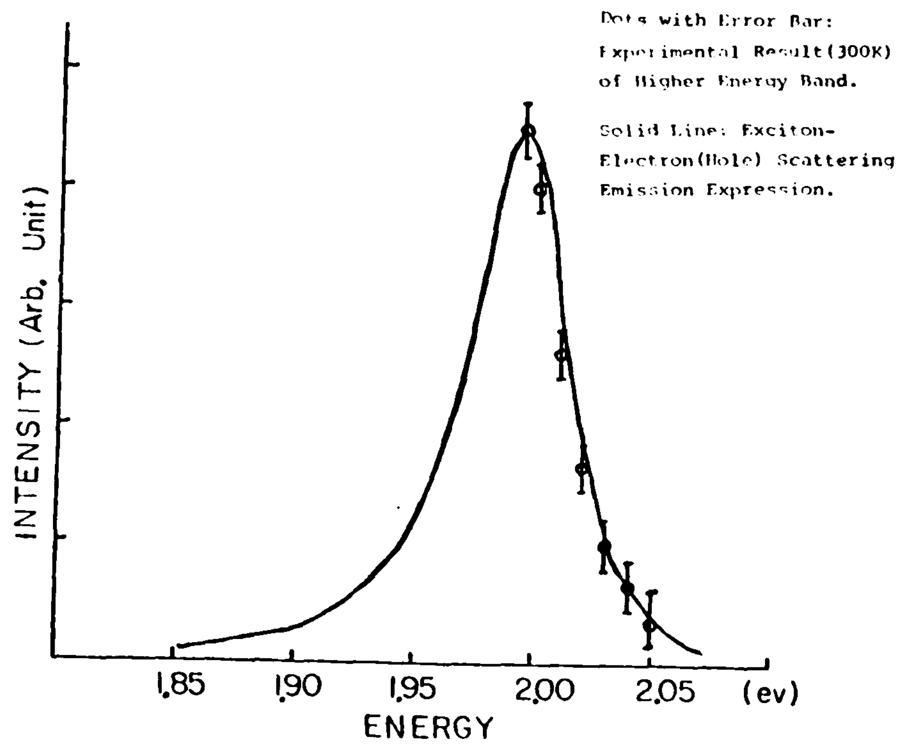

Fig.3.2.9

Dots with Error Bar: Experimental Result (77K) of Higher Energy Band.

Solid Line: Exciton-Exciton Scattering Emission.

$$\propto \frac{h\nu\, f(h\nu)}{(E_0-h\nu)^2 + (\hbar\Gamma/2)^2 E_0^2}\, \frac{N_x^2}{kT_L} \int_0^\infty d\xi \int_0^\infty dt\, \frac{\xi^{1/2}}{(1+\xi/E_x^b)^4}\, \exp\left[-t-\frac{1}{4t}\left(\frac{E_x^1 - E_x^b - h\nu - \xi}{kT_L}\right)^2\right]$$

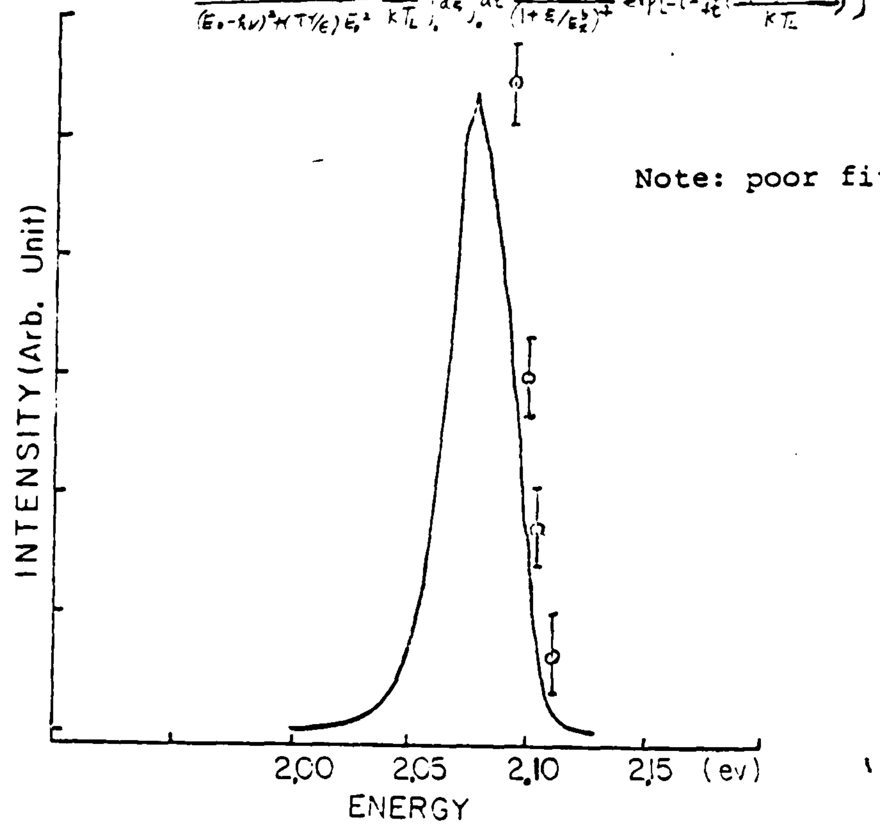

Fig.3.2.10

Dots with Error Bar: Experimental Result(300K)
of Higher Energy Band.
Solid Line: Exciton-Exciton Scattering Emission.

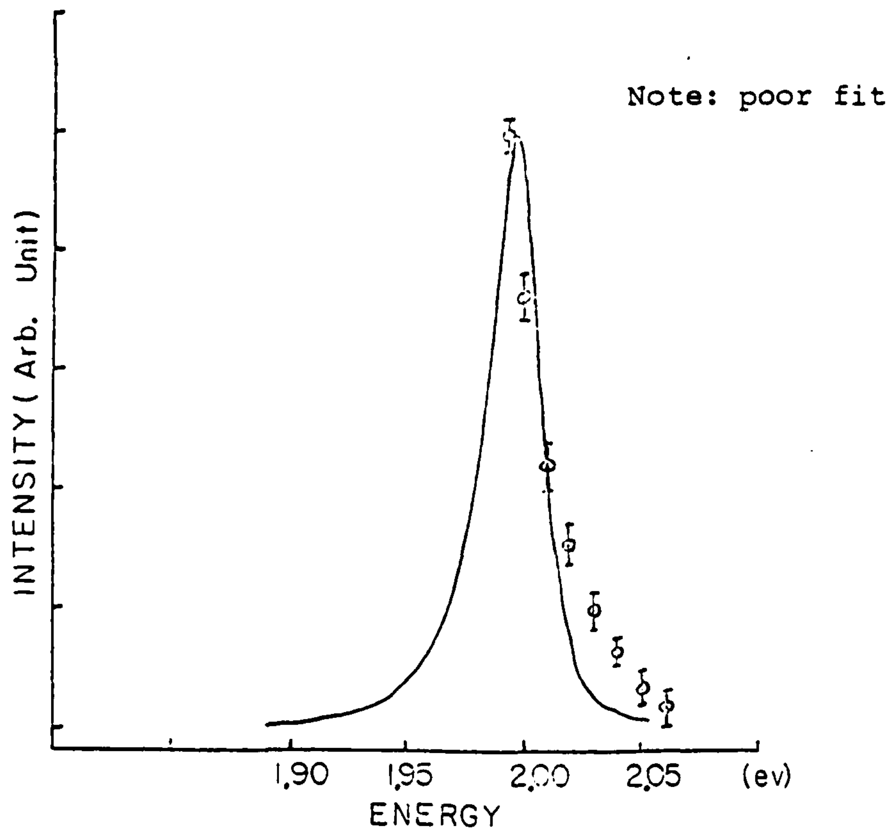

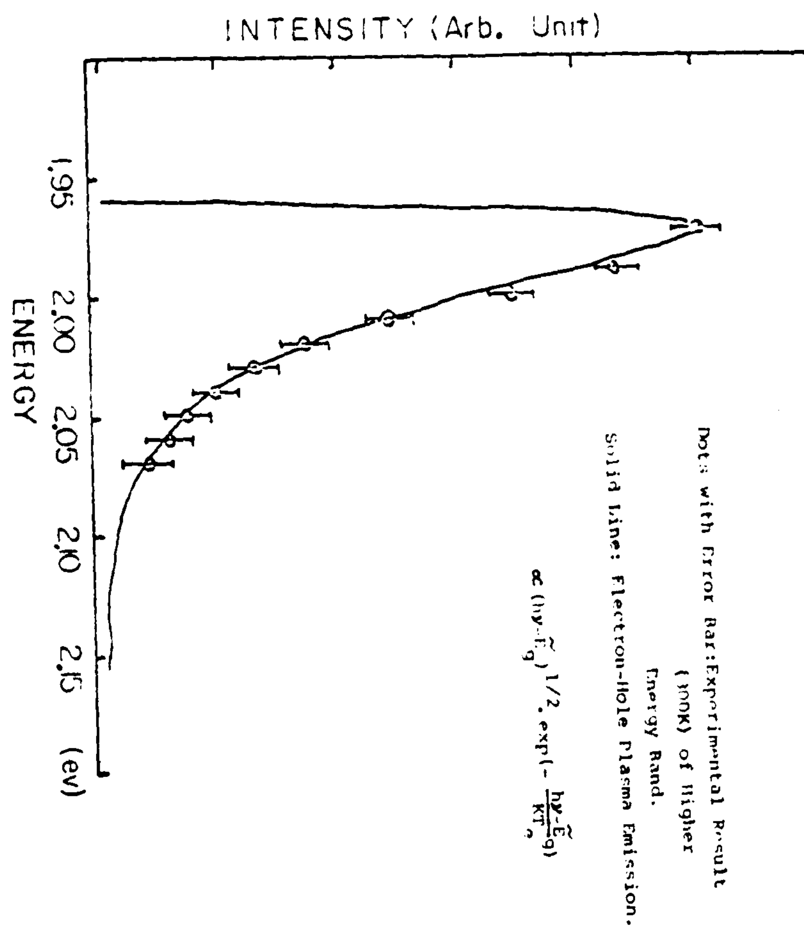

Fig.3.2.11

Fig.3.2.12

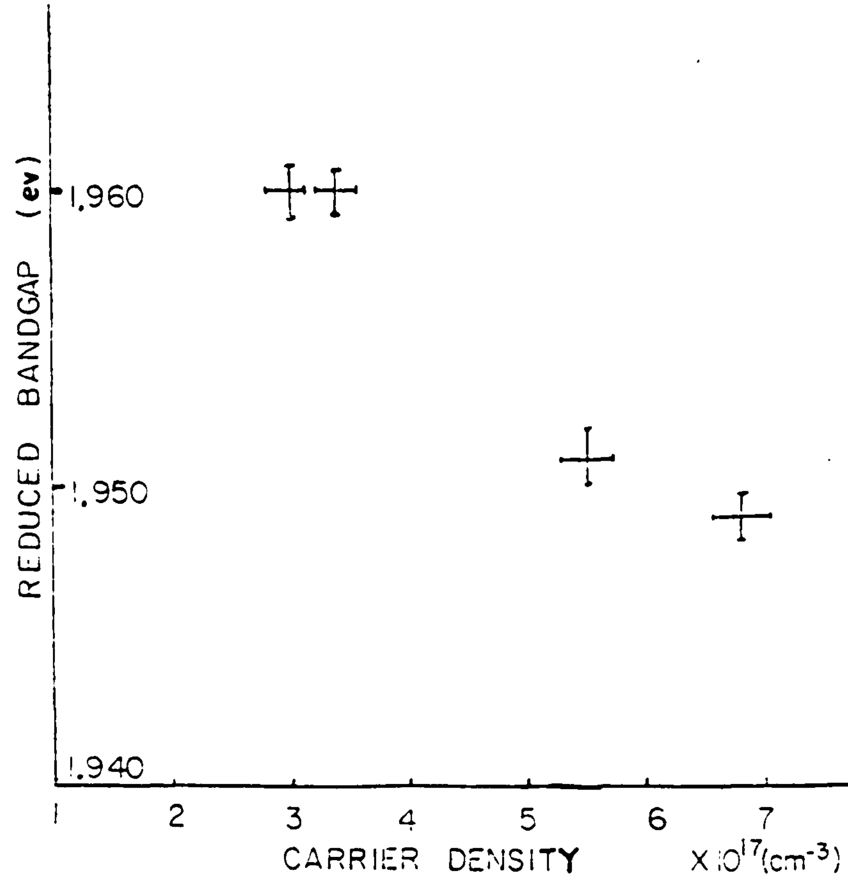

Fig.3.3.1

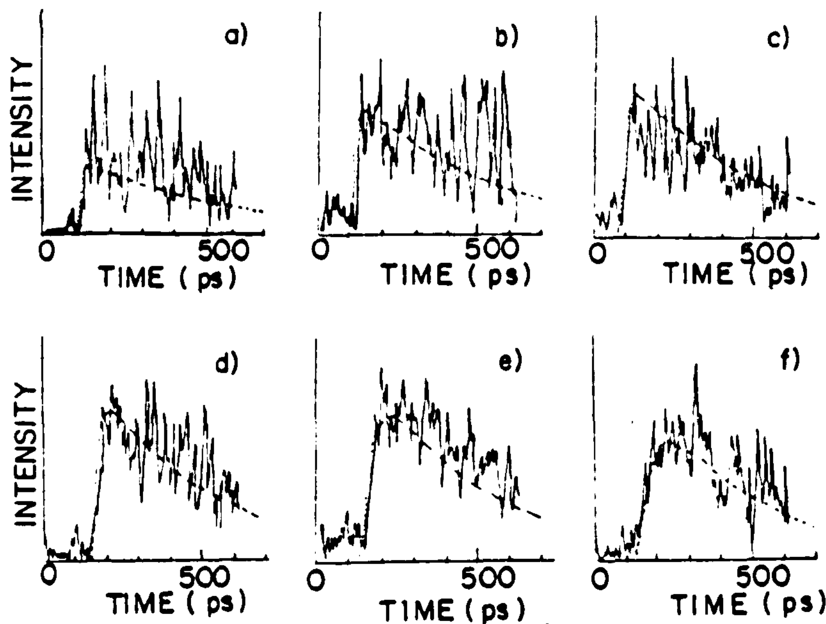

a) $N = 1.8 \times 10^{18} cm^{-3}$ b) $N = 3 \times 10^{18} cm^{-3}$ c) $N = 4.8 \times 10^{18} cm^{-3}$

d) $N = 6.6 \times 10^{18} cm^{-3}$ e) $N = 7.5 \times 10^{18} cm^{-3}$ f) $N = 8.2 \times 10^{18} cm^{-3}$

a) τ_r=5ps, τ_d=500ps

b) τ_r=5ps, τ_d=450ps

c) τ_r=10ps, τ_d=400ps

d) τ_r=20ps, τ_d=370ps

e) τ_r=30ps, τ_d=350ps

f) τ_r=50ps, τ_d=300ps

Fig.3.3.1

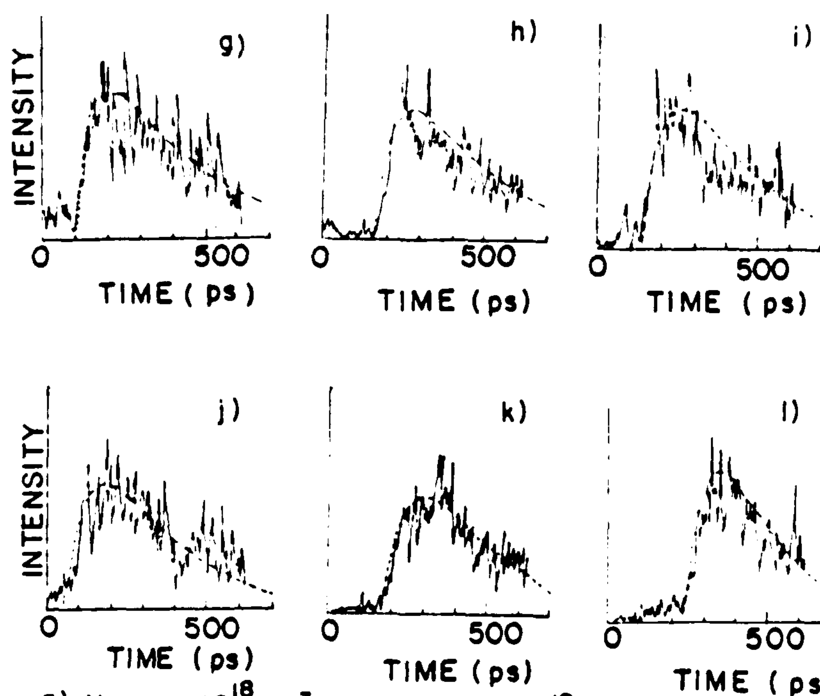

g) $N = 8.7 \times 10^{18}\ cm^{-3}$ h) $N = 1.0 \times 10^{19}\ cm^{-3}$ i) $N = 1.1 \times 10^{19}\ cm^{-3}$

j) $N = 1.2 \times 10^{19}\ cm^{-3}$ k) $N = 1.3 \times 10^{19}\ cm^{-3}$ l) $N = 1.4 \times 10^{19}\ cm^{-3}$

g) τ_r=60ps, τ_d=280ps

h) τ_r=60ps, τ_d=270ps

i) τ_r=65ps, τ_d=250ps

j) τ_r=75ps, τ_d=230ps

k) τ_r=80ps, τ_d=220ps

l) τ_r=90ps, τ_d=150ps

Fig.3.3.2

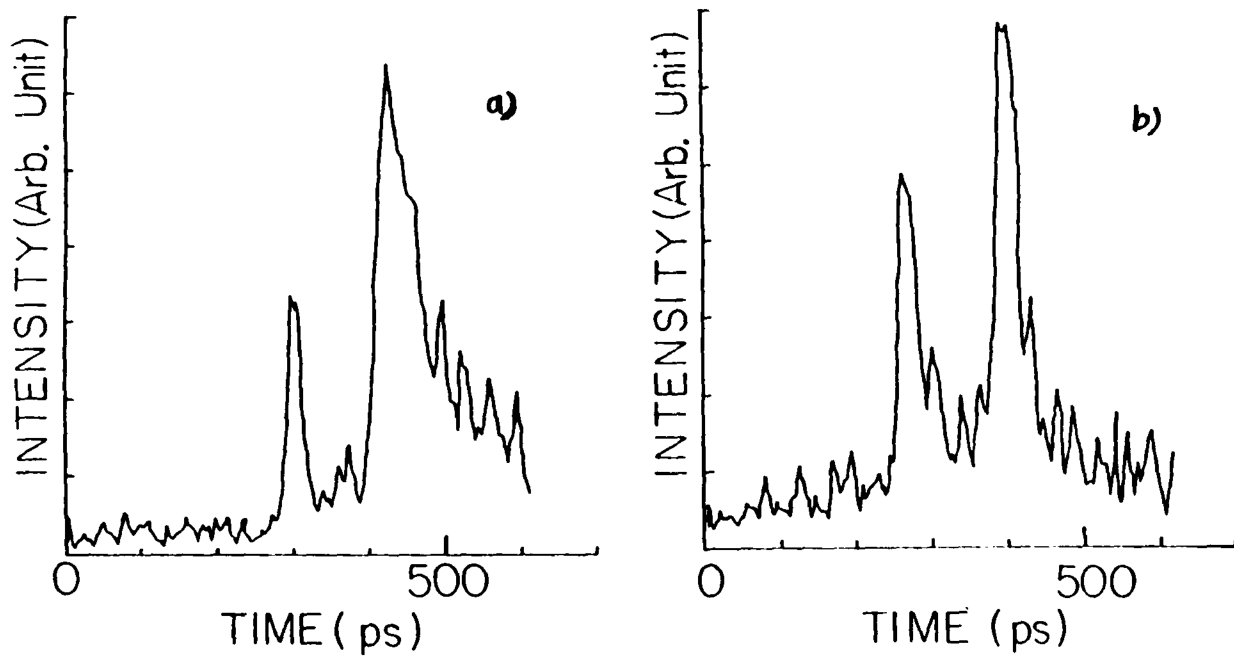

Fig.3.3.3

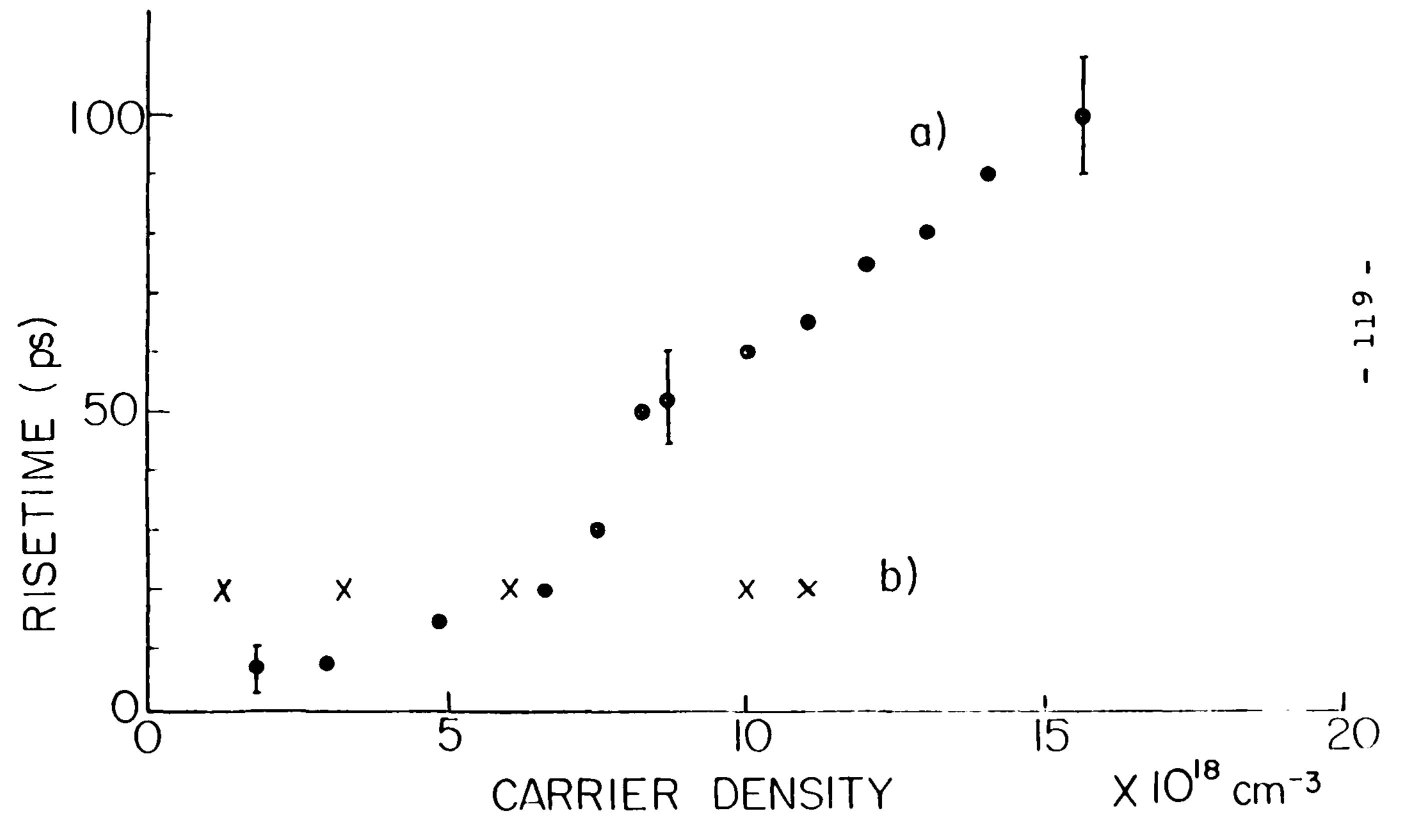

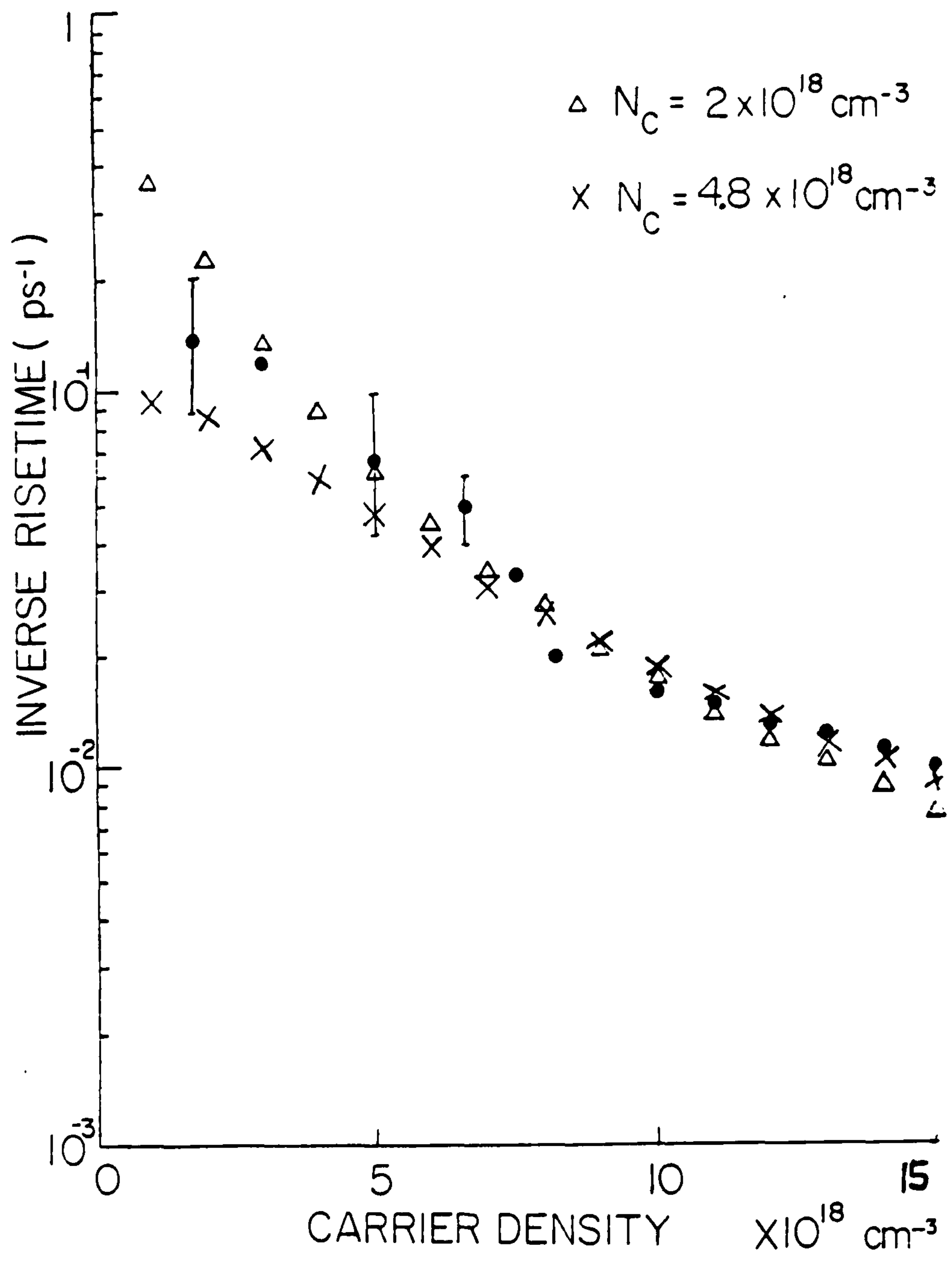

Fig.3.3.4

Chapter 4: Conclusion

In the chapter 2, the determination of the fundamental energy gap[1,2], the observation of the splitting of S-conduction band[3] and the determination of direct band gap of $CdCr_2Se_4$ were described. In the chapter 3, the dominant relaxation process of hot photogenerated carriers in GaSe was also determined to arise from the emissions of nonpolar optical phonons $A_1^{\prime(1)}$(16.7 mev) from holes[4], and the emission rate of $A_1^{\prime(1)}$ phonon was found to decrease at high density of photogenerated carriers in agreement with the theory developed by Yoffa[5].

The determination of the fundamental energy gap at 1.8 ev in $CdCr_2Se_4$ was rather difficult to determine by optical absorption because the absorption edge at 1.2 ev is far below the fundamental gap energy[6]. The splitting of S-conduction band was determined for the first time by photoluminescence spectra. This observation enables us to study the exchange effect between the itinerant conduction electrons and the local magnetic moments inside semiconductors, and the conduction band structure of a ferromagnetic semiconductor.

The relaxation processes of hot photogenerated carriers have been studied by many physicists[7-14] because they are involved in the laser annealing process within the semiconductor surfaces. There are two theories to describe the slowed relaxation processes of hot carriers: one is the

theory developed by Yoffa[5] who claims that the slowed relaxation process is due to the screening of high density carriers in semiconductors; the other theory is developed by van Driel[15] who insists that the phonons' temperature reaches that of the carriers, therefore the emission rate of phonons from carriers is slowed due to thermal equilibrium between phonons and carriers. In this thesis, the first theory fits the experimental data well and this leads us to believe that the slowed relaxation of hot carriers in semiconductors is probably due to the screening of high density carriers and not due to the thermal equilibrium between carriers and phonons. Since it is impossible to eliminate the van Driel theory from being the slowed relaxation mechanism at this time by the time resolved emission spectroscopy, a proposed experiment will be stated in the next chapter to continue this research.

References of Chapter 4:

1. T. Kambara, T. Oguchi, and K. I. Gondaira, J. Phys. C13, 1493(1980).
2. T. Oguchi, T. Kambara, and K. I. Gondaira, Phys. Rev. B22,872(1980).
3. W. Nolting and A. M. Oleś, Phys. Rev. B22, 6184(1980).
4. S. S. Yao, J. Buchert, and R. R. Alfano, Phys. Rev. B 25,6534(1982).
5. E. J. Yoffa, Phys. Rev. B23,1909(1981).
6. G. Busch, B. Magyar, and P. Wachter, Phys. Lett. 23,438 (1966).
7. R. J. Seymour, M. R. Junnarkar, and R. R. Alfano, Solid State Comm. 41,657(1982).
8. M. Pugnet, J. Collet, and A. Cornet, Sol. St. Comm. 38, 531(1981).
9. R. F. Leheny, J. Shah, R. L. Fork, C. V. Shank, and A. Migus, Sol. St. Comm. 31,809(1979).
10. D. von der Linde and R. Lambrich, Phys. Rev. Lett. 42, 1090(1979).
11. C. V. Shank, R. L. Fork, R. F. Leheny, and J. Shah, Phys. Rev. Lett. 42,112(1978).
12. C. V. Shank, D. H. Auston, E. P. Ippen, and O. Teschke, Sol. St. Comm. 26,567(1978).
13. R. G. Ulbrich, Sol. St. Electonics, 21,51(1978).
14. C. Weisbuch, Sol. St. Electronics, 21,179(1978).
15. H. M. van Driel, Phys. Rev. B19,5928(1979).

Chapter 5: Future Work

The following research work can be extended in the future.

1. Perform the steady state photoluminescence spectra of $CdCr_2Se_4$ measured at helium temperatures and very high external magnetic field $\sim$30 Kgauss and pressures. In this thesis, only magnetic field up to 4 kgauss was applied to $CdCr_2Se_4$ when the steady state photoluminescence was measured. No change of the spectra was observed in comparison with that when no external magnetic field was on the sample. This leads us to believe that the two S-conduction bands are mixed spin-polarized. It will be interesting to know how the two conduction bands of a ferromagnetic semiconductor change with increasing external magnetic field and what happen when pressure is applied.
2. Perform time resolved subpicosecond absorption spectroscopy measured at low photogenerated carrier density $\leq 5\times10^{18}cm^{-3}$ in GaSe. Since the risetime of the picosecond laser time resolved photoluminescence is within the resolution of the measuring system($\sim$20 ps) when the the carrier density is below $5\times10^{18}cm^{-3}$, it is important to know whether the unscreened emission rate of phonon is twenty-five times or five times larger than that at carrier density $\sim10^{19}cm^{-3}$ in order to justify Yoffa's theory. The time resolved absorption measurement by subpocosecond laser can solve the above

question.

3. Perform time resolved picosecond Raman scattering in GaSe. Since the theory developed by van Driel has not been proved to be correct or incorrect. The time resolved phonon temperatures can be measured from the intensity ratio of the Stokes line to the anti-Stokes line of $A_1'^{(1)}$ phonon in GaSe.

Appendix 1: The intensity dependence of exciton emission, exciton-exciton scattering emission, exciton-carrier scattering emission, and electron-hole recombination emission with respect to the excitation intensity.

a). When both electrons(holes) and excitons are photogenerated in semiconductors, the following two rate equations can be written:

$$dn/dt=J-(A+A')np+1/2(C+C')n_{ex}^{2} \quad (1)$$

$$dn_{ex}/dt=Anp-n_{ex}/\tau-(B+B')nn_{ex}-(C+C')n_{ex}^{2} \quad (2)$$

where

J : excitation = electron-hole pair creation

$n(=p)$: the electron's(hole's) density;

n_{ex} : the excitonic density;

$(A+A')np$: the electron-hole recombinations, Anp is the creation of excitons, $A'np$ is the radiative and nonradiative direct recombination;

$1/2(C+C')n_{ex}^{2}$: number of electron-hole pairs created by exciton-exciton scattering process;

n_{ex}/τ : radiative or nonradiative recombination of free excitons;

$(B+B')nn_{ex}$: exciton-electron scattering recombination, Bnn_{ex} is radiative and $B'nn_{ex}$ is nonradiative;

$(C+C')n_{ex}^{2}$: recombination due to exciton-exciton

processes, Cn_{ex}^2 is radiative and
$C'n_{ex}^2$ is nonradiative.

In the steady state case, $dn/dt = dn_{ex}/dt = 0$, eq.(1) and (2) become

$$J = (A+A')n^2 - 1/2(C+C')n_{ex}^2 \qquad (3)$$

$$An^2 = n_{ex}/\tau + (B+B')nn_{ex} + (C+C')n_{ex}^2 \qquad (4)$$

(i) Under weak excitation case, $(B+B')nn_{ex}$ and $(C+C')n_{ex}^2$ are negligible. From eq.(3),

$$J = (A+A')n^2 \qquad (5)$$

and from eq.(4),

$$An^2 = n_{ex}/\tau \qquad (6)$$

therefore $J \propto n^2 \propto n_{ex}$ ......(7)

The intensity of exciton emission is proportional to n_{ex} or J;

The intensity of electron-hole recombination is proportional to np or J.

(ii) Under high excitation case, $(C+C')n_{ex}^2$ is dominant. From eq.(4),

$$An^2 = (C+C')n_{ex}^2; \qquad (8)$$

from eq.(3),

$$n \propto n_{ex} \propto J^{1/2} \qquad (9)$$

Therefore,

the intensity of exciton-exciton scattering emission is proportional to n_{ex}^2 or J;

the intensity of exciton-carrier scattering emission is proportional to nn_{ex} or J; and
the intensity of electron-hole recombination emission is proportional to np or J.

b). When only electrons and holes are photogenerated in semiconductors, the following equations can be written:

$$dn/dt=J-nK_{NR}-K_{RAD}np \quad \text{.........................(10)}$$

$$dp/dt=J-pK_{NR}-K_{RAD}np \quad \text{.........................(11)}$$

where $K_{NR}n$, $K_{NR}p$ are nonradiative terms, $K_{RAD}np$ is radiative term.

In the steady state case, $dn/dt=dp/dt=0$, therefore, when $n=p$,

$$J=nK_{NR}+n^2K_{RAD} \quad \text{.............................(12)}$$

(i) Under weak excitation case, n^2K_{RAD} can be neglected, and

$$J=K_{NR}n \quad \text{..(13)}$$

The intensity of electron-hole recombination emission is proportional to np or J^2.

(ii) Under high excitation case, $K_{RAD}n^2$ is dominant, therefore, $J=K_{RAD}n^2$..........................(14)

The intensity of electron-hole plasma emission is proportional to np or J.

Appendix 2: The computer programming to calculate eq.(3.1.2)

```
      DOUBLE PRECISION E(40),EE(40),EH(40),FE(40),FH(40),
      A0(40),A(40),W(40),DT,T,AN,AM,H,EG,B,AK,AH,B1,B2,DE,
      G(40),Q(40),FIL,AP(40),CNE,CNH,FFE,FFH,FF(100),
      AA(100),AEE,AEH
      TYPE 100
100   FORMAT(2X,'ENTER THE TIME DELAY IN PS, THE CARRIER
    1 TEMPERATURE IN K, THE DENSITY IN CM**-3(E8.2), THE
    2 ELECTRON EFFECTIVE MASS IN M0, THE HOLE EFFECTIVE
    3 MASS IN M0, THE REDUCED BAND GAP ENERGY IN EV, THE
    4 ABSORPTION BACKGROUND IN O.D.')
      ACCEPT 200,DT,T,AN,AM,H,EG,B
200   FORMAT(2G,E8.2,4G)
      AK=1.38
      AH=6.62
      CNE=(5.28D+15)*(AM*T)**1.5
      FFE=AN/CNE
      CNH=(5.28D+15)*(H*T)**1.5
      FFH=AN/CNH
210   FORMAT(2X,'B1=',G,3X,'B2=',G,3X,'AEE=',G,3X,'AEH=',
    1 G)
      A0(1)=0.
      A0(2)=0.
      A0(3)=0.
      A0(4)=0.
```

```
A0(5)=0.
A0(6)=0.
A0(7)=0.05
A0(8)=0.1
A0(9)=0.29
A0(10)=0.36
A0(11)=0.48
A0(12)=0.61
A0(13)=0.62
A0(14)=0.62
A0(15)=0.61
A0(16)=0.61
A0(17)=0.6
A0(18)=0.62
A0(19)=0.62
A0(20)=0.63
A0(21)=0.63
A0(22)=0.64
A0(23)=0.64
A0(24)=0.66
A0(25)=0.66
A0(26)=0.67
A0(27)=0.67
A0(28)=0.68
A0(29)=0.70
A0(30)=0.70
```

```
A0(31)=0.71
A0(32)=0.72
FF(1)=0.76515
FF(2)=0.82756
FF(3)=0.89388
FF(4)=0.96422
FF(5)=1.0387
FF(6)=1.1173
FF(7)=1.2003
FF(8)=1.2875
FF(9)=1.3791
FF(10)=1.4752
FF(11)=1.5756
FF(12)=1.6806
FF(13)=1.7900
FF(14)=1.9038
FF(15)=2.0221
FF(16)=2.1449
FF(17)=2.2720
FF(18)=2.4035
FF(19)=2.5393
FF(20)=2.6794
FF(21)=2.8237
FF(22)=2.9722
FF(23)=3.1249
FF(24)=3.2816
```

```
FF(25)=3.4423
FF(26)=3.6070
FF(27)=3.7755
FF(28)=3.9480
FF(29)=4.1241
FF(30)=4.3040
FF(31)=4.4876
FF(32)=4.6747
FF(33)=4.8653
FF(34)=5.0595
FF(35)=5.2571
AA(1)=0.0
AA(2)=0.1
AA(3)=0.2
AA(4)=0.3
AA(5)=0.4
AA(6)=0.5
AA(7)=0.6
AA(8)=0.7
AA(9)=0.8
AA(10)=0.9
AA(11)=1.0
AA(12)=1.1
AA(13)=1.2
AA(14)=1.3
AA(15)=1.4
```

```
      AA(16)=1.5
      AA(17)=1.6
      AA(18)=1.7
      AA(19)=1.8
      AA(20)=1.9
      AA(21)=2.0
      AA(22)=2.1
      AA(23)=2.2
      AA(24)=2.3
      AA(25)=2.4
      AA(26)=2.5
      AA(27)=2.6
      AA(28)=2.7
      AA(29)=2.8
      AA(30)=2.9
      AA(31)=3.0
      AA(32)=3.1
      AA(33)=3.2
      AA(34)=3.3
      AA(35)=3.4
      IF(FFE-0.76515)40,30,30
30    DO 10 I=1,35
      IF(FFE-FF(I))11,11,10
10    CONTINUE
11    AEE=AA(I)
      B1=DEXP(-AEE)
```

```
50      IF(FFH-0.76515)80,60,60
60      DO 70 L=1,35
        IF(FFH-FF(L))71,71,70
70      CONTINUE
71      AEH=AA(L)
        B2=DEXP(-AEH)
        GO TO 110
40      B1=2D-6/AN*1D+21*((2*3.14*AM*9.1*AK*T)/AH**2.)**1.5
80      B2=2D-6/AN*1D+21*((2*3.14*H*9.1*AK*T)/AH**2.)**1.5
        GO TO 50
110     TYPE 210,B1,B2,AEE,AEH
        J=(EG-1.942)/0.005
        TYPE 220,J
220     FORMAT(2X,'J=',I2)
        K=32-J
        E(1)=EG
        DE=0.005
        DO 300 I=1,K
        E(I)=E(1)+DE*(I-1)
        EE(I)=(E(I)-E(1))*H/(AM+H)
        EH(I)=(E(I)-E(1))*AM/(AM+H)
        G(I)=EE(I)*300./(0.027*T)
        Q(I)=EH(I)*300./(0.027*T)
        FE(I)=(1+B1*DEXP(G(I)))**-1
        FH(I)=(1+B1*DEXP(Q(I)))**-1
        AP(I)=A0(I+J)
        A(I)=AP(I)*(1-FE(I))*(1-FH(I))+B
```

```
300       W(I)=1239.4/E(I)
          TYPE 500,DT
500       FORMAT(1X,'ENTER THE NAME FOR THE REDUCED ABSORPTION
     1    AT TIME DELAY =',G)
          ACCEPT 600,FIL
600       FORMAT(A10)
          CALL OFILE(21,FIL)
          DO 700 I=1,K
700       WRITE(21,800)W(I),A(I)
800       FORMAT(2G)
          END
```

Appendix 3: The derivation of eq.(3.1.5)

The probability per unit time of a carrier being scattered out of K is

$$\frac{1}{\tau} = \frac{2\pi}{\hbar} \sum_{\vec{q}} [|\langle\vec{K}+\vec{q}, N_{\vec{q}}-1 | H' | \vec{K}, N_{\vec{q}}\rangle|^2 \delta(\mathcal{E}_{\vec{K}+\vec{q}}, N_{\vec{q}}-1 - \mathcal{E}_{\vec{K},N_{\vec{q}}}) + |\langle \vec{K}-\vec{q}, N_{\vec{q}}+1 | H' | \vec{K}, N_{\vec{q}}\rangle|^2 \delta(\mathcal{E}_{\vec{K}-\vec{q}}, N_{\vec{q}}+1 - \mathcal{E}_{\vec{K},N_{\vec{q}}})] \quad (1)$$

where the first term is the transition probability due to phonon absorption, the second due to emission. $N_{\vec{q}}$ is the steady state average number of phonons with wave vector $\vec{q}$. After the integration over the θ, ϕ angles of $\vec{q}$, the probability per unit time of optical mode scattering is

$$\frac{1}{\tau_{op}} = \frac{mV}{2\pi\hbar^3 K}\left[\int_{k(1+\hbar\omega_0/\varepsilon)^{1/2}-k}^{k(1+\hbar\omega_0/\varepsilon)^{1/2}+k} |\langle\vec{K}+\vec{q}|H'_{op}|\vec{K}\rangle|^2 q\,dq + \int_{k-k(1-\hbar\omega_0/\varepsilon)^{1/2}}^{k+k(1-\hbar\omega_0/\varepsilon)^{1/2}} |\langle\vec{K}-\vec{q}|H'_{op}|\vec{K}\rangle|^2 q\,dq\right] \quad (2)$$

Since $|\langle\vec{K}\pm\vec{q}\,|\,H'_{op}\,|\,\vec{K}\rangle|^2 = \frac{D^2\hbar}{2V\rho\omega_0}\left\{N_q + \frac{1}{2} + \frac{\delta N_k}{2}\right\}$ (3)

where D is the deformation potential, we find

$$\frac{1}{\tau_{op}} = \frac{D^2 m_t m_\ell^{1/2}}{2^{1/2}\pi\hbar^3\rho\omega_0}\left[N_q(\varepsilon+\hbar\omega_0)^{1/2} + (N_q+1)(\varepsilon-\hbar\omega_0)^{1/2}\right] \quad (4)$$

The rate of change of carrier energy $(d\mathcal{E}/dt)_{op}$ due to the nonpolar optical phonon scattering is given by the phonon energy $\hbar w_0$ times the difference between $1/\tau$ for phonon absorption and $1/\tau$ for phonon emission.

$$\left(\frac{d\varepsilon}{dt}\right)_{op} = \frac{D^2 m_t m_l^{1/2}}{2^{1/2}\pi\hbar^2\rho}\left[N_q(\varepsilon+\hbar\omega_o)^{1/2} - (N_q+1)(\varepsilon-\hbar\omega_o)^{1/2}\right] \tag{5}$$

For a Maxwell-Boltzmann distribution at T_e, the average rate of change of carrier energy due to nonpolar optical phonon scattering is found to be

$$\left\langle\frac{d\varepsilon}{dt}\right\rangle_{op} = -\left(\frac{2}{\pi}\right)^{1/2}\frac{D^2 m_t m_l^{1/2}}{\pi\hbar^2\rho}(k_o T_e)^{1/2}\frac{e^{(x_o-x_e)}-1}{e^{x_o}-1}\frac{x_e}{2}e^{x_e/2}K_1\left(\frac{x_e}{2}\right) \tag{6}$$

where $x_e=\hbar w_o/k_oT_e$, $x_o=\hbar w_o/k_oT_o$, and K_1 is a Bessel function of the second kind with imaginary argument.

Appendix 4: The computer programming to calculate eq.(3.1.6)

```
EX GASE8.F4 SYS:PORT/LIB
        EXTERNAL F
        REAL TT,A,RES,ANS,ER,B
        COMMON A
5       TYPE 10
10      FORMAT(2X,'ENTER THE VALUES OF DELAY TIME, A, AND
     1  FINAL TEMPERATURE.')
        ACCEPT 20,TT,A,B
20      FORMAT(3F)
        CALL QUAD(F,2000.,B,.1,ANS,ER)
        TYPE 40,ANS,B
40      FORMAT(2X,'ANS=',F,3X,'B=',F)
        RES=TT-ANS
        TYPE 30,RES
30      FORMAT(2X,'RES=',F)
        IF(RES .NE. 0)GO TO 5
        STOP
        END
        REAL FUNCTION F(T)
        REAL A,T,F
        COMMON A
        F=A*(T**-0.5)*EXP(-96.5/T)*(EXP(0.643-193./T)-1.)**
     1 (-1.)*(EXP(0.643)-1.)
        RETURN
```

END

Appendix 5: The computer programming to calculate eq. (3.2.1)

```
        DOUBLE PRECISION FIL,E(70),PS(70),E0,T,TE,X,BK
        TYPE 100
100     FORMAT(2X,'ENTER THE VALUES OF THE EXCITON ENERGY IN
     1  EV, THE LATTICE AND THE ELECTRON TEMPERATURES IN
     2  K.')
        ACCEPT 200,E0,T,TE
200     FORMAT(3G)
        DO 300 I=1,70
        E(1)=1.800
        E(I)=E(1)+(I-1)*0.005
        X=0.48E+4/TE*DSQRT((E0-E(I))**2.*(TE/T+0.97))
        CALL BESK(X,1,BK,IER)
        TYPE 250,I,X,BK
250     FORMAT(2X,'I=',I2,2X,'X=',G,2X,'BK=',G)
        PS(I)=TE*DSQRT((E0-E(I))**2./(TE/T+0.97))*BK*DEXP(
      1 0.47E+4/TE*(E0-E(I)))/((E0-E(I))**2.+0.25E-3*E0**2.)
300     TYPE 350,PS(I),I
350     FORMAT(2X,'PS(I)=',G,2X,'I=',I2)
        TYPE 400
400     FORMAT(2X,'ENTER THE FILE NAME FOR THE OUTPUT.')
        ACCEPT 500, FIL
500     FORMAT(A10)
        CALL OFILE(21,FIL)
        DO 600 I=1,70
600     WRITE(21,700)E(I),PS(I)
```

```
700     FORMAT(2G)
        END
```

Appendix 6: The computer programming to calculate eq.(3.2.2)

```
        EXTERNAL FCT
        DOUBLE PRECISION FCT,HNI,E01S,PIA,BKT,Y,EXB,BB,AA,
        1YY,FILENAME
        COMMON Y,EXB,BKT
        TYPE 100
100     FORMAT(2X,'ENTER E01S,PIA,BKT,EXB')
        ACCEPT 101,E01S,PIA,BKT,EXB
        TYPE 102
        ACCEPT 103,FILENAME
102     FORMAT(2X,'ENTER FILENAME')
103     FORMAT(A10)
101     FORMAT(4F)
        CALL OFILE(20,FILENAME)
        DO 1 I=1,101
        BB=I
        Y=-31.0+BB*.5
        HNI=E01S*1000.0+Y
        AA=HNI/((E01S*1000.0-HNI)**2+PIA*(E01S*1000.0)**2)/
     1  BKT
        CALL DQL24(FCT,YY)
        AA=AA*YY
        IF(AA.LE.1.0D00)AA=1.0
        AA=DLOG10(AA)
1       WRITE(20,105)Y,AA
```

```
105     FORMAT(2F)
        END
        FUNCTION FCT(AKSI)
        DOUBLE PRECISION FCT,AKSI,Y,E01S,HNI,ARKI,EXB,BKT,
        1A,B,C,D
        COMMON Y,EXB,BKT
        ARKI=DABS((-Y-EXB-AKSI)/BKT)
        X=ARKI
        CALL BESK(X,1,BK,IER)
        A=1.0+AKSI/EXB
        D=DEXP(AKSI)/A**4.
        FCT=ARKI*DSQRT(AKSI)*BK*D
        RETURN
        END
```

Appendix 7: The derivation of eq.(3.3.2)

The phonon emission rate is related directly to the carrier excitation spectrum, which is

$$\mathrm{Im}\frac{1}{\epsilon(\vec{q},\omega)} = \frac{\epsilon_2}{\epsilon_1^2+\epsilon_2^2} \tag{1}$$

where ϵ_1 and ϵ_2 are the real and imaginary parts of the complex dielectric function $\epsilon(\vec{q},w)$. Within the random -phase approximation,

$$\epsilon_2(\vec{q},\omega) = \frac{4\pi^2 e^2}{\Omega q^2}\sum_{ij}\sum_{\vec{K}\sigma} f^{i}_{\vec{K}\sigma}(1-f^{j}_{\vec{K}+\vec{q},\sigma})\,\delta(\hbar\omega-[\Delta E(\vec{K},\vec{q})]_{ij}) \tag{2}$$

where Ω is the volume. The sum Σ_{ij} ranges over all pairs of valleys i and j (including i=j) where the transitions take a carrier from valley i to valley j. The occupation probability of a state in the ith valley with momentum $\vec{K}$ and spin σ is $f^{i}_{\vec{K}\sigma}$ and $[\Delta E(\vec{K},\vec{q})]_{ij}$ is the difference in energy between electronic states $(\vec{K}+\vec{q},\sigma)_j$ and $(\vec{K},\sigma)_i$. Assuming occupation probabilities are essentially Boltzmann, $f^{i}_{\vec{K}\sigma} \approx \exp(-\beta E^{i}_{\vec{K}})$ and $f(1-f) \approx f$. Eq.(2) can then be written

$$\epsilon_2(\vec{q},\omega) = \epsilon_0 \sum_{ij}(\hbar\omega_{pi})^2 f_{ij}\frac{(\hbar\Gamma_{ij})(\hbar\omega)}{[(\hbar\Omega_{ij})^2-(\hbar\omega)^2]^2+(\hbar\Gamma_{ij})^2(\hbar\omega)^2} \tag{3}$$

where $w_{pi}=(4\pi N_i e^2/\epsilon_0 m_i^*)^{1/2}$, N_i is the number of carriers in valleys i, ϵ_0 is the bulk dielectric function, f^{ij} is the effective oscillator strength for the transition $f_{ij}=Z_{ij}(m_j^*/m_i^*)^{1/2} h\,\Omega_{ij}/E_q$, Z_{ij} is the number of intravalley or intervalley transitions with

resonances at $\hbar w = \hbar \Omega_{ij}$. Eq. (3) can then be written as

$$\text{Im}\frac{1}{\epsilon(\vec{q},\omega)} \simeq \frac{1}{\epsilon_0}\sum_{ij} \frac{Z_{ij}(\hbar\omega_{pi})^2(m_j^*/m_i^*)^{1/2}(\hbar\Gamma_{ij})(\hbar\omega)^2/E_q\,\delta_{q,q_{0ij}}}{Z_{ij}^2(\hbar\omega_{pi})^4(m_j^*/m_i)(\hbar\omega/E_q)+(\hbar\Gamma_{ij})^2(\hbar\omega)^2} \tag{4}$$

The rate for emission of phonons (wave vector $\vec{q}$, frequency w) is given within the random phase approximation by the golden rule to be

$$R_{\vec{q},\omega} = \frac{2\pi}{\hbar}\sum_{ij}\sum_{\vec{K}\sigma}\left|\frac{V^{ij}_{\vec{K}+\vec{q},\vec{K}}}{\epsilon}\right|^2 f^i_{\vec{K}+\vec{q},\sigma}(1-f^j_{\vec{K}\sigma})\,\delta(\hbar\omega-(E^i_{\vec{K}+\vec{q}}-E^j_{\vec{K}})) \tag{5}$$

$V^{ij}_{\vec{K}+\vec{q},\vec{K}}$ is the unscreened matrix element for the transition of an electron from state $(\vec{K}+\vec{q})_i$ to $(\vec{K})_j$ via phonon emission. Because the carrier temperature greatly exceeds the lattice temperature, phonon absorption makes negligible contribution to the net energy relaxation rate of the carriers. With the usual assumption that V does not depend strongly on electronic state K. Eq. (5) becomes

$$R_{\vec{q},\omega} = \frac{\Omega e^{-\beta\hbar\omega}}{\pi\hbar e^3\epsilon_0^2}\sum_{ij}|V_q^{ij}|^2 Z_{ij}\frac{(\hbar\omega_{pi})^2}{(\hbar\Gamma_{ij})}\frac{(m_j^*)^{3/2}}{(m_i^*)^{1/2}}\delta_{\vec{q},\vec{q}_{0ij}} \Big/ \left[1+\frac{Z_{ij}(\hbar\omega_{pi})^4}{(\hbar\Gamma_{ij})^2E_q^2}\frac{m_j^*}{m_i^*}\right] \tag{6}$$

The carrier density dependence of the various emission rates can be seen more clearly by recognizing that $(\hbar w_{pi})^2 \sim N_i$ where N_i is the density of carriers in valley i. The critical value of N_i for the onset of screening is

$$(N_{ic})_{ij} = \frac{\epsilon_0(\hbar\Gamma_{ij})q_{0ij}^2}{8\pi e^2 Z_{ij}}\left[\frac{m_i^*}{m_j^*}\right]^{3/2} \tag{7}$$

$\hbar\Gamma_{ij} = (2E_q/\beta)^{1/2}$ for intravalley transition, $q_{0ii} \equiv (2m_i^*\omega/\hbar)^{1/2}$ for intravalley transitions in nonpolar crystal, and $q_{0ii} \equiv (\beta m_i^*/3)^{1/2}\omega$ for polar crystal. Eq.(6) becomes

$$R^{ij}_{q,\omega} \sim N/[1+[\frac{N}{N_{cij}}]^2] \tag{8}$$

The emission frequency $\nu^{ij}_{q,\omega} = R^{ij}_{q,\omega}/N$ is then

$$\nu^{ij}_{\vec{q},\omega} \sim 1/[1+[\frac{N}{N_{cij}}]^2]. \tag{9}$$

Appendix 8: The derivation of eq.(3.1.2)

According to the Golden rule for the optical absorption in a semiconductor, the absorption constant is

$$\alpha \propto \int d^3k_e \int d^3k_h |M|^2 (1-f_e)(1-f_h)\, \delta(\tilde{k}_e - \tilde{k}_h)\, \delta(\hbar\omega - E_g - E_e - E_h) \tag{1}$$

where f_e, f_h are the Fermi distributions of electrons and holes. Before the sample is excited by the pump pulse, the optical absorption due to the probe pulse is

$$\alpha_0 \propto \int d^3k_e \int d^3k_h |M|^2 \delta(\tilde{k}_e - \tilde{k}_h)\, \delta(\hbar\omega - E_g - E_e - E_h)$$

where f_e and f_h due to the thermal effect can be neglected because the sample is nondegenerate at room temperature. Therefore

$$\alpha_0 \propto \int dE_e\, E_e^{1/2} |M|^2 \delta(\hbar\omega - E_g - E_e - E_h) \propto (\hbar\omega - E_g)^{1/2} \tag{2}$$

After the sample is excited by the pump pulse, the optical absorption due to the probe pulse is

$$\alpha \propto \int d^3k_e \int d^3k_h |M|^2 (1-f_e)(1-f_h)\, \delta(\tilde{k}_e - \tilde{k}_h)\, \delta(\hbar\omega - E_g - E_e - E_h)$$

$$E_h = \hbar^2 k_h^2/2m_h = \hbar^2 k_e^2/2m_h = \frac{m_e}{m_h} E_e \quad , \quad E_e + E_h = E_e\left(1 + \frac{m_e}{m_h}\right) = \hbar\omega - E_g$$

$$E_e = (\hbar\omega - E_g)\frac{m_h}{m_e + m_h} \quad , \quad E_h = (\hbar\omega - E_g)\frac{m_e}{m_e + m_h}$$

and

$$\alpha \propto \int dE_e\, E_e^{1/2} |M|^2 (1-f_e)(1-f_h)\, \delta(\hbar\omega - E_g - E_e - E_h) \propto (\hbar\omega - E_g)^{1/2} (1-f_e)(1-f_h)$$

From eq.(2), $f_e = 1/(1+\exp(E_e - \mu_e)/kT_e)$, $f_h = 1/(1+\exp(E_h - \mu_h)/kT_h)$,

$$\alpha = \alpha_0 (1-f_e)(1-f_h). \tag{3}$$

Appendix 9: The concepts of the exchange and correlation energies in electron-hole plasma

Inside electron-hole plasma, a large positive(ie. repulsive) contribution to the ground state energy is kinetic energy

$$E_k = \frac{3}{5}\left(\frac{\hbar^2 k_F^2}{2m_e} + \frac{\hbar^2 k_F^2}{2m_h}\right) \tag{1}$$

where k_F is the Fermi wave vector. There are two negative energy contributions to the ground state energy. The leading correction is the exchange energy between the electrons and the holes separately. This is an attractive contribution arising from the reduction in Coulomb energy because of the spatial correlation imposed by the Pauli principle on electrons(or holes) in the same spin state. Its value is wellknown

$$E_{exch} = -3e^2 k_F / 2\pi K \tag{2}$$

The remaining term is known as the correlation energy. As its name implies, this term arises from the correlations between particles in unlike quantum states. In the electron-hole plasma, there are two types. The first is electron-hole correlation, which is between oppositely charged particles. The second is the electron-electron(or hole-hole) correlation between particles of like charge but opposite spin. These terms can be evaluated only

approximately. The first attack on the problems was by Hanamura who used a high density expansion to estimate this energy, with $m_e = m_h$,

$$E_{corr.} = 0.497 \ln r_s - 0.33 \tag{3}$$

Appendix 10: The concept of screening on the carrier-nonpolar optical phonon interaction

For polar crystal, the electrons can interact strongly with the long range polarization field created by the short wavevector polar LO-phonons, and this interaction can be screened when the carrier density reaches 6×10^{16} cm^{-3} in GaAs. The distance between two carriers at this density is 250 Å. However in nonpolar crystal, the interaction between electrons and nonpolar optical phonons are short range and it is more difficult to screen this interaction compared with that in polar crystal. For example, in Si, the intravalley transitions of electrons with nonpolar optical phonons will not be screened until 1.4×10^{19}cm^{-3}. At this density, the average distance between two carriers is $\sim$40Å which is very short compared with 250Å for GaAs. This is due to the fact that in nonpolar crystal the nonpolar optical phonons do not generate long range field to affect the electronic motion and the electrons interact with nonpolar optical phonons through short range deformation potential.